Designing Heterogeneous-Based Cascade Catalytic Systems for Carbon Dioxide Hydrogenation

by

Yuan Chen

A dissertation submitted in partial fulfillment
of the requirements for the degree of
Doctor of Philosophy
(Chemical Engineering)
in the University of Michigan
2016

Doctoral Committee:

Professor Levi T. Thompson, Jr., Chair
Professor Jun Ni
Professor Melanie S. Sanford
Professor Phillip E. Savage, Penn State University
Professor Johannes W. Schwank

Fortune does favor the bold and you never know
what you're capable of if you don't try.

— Sheryl Sandberg

This dissertation is dedicated to my Mom and Dad,

张全灵 和 陈卫明

You raise me up and I love you dearly.

ACKNOWLEDGEMENTS

I was so blessed to be surrounded and helped by a number of talented people during my study at the University of Michigan. First, I would like to sincerely thank my research advisor, Prof. Levi Thompson. His tremendous support, trust, and guidance have allowed me to grow as a better researcher and individual. I also greatly appreciate his patience in helping me strengthen my communication skills on both writing and public speaking. I am especially grateful for the extra effort he was willing to make, given I am not a native speaker. Above all, I want to thank him for seeing my potential and constantly encouraging me to get there. His advice will remain with me throughout my professional and personal life.

I would also like to express my gratitude to other members of my dissertation committee. Prof. Schwank, my academic grandpa, who always nicely grasped the big picture when I seemed to get stuck in details. I want to thank him for asking thought-provoking questions and always encouraging me to approach a problem from different angles.

I want to thank Prof. Sanford for her constructive input on my dissertation work, especially our collaboration on creating homo-/heterogeneous cascade systems. Prof. Sanford taught me how to select meaningful information from large amounts of data and move forward effectively to reach the project goal.

I am also thankful to Prof. Savage for providing his insights on the sustainability and the reaction kinetics for the cascade systems described in this dissertation. Prof. Savage wasalso extremely supportive of my participation in a number of extracurricular activities, such as recruiting and graduate symposia, during my graduate study.

I would also like to thank Prof. Ni for serving as my cognate committee member and guiding me to consider the economic viability and implementation of the overall process. Prof. Ni was also an incredible mentor during my study at Michigan and offered me many suggestions on personal and career development.

I am also grateful to all the past and present Thompson Research Group members: Olabode Ajenifujah, Dr. Tanya Breault, Dr. Amin Bazyari, Sarah Carl, Dr. Saemin Choi, Abdoulaye Djire, Allison Frank, Ryan Frank, Dr. Galen Fisher, Dr. Jason Gaudet, Dr. Krista Hawthorne, Dr. Iljeong Heo, Jennifer Joz, Jonathan Kucharyson, Sydney Laramie, Dr. Adam Lausche, Tapiwa Mushove, Dr. Kanado Okada, Dr. Priyanka Pande, Sarah Paleg, Dr. Joshua Schaidle, Dr. Aaron Shinkle, Dr. Neil Schweitzer, Siu on Tung, Digna Vora, Wei-Chung Wen, and Brian Wyvratt. I would not have been able to make so much progress on my research project without each one's help and support.

I would like to especially acknowledge a few individuals from this group. First, I want to thank Dr. Saemin Choi, who constantly encouraged me during the frustrating moments and generously shared with me his experience both in research and in life. We also co-authored three journal articles through which he helped me significantly on improving my writing skills. Second, Brian Wyvratt was a great colleague during my graduate study and will continue to be a good friend. He helped me through the difficult time when I switched my project to work on heterogeneous catalysis and patiently showed

me almost every single piece of equipment for catalyst characterization. We also constantly had great discussions on each other's research projects, especially on the experiment design and data analysis. Third, I want to acknowledge Dr. Jason Gaudet, who generously provided me helpful guidance on the reactor design and data analysis when I first started the cascading CO_2 hydrogenation project. Fourth, I am deeply grateful to Dr. Tanya Breault, who offered me tremendous help in writing manuscripts. Whenever I sent her a draft, she always gave me her insightful feedback as soon as possible and was always willing to proofread the edited version. I would not have been such a productive writer without her kindness and support. In addition, I want to thank Siu on Tung for patiently spending several late nights collecting high quality SEM micrographs for the selected heterogeneous catalysts. Finally, I want to thank my undergraduate students, Evan Roberts and Tianshu Ji, and my master's student, Digna Vora, who worked diligently and made great contributions to a number of experiments included in this dissertation. I also want to thank them for teaching me how to be a good research mentor.

Additionally, I would like to acknowledge the funding sources for this research, the Center for Enabling New Technologies Through Catalysis (CENTC), an innovation center under the National Science Foundation, through the grant CHE-1205189. I received not only the financial support but also intellectual support through the monthly video conference, where I had great opportunities to showcase my research and learn from the work of other researchers. I have also gained valuable networking experiences and made a lot of friends through the annual meeting and summer school hosted by CENTC. From CENTC, I would like to specially acknowledge Dr. Karen Goldberg and Dr. Alex Miller, who were patient in answering my questions regarding homogeneous catalysis and made

insightful comments on my research. I am also extremely grateful to the CENTC staff, Nadine Gruhn, Lynsey Tafreshi, Eve Perara, and Tamara Yurkanin. They were so responsive to every single question or request that I raised and kept all the CENTC events running in a highly organized way, so that we got the best experience.

From the Chemical Engineering department, I would like to thank the graduate coordinator, Susan Hamlin, for assisting with several administrative tasks on course selection, exam scheduling and visa paperwork for international scholars. I would also like to acknowledge Shelley Fellers, Barbara Perry, and Jennifer Downey for their time and assistance on various tasks especially on order forms and travel reimbursement.

Last but not least, I must thank my family. Their unconditional love and support have propelled me to move forward no matter how many challenges I faced on this arduous and rewarding journey. I want to thank my parents, who gave me infinite courage and support to pursue my dream. I am grateful to have the Chen, Bi, and Zhang families to always stand by my side and encourage me to achieve further. Finally, I want to thank my husband, Yuqiang, who has always been there for me, sharing every single piece of my happiness and frustration, and who drives me to become a better and more confident person.

TABLE OF CONTENTS

LIST OF FIGURES

LIST OF TABLES

LIST OF APPENDICES

LIST OF ABBREVIATIONS

AM – Ammonium molybdate

AN – Aniline

ASF – Anderson-Schulz-Flory

BAL – Butyraldehyde

BOH – Butanol

BET – Brunauer–Emmett–Teller

CAL – Crotonaldehyde

CHA – Cyclohexylamine

COH – Crotyl alcohol

DFT – Density functional theory

DME – Dimethyl ether

DMF – Dimethylformamide

DMSO-d6 – Dimethyl sulfoxide-d6

E_A – Activation energy

EDX – Energy Dispersive X-ray Spectroscopy

FAME – fatty acid methyl ester

FE – Faradaic efficiency

FID – Flame ionization detector

FTS – Fischer-Tropsch Synthesis

GC – Gas chromatograph(y)

GDL – Gas-diffusion layer

HER – Hydrogen evolution reaction

H_2-TPR – Hydrogen temperature programmed reduction

HMF – 5-hydroxymethyl furfural

LCA – Life cycle assessment

ICP-OES – Inductively coupled plasma optical emission spectrometry

LLDPE – Low-density polyethylene

MEA – Membrane electrode assembly

MS – Mass spectroscopy

MSR –Methanol steam reforming

MTG – Methanol-to-gasoline

MTO – Methanol-to-olefin

NEt_3 – Triethyl amine

NMR – Nuclear magnetic resonance

RWGS – Reverse water-gas shift

SEM – Scanning electron microscopy

SPE – Solid-polymer electrolyte

TCD – Thermal conductivity detector

THF – Tetrahydrofuran

TMC – Transition metal carbides

TPR – Temperature programmed reaction

WGS – Water-gas shift

XRD – X-ray diffraction

ABSTRACT

The search for sustainable and economical chemical processes is a key priority for the chemical industry. Cascade catalysis presents a promising technology to meet this need by combining multiple catalysts to drive a sequence of catalytic steps in one reactor. These catalysts work cooperatively to achieve desired products with higher selectivity/atom efficiency than from using any single catalyst alone. Consequently, this cascade approach enables efficient use of feedstock and reduces the operational work-up between catalytic sub-steps, leading to both time and cost benefits. Research described in this dissertation investigates the use of heterogeneous-based cascade catalytic systems to advance carbon dioxide hydrogenation for producing value-added products. Carbon dioxide is an abundant and nontoxic carbon source; its conversion provides sustainable routes for chemical synthesis and opportunities to balance green-house gas emissions that are linked to climate change.

In this dissertation, copper- and molybdenum carbide-based heterogeneous catalysts were evaluated for the hydrogenation of carbon dioxide and subsequent intermediates, i.e. formic acid and formate esters, to produce methanol. Catalysts identified from these sub-reactions were combined to devise several cascade systems for carbon dioxide hydrogenation. A series of mixed homo-/hetero-geneous cascade systems were first targeted via pathways at both Lewis acidic and basic conditions. Surface interactions between homogeneous and heterogeneous catalysts seemed to play an important role in

catalytic performance, ultimately leading to catalyst deactivation and ineffective cascade systems. Several heterogeneous-based cascade systems were developed to eliminate these interactions; these systems worked cooperatively to produce methanol and/or dimethyl ether. For example, a system containing an iridium- and a copper-based catalyst enhanced the methanol production by threefold (via the formic acid intermediate) compared to employing each catalyst alone. The study was further extended to evaluate several molybdenum carbide supported metal catalysts to produce alcohols and hydrocarbons. The role of temperature and metal type on reaction performances and pathways was also elucidated. In addition to developing novel heterogeneous cascade systems for carbon dioxide hydrogenation, research described in this dissertation also provides useful insights for designing similar types of catalytic systems for other challenging and multi-step chemical transformations of interest.

CHAPTER 1

INTRODUCTION

1.1 Cascade Catalysis: An Emerging Strategy for Chemical Synthesis

By 2040, the world's population is expected to reach 9 billion, requiring at least a 25% increase in the energy supply or the equivalent of ~150 quadrillion BTU, to maintain current lifestyles [1] (Figure 1.1). The development of more sustainable and efficient processes for chemical production is greatly desired to meet the increasing demand for energy and materials as a result of the rapid population growth.

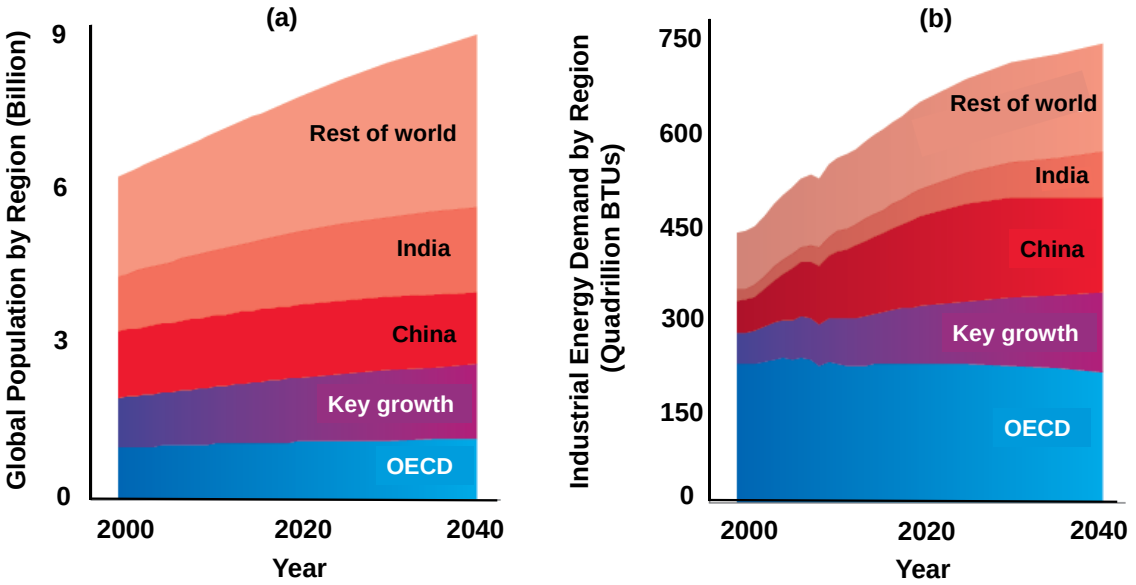

Figure 1.1 Current and projected data from year 2000-2040 for (a) global population and (b) global energy demand. Adapted from 2014 Energy Outlook [1]. Key growth includes Turkey and Mexico. OCED: Organization for Economic Cooperation and Development.

Cascade (or tandem) catalysis represents a promising technology for sustainable and economical chemical synthesis. By definition, cascade catalysis is the involvement of multiple catalytic sites to drive a series of reactions sequentially within one-synthetic operation [4]. Figure 1.2 schematically shows the working principles associated with a typical cascade system. The product generated by one catalyst is passed onto the next catalyst as an intermediate until the final product is obtained through a sequence of closely coupled catalytic reactions. Consequently, cooperation between these catalysts enables more efficient use of the starting materials, delivering the final desirable products in a more selective and atom efficient manner compared to processes using a single catalyst [2, 5, 6]. High selectivity towards final products is highly desirable in developing cost effective processes, as it reduces the down-stream separation requirements, which account for the majority of the costs in many chemical processes [7]. In some cases, this cascade approach also shifts the chemical equilibrium by converting an unstable intermediate *in situ* to a lower energy species, leading to increased product yields [4]. Furthermore, cascade catalysis offers more degrees of freedom with respect to designing the catalytic system, as catalysts for each single reaction step can be identified and tuned independently for optimal performance [5].

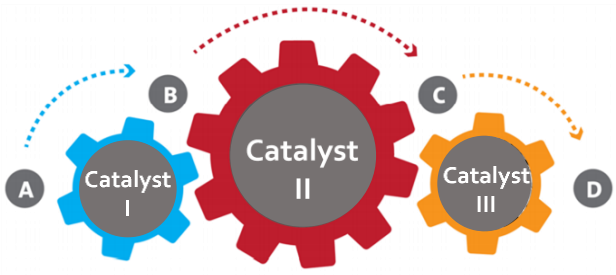

Figure 1.2 Schematic diagram for cascade catalysis. Adapted from [2].

Broader descriptions of cascade catalysis also include a single site catalyst that triggers a sequence of reactions (also known as auto-tandem or domino system [8]) or a single catalyst that possesses multiple catalytic sites working in concert to drive the reaction steps sequentially within a transformation [6]. This dissertation principally covers the examples of cascade systems based on multiple catalysts.

1.2 Cascade Catalysis Examples

Cascade catalytic systems can be categorized based on roles of the substrates, additional reagents, and active sites for each reaction. The four most common patterns are illustrated in Figure 1.3. Pattern (i) is the most straightforward case where A is converted to B by catalyst I, and B is then converted by catalyst II to produce the desired product (P). Pattern (ii) is very similar to pattern (i) except that A participates in both catalytic cycles. This type of chemistry is common for polymerization reactions. For Pattern (iii), C has to be added as an additional reagent to enable one of the catalytic cycles. As for Pattern (iv), it first involves the parallel transformation of A to B using catalyst I and C to D using catalyst II. Intermediates B and D will then participate in a reaction using catalyst III to deliver P. This pattern is extremely useful for generating complex molecules for fine chemical or pharmaceutical applications [4].

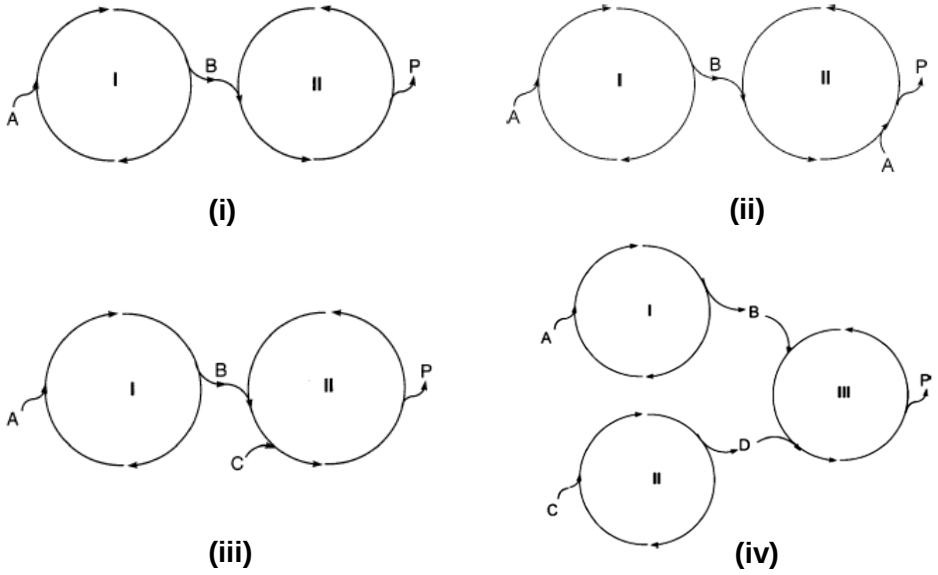

Figure 1.3 Four typical patterns of cascade catalysis. A = substrate, B or D = intermediate, C = additional reagent, P = products. Taken from [4].

Applying the concept of cascade catalysis to artificial processes opens a broad spectrum for chemical syntheses, both for homogeneous and heterogeneous-based catalytic systems. The next few paragraphs will introduce the advantages and limitations for both homogeneous and heterogeneous cascade systems. We also provide several examples in each case to demonstrate how a cascade system achieves a desired transformation that would be ineffective or unachievable via a single catalytic material. [5]

1.2.1 Homogeneous Cascade Catalysis

Nature provides a number of examples of cascade catalysis through multi-enzymatic systems to achieve products with high molecular complexity starting with easily-accessible substrates, such as plant photosynthesis [9] and polyketide biosynthesis [10]. These multi-enzymatic systems serve as models for the development of homogeneous cascade systems. The use of cascade catalysis in homogeneous processes significantly reduces the need for isolation, purification, and work-up between catalyst steps. This

advantage not only leads to cost and time benefits but also provides more environmental-friendly synthesis protocols, because the use of toxic reagents (usually required for purification) are significantly reduced. [5] A major limitation when applying homogeneous cascade catalysis in a one-pot reactor is the potential irreversible interactions between substrates and catalysts. These interactions can cause side reactions that ultimately lead to ineffective catalytic systems [11]. Nevertheless, significant progress has been made on developing homogenous cascade systems for organic synthesis, as illustrated by the following examples.

Homogeneous cascade catalysis has been demonstrated to be an effective technique for catalyzing carbonylation reactions [12]. Figure 1.4 shows the scheme for a recent study [13] on the formation of valuable α-methyl-branched aldehydes from terminal alkenes via hydroformylation, a common type of carbonylation reaction. Terminal alkenes are abundant and cheap biosubstrates; however, their direct hydroformylation normally leads to linear aldehydes. These linear aldehydes are not as valuable or useful when compared to their branched aldehyde isomers (with a carboxylic group), which is an important building block for the production of fine chemicals and pharmaceuticals [14]. In the cascade system described in Figure 1.4, the Pd-PPh_3 catalyst was first used to isomerize the terminal alkene to an internal alkene, a scarce and expensive intermediate. This step was followed by hydroformylation of the internal alkene using a Rh/L1 catalyst (with the addition of syngas), to produce α-methyl- branched aldehyde. A total TOF (for terminal alkene conversion) of 0.001 s^{-1} was attained at 25 ℃, with up to 85% selectivity achieved for the desired branched aldehyde, a significant improvement (by ~ 60%) compared to the performance using a single Rh/L1 catalyst alone [13]. This cascade system opens new

opportunities for transforming terminal alkenes, the inexpensive bioavailable substrates, to valuable and complex pharmaceutical products or building blocks, such as the branched aldehyde described in this example.

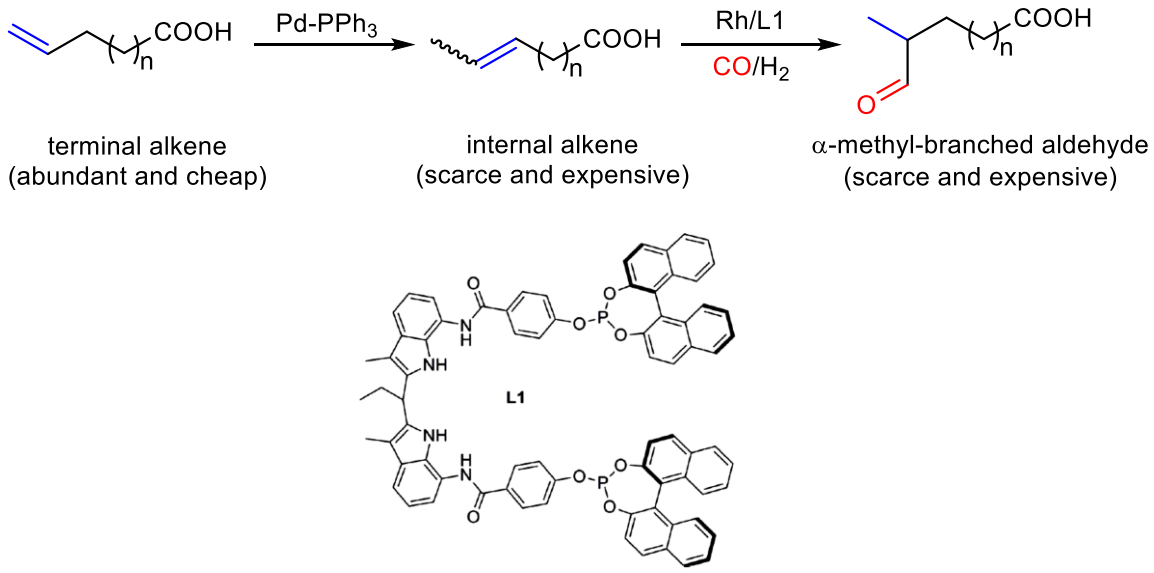

Figure 1.4 Homogeneous cascade system of terminal olefins to α-methyl-branched aldehydes. Adapted from [13].

Homogeneous cascade catalysis also plays an important role in polymer synthesis, generating polymer structures with desired features that are challenging to obtain using a single catalyst. Figure 1.5 shows the copolymerization of ethylene to produce linear low-density polyethylene (LLDPE) [15]. The traditional synthesis of LLDPE requires an alpha olefin (e.g. 1-butene) comonomer added with the ethylene. [16] In this cascade system, the alpha olefin was first generated from ethylene using an oligomerization catalyst (I in Figure 1.5) such as a $Ti(OC_4H_9\text{-}n)_4\text{-}AlR_3$(R = CH_3, C_2H_6,i -C_4H_9) catalyst reported by Pillai and coworkers [17]. A copolymerization catalyst (II in Figure 1.5), such as a Ziegler-Natta catalyst, was then used to convert the ethylene and alpha olefin to the desired LLDPE. This

cascade system fully utilized the easily-accessible ethylene substrate, removing the need for adding a comonomer.

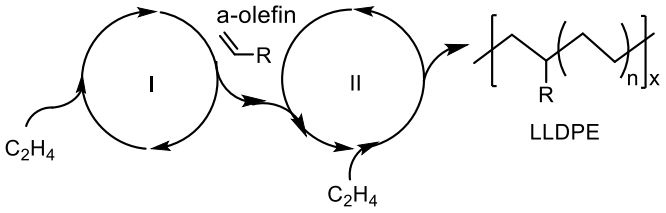

Figure 1.5 Homogeneous cascade system of ethylene copolymerization to produce linear low-density polyethylene (LLDPE). Adapted from [4].

Alkane metathesis has recently received considerable attention as a useful reaction to convert the low-value middle-chain length hydrocarbons (e.g. n-hexane) to valuable long chain hydrocarbons (>C_9) that are suitable for transportation fuels [18]. To this end, the literature examples on the direct metathesis of alkane are limited and suffer from low yields to the desired higher molecular weight hydrocarbons (> C_9), due to the difficulty of activating and rearranging C-H bond in alkanes [19, 20] Alternatively, alkane metathesis can be accomplished indirectly through a cascade pathway by first dehydrogenating the alkane to an alkene and performing the corresponding alkene metathesis, followed by the hydrogenation of the resulting alkenes to alkanes. The example shown in Figure 1.6 utilized a homogeneous cascade system that combines an Ir-pincer type complex (Cat. I and II) for the transfer dehydrogenation cycle (initial and final step in Figure 1.5) and a Schrock-type (Cat. III) catalyst for alkene metathesis (middle step in Figure 1.5). [18] This system successfully accomplished alkane metathesis by converting n-hexane to a series of hydrocarbons ranging from C_2-C_{15}. A total TOF of 0.0015 s^{-1} and a molar yield of 3.8% to the C_9+ alkanes was achieved at 125 ℃ for 24 h; control experiments with each single

catalyst alone showed inactivity for alkane metathesis. This example demonstrated the feasibility of performing alkane metathesis using homogeneous cascade catalysis. However, the overall yield to the desired C_9+ hydrocarbons still remained relatively low, due to the decomposition of Cat. III. A more robust catalyst for olefin metathesis is desired to enhance the reaction performance.

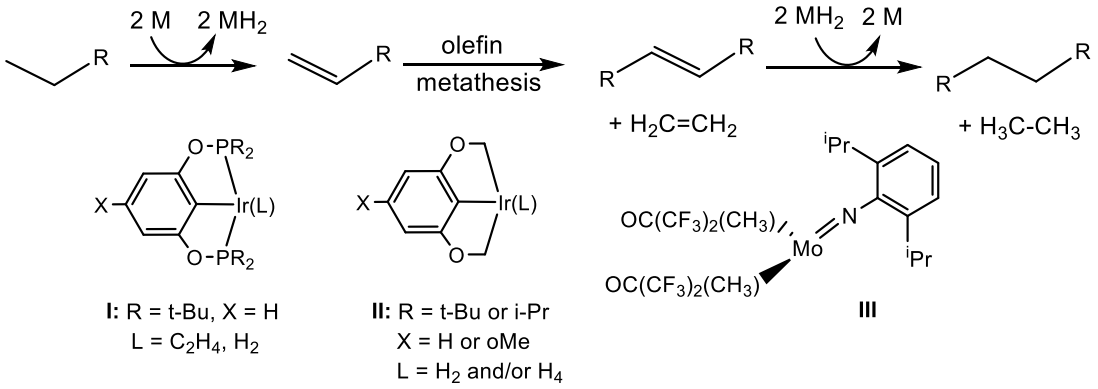

Figure 1.6 Homogeneous cascade system of linear alkane metathesis. M is the active metal center in the transfer dehydrogenation cycle. Catalysts I or II is for dehydrogeantion and catalyst III (Schrock-type) is for olefin metathesis. Adapted from [18].

1.2.2. Heterogeneous Cascade Catalysis

The classic heterogeneous catalyst design has focused on identifying a single catalyst that works most effectively for the rate-limiting step of a targeted transformation. [21] One drawback to using this strategy for a multi-step reaction is the difficulty of tailoring a single catalyst to efficiently perform all the steps within the process. Therefore, the overall reaction rate is always limited by certain step(s). The first generation of heterogeneous cascade systems are bifunctional catalysts, where multiple active sites exist on the same support to facilitate different catalytic cycles sequentially [22-24]. Only in the last two decades have heterogeneous cascade systems containing multiple catalysts been

demonstrated, where different components or interfaces of heterogeneous catalysts have been combined to advance complex multi-step transformations [5, 6, 25]. Heterogeneous systems hold promise for providing enhanced compatibility between catalysts components, better thermal stability, more cost-effective materials, and easier separation from the reaction mixtures compared to most of their homogeneous counterparts.

Figure 1.7 illustrates a bilayer cascade system that converts CH_3OH and ethylene selectively to propanal [25]. The system effectively utilized two metal/metal oxide interfaces in the CeO_2-Pt-SiO_2 nanocrystalline material, where the Pt-CeO_2 interface catalyzed the CH_3OH decomposition to provide syngas (a mixture of CO and H_2) and the syngas and ethylene were then converted at the Pt-SiO_2 interface to produce propanal. This bilayer cascade system afforded a total turnover frequency (TOF) for propanol of 2.6×10^{-2} s^{-1} at 190 ℃ and 1 bar with a reaction mixture of $CH_3OH/C_2H_4/N_2$ = 5%/1%/95%; the TOF for propanol achieved on each single interface was only on the order of 10^{-4}~$10^{-3}s^{-1}$. As this system directly used the syngas from CH_3OH decomposition, it removed the need of externally feeding syngas to the reactor system. Furthermore, the two interfaces shared the same layer of Pt to catalyze the two sub-steps in this process, which optimized the use of precious metal. In addition, the interfaces in this nanocrystalline material could be modified independently for desired chemical transformations.

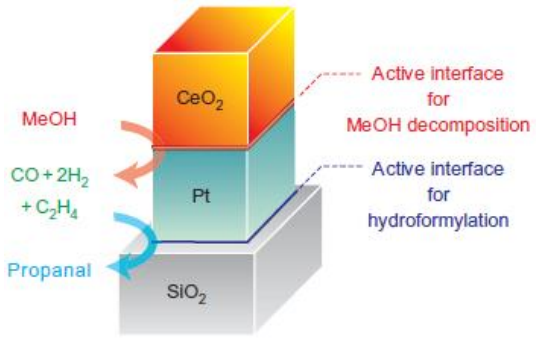

Figure 1.7 Heterogeneous bilayer cascade system of ethylene hydroformylation with methanol. Adpated from [25].

The use of a heterogeneous cascade system is also advantageous for acid-base-catalyzed processes, where the acid/base sites can be added onto the same solid supports or be introduced as a mixture of two solid catalysts. This combination is typically not feasible in homogeneous processes due to the fast neutralization between the acid and base species.[6] The example in Figure 1.8 shows a heterogeneous acid-base cascade system for the integrated production of biodiesel and solketal [26], a compound with various applications as a fuel additive, surfactant and flavoring agent. [27, 28] The first step in the cascade system involved a basic catalyst for the transesterification of triglyceride and CH_3OH to glycerol and fatty acid methyl ester (FAME), i.e. the biodiesel. The second step used glycerol and acetone as the starting materials over an acid catalyst to generate solketal. The catalytic system contained a physical mixture of 1,5,7-triazabicyclo[4.4.0]-dec-5-ene bound to polystyrene (TBD-PS) as the basic catalyst and Nafion NR-50 as the acid catalyst. In addition to the catalyst mixture, a zeolite membrane was also introduced to the cascade system to eliminate H_2O from the reaction media. The removal of H_2O shifted the chemical

equilibrium of second step in this cascade transformation which led to significantly improved product yields.

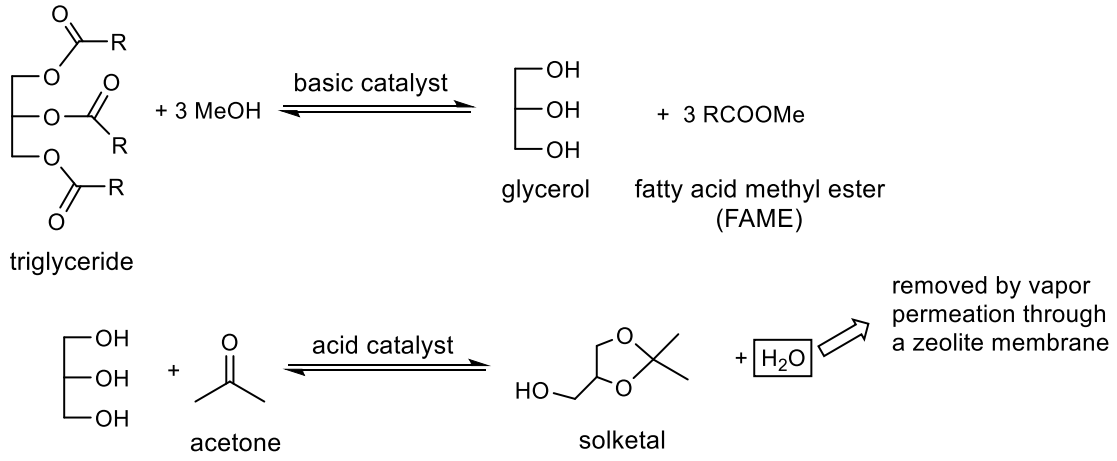

Figure 1.8 Heterogeneous acid-base cascade system for integrated production of biodiesel and solketal. Adapted from [26].

Recently, heterogeneous catalysis has also been demonstrated to be effective to sequentially drive a series of typical reactions involved in biomass conversion, such as dehydration, condensation, isomerization, and hydrogenation [29-31]. Figure 1.9 illustrates a cascade system for converting D-glucose to 5-hydroxymethyl furfural (HMF) [29], an important precursor for synthesizing value-added polymers, such as polyurethanes and polyamides, as well as for biofuels [32, 33]. Glucose is the most abundant monosaccharide and the cheapest hexose, making it a promising feedstock for producing HMF. [34] In this cascade transformation, two types of acid sites on beta-zeolite were utilized, where the Lewis acid site catalyzed the isomerization from D-glucose to D-fructose and the Bronsted acid site dehydrated D-fructose to produce HMF. The amount of each acid site can be tuned by modifying the synthesis protocols, such as the calcination temperatures and time [35, 36]. Materials with different densities of acid sites led to different HMF selectivities. This

simple one-pot synthesis of HMF using a heterogeneous multifunctional zeolite also effectively eliminated the need for using enzymes or environmentally-unfriendly catalysts and solvents as reported previously for the same transformation. [37-39]

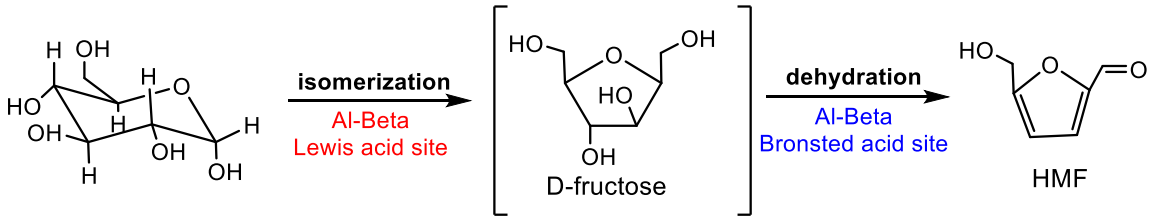

Figure 1.9 Cascade system for the synthesis of 5-hydroxymethyl furfural (HMF) from D-glucose using bifunctional beta zeolite catalyst. Adapted from [6].

1.2.3 Considerations and Challenges for Cascade Catalysis

When combining multiple catalysts for a cascade transformation, a number of factors must be considered. The primary factor that enables the cascade system is compatibility, where all the catalyst materials, reactants, products, and solvents have to work together without any undesirable interaction/deactivation phenomena under the operating conditions. In addition, the activity for each active site should be matched such that the overall process is not starved or overwhelmed by a specific step; this also ensures the efficient use of the substrate and intermediate for the overall cascade transformation. Finally, a common set of operating conditions has to work for all the specific sub-steps within the overall transformation. Defining the operating conditions creates a significant challenge, as the favored thermodynamic conditions for each catalytic cycle can be significantly different. The level of difficulty will also gradually increase with the number of catalytic cycles in the overall process.

The concept of "cascade catalysis", where all the operations are performed in a one-pot reactor, should be distinguished from the idea of "cascading reactors" [40], where each reaction is conducted independently in a series of reactors (Figure 1.10). The major difference is whether the intermediate generated from the previous step is immediately consumed in the same reactor or is delivered to the next reactor. The difference in intermediate lifetime can result in different reactivities. Cascade catalysis is capable of consuming the unstable intermediates *in-situly*, which potentially enhances the overall conversion by shifting the chemical equilibrium for the intermediate formation. It also allows easy setup and maintenance and is viable for both batch and flow operations. The cascading reactor systems in series are typically applied in flow systems [41] and are more effective for separating incompatible catalysts/active sites. A cascading reactor system should be considered when material compatibility becomes the major concern or the sub-reaction cannot be operated at similar conditions for a targeted cascade transformation.

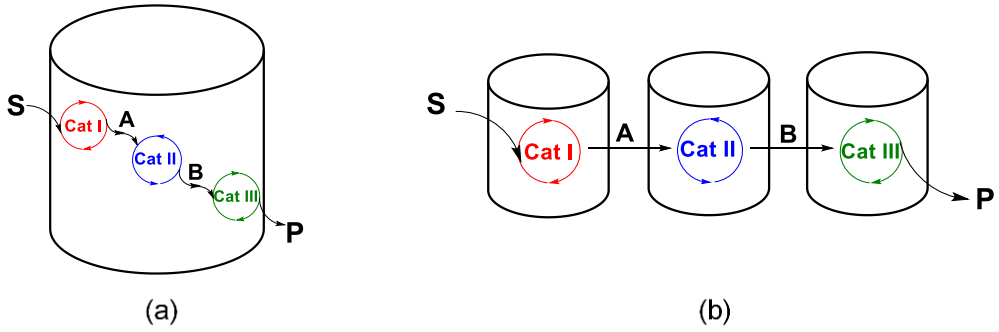

Figure 1.10 Schematic diagrams of (a) one-pot reactor using cascade catalysis and (b) cascading reactors operated in series.

1.3 CO_2 Hydrogenation: Motivation and State-of-the-Art

Natural gas and petroleum are the principal resources used to produce most chemicals. In addition, the production of chemicals is among the most energy-intensive segments of the industrial sector, accounting for the consumption of ~5 quadrillion BTU per year [42] in the United States, most of which comes from fossil fuels. The energy demand for chemicals production is projected to increase by 35% in 2040 [1] as shown in Figure 1.11. Growing concerns about climate change and diminishing fossil resources are driving the development of renewable and non-fossil-based feedstocks for the production of chemicals.

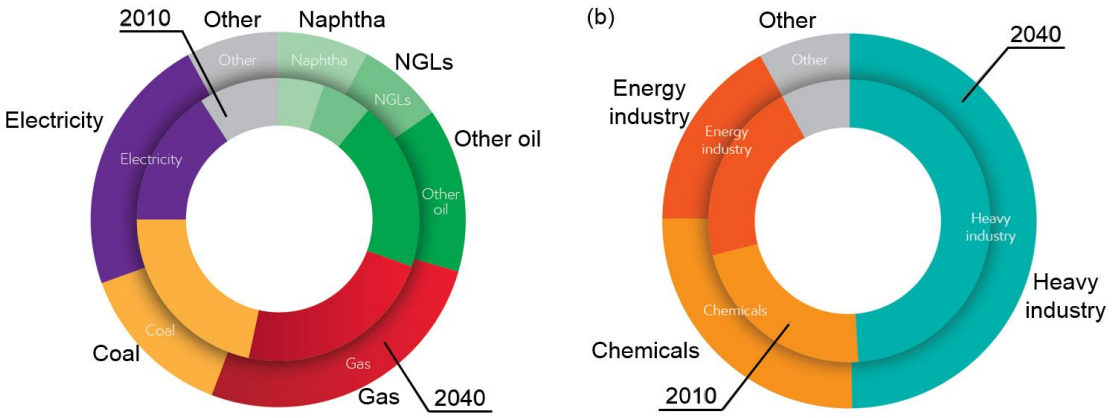

Figure 1.11 Relative industrial energy demand in 2010 and projection in 2040 (a) by fuel and (b) by sector. Adapted from [1].

Carbon dioxide has attracted considerable attention as a C_1 building block for the production of fuels and chemicals [43-47]. With the advances in capture technologies, CO_2 could become available at low cost and its conversion to value-added chemicals could be

cost-competitive [44]. Furthermore, large-scale CO_2 conversion provides opportunities to balance green-house gas emissions that are linked to climate change. [3, 48]

Presently the conversion of CO_2 is limited to a few products including urea (146 Mton/year [49]), CH_3OH via the reverse water-gas shift (RWGS) then CO hydrogenation (5 Mton/year [50]), and salicylic acid (170 kTon/year [47]). The most promising strategy for the large-scale conversion of CO_2 is through hydrogenation processes, producing alcohols and hydrocarbons. [44, 51] However, CO_2 hydrogenation is quite challenging due to its stability, the lack of sufficiently active and selective catalytic materials, and the lack of cost-effective, non-fossil fuel sources of hydrogen (e.g. via H_2O splitting) [45]. Additional work is still needed for the commercial scale implementation of CO_2 hydrogenation processes. Centi et al. projected a timeline for the commercial use of CO_2 for sustainable chemical production as shown in Figure 1.12. They proposed that an artificial leaf system coupling the photochemical H_2O splitting and CO_2 hydrogenation could be commercially employed to produce several important chemicals/intermediates such as CH_3OH, dimethyl ether, and olefins. [3]

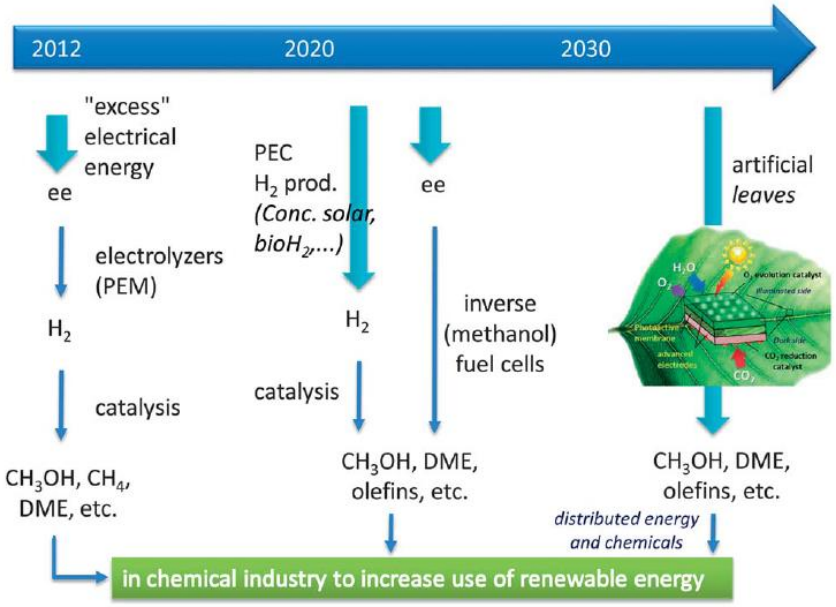

Figure 1.12 Projected timeline for the use of CO_2 and renewable energy to increase resource and energy efficiency in the chemical production chain. Adapted from [3].

As CO_2 is thermodynamically stable, its conversion to a number of valuable chemicals are energy demanding (Figure 1.13). Furthermore, most of the CO_2 conversion reactions involve multi-electron transfer, and the use of a single catalyst may not be sufficient to drive the reaction [52]. To this end, most of examples of CO_2 hydrogenation catalysis in the literature focus on developing a single catalyst with the addition of various promoters to achieve the desired products [43, 53, 54]. To carry out a multi-step reaction over a single catalyst, a rate-determining step always exists, limiting the overall reaction rate. As an alternative to a single catalytic system, cascade systems have been devised to perform CO_2 hydrogenation to achieve higher atom efficiency/selectivity to desired products. Meanwhile, these systems provide higher degrees of freedom to tune the catalytic performance by independently modifying the catalysts for each individual sub-step.

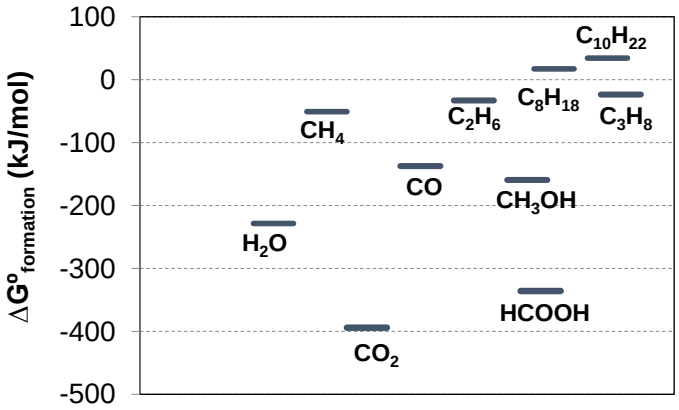

Figure 1.13 Standard Gibbs free energy of formation for CO_2 and a series of carbon-containing chemicals. [55]

1.4 Cascade Catalysis for CO_2 Hydrogenation

The first cascade catalytic system for CO_2 hydrogenation was demonstrated by Huff and Sanford [56]. They used three homogeneous catalysts consisting of $(PMe_3)_4$Ru-(Cl)(OAc), $Sc(OTf)_3$, and (PNN)Ru(CO)(H) to hydrogenate CO_2 to CH_3OH through formic acid and alkyl formate intermediates (Figure 1.14). While each catalyst individually achieved at least 100 turnovers (TON) for its targeted sub-step [57, 58], the measured TON for CH_3OH production was only 2.5 at 135 ℃, 10 bar CO_2, 30 bar H_2, and 16h when combining the three catalysts in one-pot. This underperformance was caused by the incompatibility of (PNN)Ru(CO)(H) with $Sc(OTf)_3$ as well as with CO_2 reactant. Physical separation of $Sc(OTf)_3$ from (PNN)Ru(CO)(H) by performing the reactions in two separate vessels significantly improved the CH_3OH TON to 21. While the mechanisms that contributed to the observed incompatibility were identified [59, 60], suitable catalysts still need to be sought for ester hydrogenation that can be employed in this cascade system.

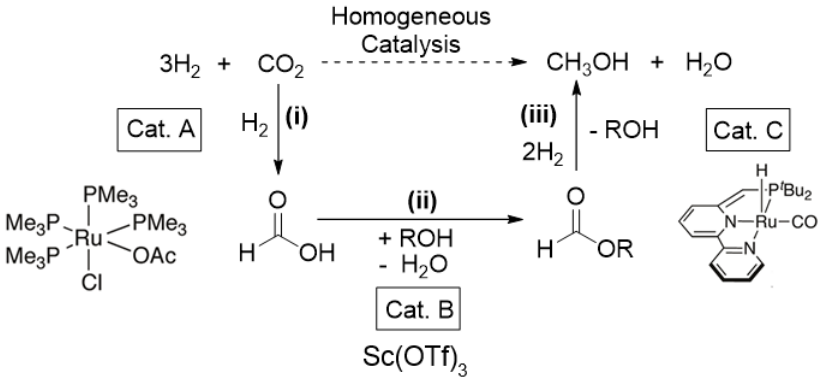

Figure 1.14 Homogeneous cascade system for CO_2 hydrogenation to CH_3OH through formic acid and alkyl formate intermediates using $(PMe_3)_4Ru(Cl)(OAc)$, $Sc(OTf)_3$, and (PNN)Ru(CO)(H) catalysts. Adapted from [56].

A recent study by Wesselbaum [61] et al. also reported a homogeneous cascade system using the same pathway, via formic acid and alkyl formate intermediates, involving a (Triphos)Ru-phosphine and a $HNTf_2$.acid catalyst. As shown in Figure 1.15, the (Triphos)Ru-phosphine catalyst catalyzed both the conversion of CO_2 to formic acid (step i) and ester hydrogenation (step iii); $HNTf_2$ (triflimide) acted as the catalyst for esterification (step ii). The highest TON of 221 was achieved for CH_3OH at 20 bar CO_2, 60 bar H_2, and 140 ℃ at 24 h. This example was by far the first demonstration of a single homogeneous catalyst that can catalyze both step (i) and (iii) for this transformation, which eliminated the issue of catalyst incompatibility.

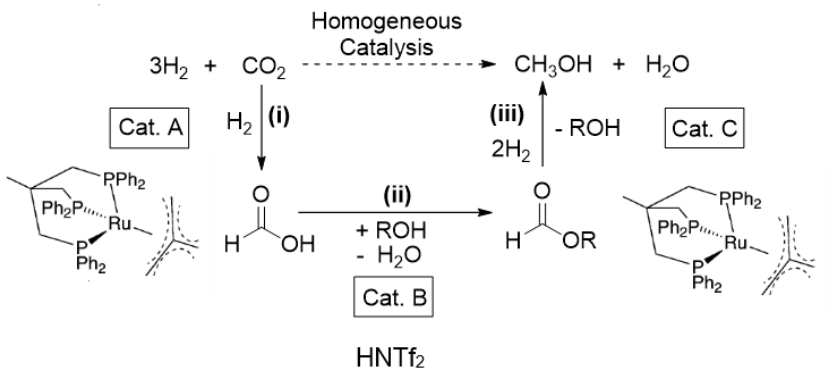

Figure 1.15 Homogeneous cascade system for CO_2 hydrogenation to CH_3OH through formic acid and alkyl formate intermediates using (Triphos)Ru-phosphine and $HNTf_2$ catalysts. Adapted from [61].

Fan et al. reported the use of Cu/ZnO and Cu/Cr_2O_3 catalysts for the liquid phase CO_2 hydrogenation to CH_3OH in ethanol, through formic acid and ethyl formate intermediates [62]. Table 1.1 shows the conversions and selectivities for CO_2 hydrogenation over three studied catalysts from this work. The presence of both ethyl formate and CH_3OH in the products suggested that the reactions proceeded through the formic acid/ethyl formate intermediates. The production of CO indicated that these Cu-based catalysts also catalyzed RWGS reaction. The best performance was achieved over a Cu/ZnO (Cu-Zn) catalyst, with a 7.5% CO_2 conversion and a 73% selectivity to CH_3OH. They also reported that the CH_3OH production was significantly enhanced when introducing ethyl formate into the reaction, indicating that the overall rate was limited by the formation of ethyl formate in the system. This finding suggested that alone the Cu-based catalysts did not provide equally matched active sites for each sub-step of the system. The combination of multiple heterogeneous catalysts for each sub-step could provide opportunities to match active sites and optimize the overall catalytic performance of the system.

Table 1.1 Conversion and selectivity for liquid phase CO_2 hydrogenation.[a]

Catalyst	CO_2 Conversion (%)	Selectivity (%)			
		Ethyl formate	CH_3OH	CO	CH_4
Cu-Cr-O	5.2	17	60	21	1.2
Pd-Cu-Cr-O	4.1	29	51	17	0
Cu-Zn-O	7.5	6.2	73	20	0

[a]Reactions were performed at 200 ℃, 7.5 bar CO_2, 22.5 bar H_2 using 200 mg catalyst in 10 mL ethanol. Taken from [57].

1.5 Research Goal and Thesis Layout

The overall goal for the research described in this dissertation was to explore the feasibility of using heterogeneous catalysts to create cascade catalytic systems for CO_2 hydrogenation. The following objectives were established to achieve this goal:

1) Identify heterogeneous catalysts to substitute for the incompatible catalyst described earlier for the homogeneous cascade system for CO_2 hydrogenation to CH_3OH through formic acid and ester intermediates. In particular, the catalysts for the ester hydrogenation step.
2) Design and evaluate cascade systems coupling homogeneous and heterogeneous catalysts for CO_2 hydrogenation to CH_3OH.
3) Design and evaluate all-heterogeneous-based cascade systems for CO_2 hydrogenation to CH_3OH, dimethyl ether, and hydrocarbons.
4) Investigate key reaction parameters and their effects on reaction activities, selectivities, and pathways for liquid phase low temperature CO_2 hydrogenation.

With the research goals and objectives identified, this dissertation is divided into seven chapters. A brief description of each remaining chapter is provided in the following.

Chapter 2: Identifying Heterogeneous Catalysts for Ester Hydrogenation

This chapter discusses the physical and catalytic properties of a series of heterogeneous catalysts for the ester hydrogenation reaction using ethyl formate as the model reactant. Reaction rates, selectivities, and possible mechanisms are described for catalysts that were evaluated. The selectivity of this reaction is closely linked to the acidity/basicity of the catalytic support. Extended studies are performed using Cu and/or Pd promoted Mo_2C catalysts to identify the effect of metal deposition and temperature on reaction performance.

Chapter 3: Coupling Homogeneous and Heterogeneous Catalysts for Cascading CO_2 Hydrogenation to CH_3OH

This chapter explores the possibility of combining several homogeneous and heterogeneous catalysts to promote low temperature ($\leq$ 135 °C) CO_2 hydrogenation to CH_3OH. The study targets a series of cascade systems involving various intermediates, including 1) formic acid/ester, 2) amide, and 3) sodium formate intermediates to drive the hydrogenation of CO_2 to CH_3OH. Interactions between the homogeneous and heterogeneous catalysts play an important role with regard to the performance of these cascade systems.

Chapter 4: Designing All-Heterogeneous Cascade Systems for CO_2 Hydrogenation

This chapter discusses the feasibility of creating all-heterogeneous-based cascade systems for CO_2 hydrogenation to CH_3OH and dimethyl ether. The study first targets

reaction pathways through formic acid or formate ester intermediates using Cu-, Ir- or Mo_2C- based heterogeneous catalysts. The production of dimethyl ether from CO_2 is also demonstrated by combining a Cu-based methanol synthesis catalyst and a zeolite catalysts.

Chapter 5: Liquid Phase CO_2 Hydrogenation over Metal/Mo_2C Catalysts

This chapter discusses the use of a series of Mo_2C-supported metal catalysts for CO_2 hydrogenation. The study investigates the influence of reaction temperature and the type of metal deposited onto Mo_2C on the reaction rates, selectivities, and reaction pathways. The catalyst stability in liquid reaction environment is also assessed by comparing the catalytic and surface/bulk properties of the pre- and post-reaction catalysts. A series of techniques are utilized including N_2 physisorption, X-ray diffraction (XRD), temperature programmed reaction (TPR), and scanning electron microscopy (SEM), to characterize the catalysts.

Chapter 6: Chemoselective Hydrogenation of Crotonaldehyde in a Solid-Polymer-Electrolyte Reactor

This chapter focuses on the chemoselective hydrogenation of crotonaldehyde in a solid-polymer electrolyte (SPE) reactor. This study first investigates the influence of the applied potential (0-1.0V) on the reaction rates, selectivities, and current efficiencies. The reaction pathways are also explored by probing the system with possible reaction intermediates, such as crotyl alcohol and butyraldehyde. The overall reactivity data are fitted to a series of rate equations to determine the reaction order and rate constant for each elementary step.

Chapter 7: Conclusions and Future Work

The final chapter revisits the key findings and accomplishments from this research. Based on these results, future directions for extending and improving the current work of cascade systems for CO_2 hydrogenation are provided.

1.6 References

[1] The Outlook for Energy: A View to 2040, ExxonMobil 2014.
[2] W. Kroutil, M. Rueping, ACS Catal. 4 (2014) 2086-2087.
[3] G. Centi, G. Iaquaniello, S. Perathoner, ChemSusChem 4 (2011) 1265-1273.
[4] J.-C. Wasilke, S.J. Obrey, R.T. Baker, G.C. Bazan, Chem. Rev. 105 (2005) 1001-1020.
[5] F.-X. Felpin, E. Fouquet, ChemSusChem 1 (2008) 718-724.
[6] M.J. Climent, A. Corma, S. Iborra, M.J. Sabater, ACS Catal. 4 (2014) 870-891.
[7] R.M. Smith, Chemical process: design and integration, John Wiley & Sons, 2005.
[8] N. Shindoh, Y. Takemoto, K. Takasu, Chemistry – A European Journal 15 (2009) 12168-12179.
[9] J. Barber, Chem. Soc. Rev. 38 (2009) 185-196.
[10] C. Khosla, Chem. Rev. 97 (1997) 2577-2590.
[11] J.M. Lee, Y. Na, H. Han, S. Chang, Chem. Soc. Rev. 33 (2004) 302-312.
[12] P. Eilbracht, L. Bärfacker, C. Buss, C. Hollmann, B.E. Kitsos-Rzychon, C.L. Kranemann, T. Rische, R. Roggenbuck, A. Schmidt, Chem. Rev. 99 (1999) 3329-3366.
[13] P. Dydio, M. Ploeger, J.N.H. Reek, ACS Catal. 3 (2013) 2939-2942.
[14] F. Agbossou, J.-F. Carpentier, A. Mortreux, Chem. Rev. 95 (1995) 2485-2506.
[15] N. Platzer, Industrial & Engineering Chemistry Product Research and Development 22 (1983) 158-160.
[16] D.L. Beach, Y.V. Kissin, Journal of Polymer Science: Polymer Chemistry Edition 22 (1984) 3027-3042.
[17] S.M. Pillai, G.L. Tembe, M. Ravindranathan, S. Sivaram, Ind. Eng. Chem. Res. 27 (1988) 1971-1977.
[18] A.S. Goldman, A.H. Roy, Z. Huang, R. Ahuja, W. Schinski, M. Brookhart, Science 312 (2006) 257-261.
[19] E. Le Roux, M. Taoufik, C. Copéret, A. de Mallmann, J. Thivolle-Cazat, J.M. Basset, B.M. Maunders, G.J. Sunley, Angew. Chem., Int. Ed. 44 (2005) 6755-6758.
[20] J.M. Basset, C. Copéret, L. Lefort, B.M. Maunders, O. Maury, E. Le Roux, G. Saggio, S. Soignier, D. Soulivong, G.J. Sunley, M. Taoufik, J. Thivolle-Cazat, J. Am. Chem. Soc. 127 (2005) 8604-8605.
[21] A. Baiker, J. Mol. Catal. A: Chem. 163 (2000) 205-220.
[22] H. Gröger, Chemistry-A European Journal 7 (2001) 5246-5251.
[23] Y. Kusunoki, T. Miyazawa, K. Kunimori, K. Tomishige, Catalysis Communications 6 (2005) 645-649.
[24] K. Sun, W. Lu, F. Qiu, S. Liu, X. Xu, Appl. Catal., A 252 (2003) 243-249.
[25] Y. Yamada, C.-K. Tsung, W. Huang, Z. Huo, S.E. Habas, T. Soejima, C.E. Aliaga, G.A. Somorjai, P. Yang, Nat. Chem. 3 (2011) 372-376.

[26] J.M. Fraile, R. Mallada, J.A. Mayoral, M. Menéndez, L. Roldán, Chemistry – A European Journal 16 (2010) 3296-3299.
[27] A. Sokołowski, A. Piasecki, B. Burczyk, J Am Oil Chem Soc 69 (1992) 633-638.
[28] M.J. Climent, A. Corma, A. Velty, Appl. Catal., A 263 (2004) 155-161.
[29] R. Otomo, T. Yokoi, J.N. Kondo, T. Tatsumi, Appl. Catal., A 470 (2014) 318-326.
[30] L. Bui, H. Luo, W.R. Gunther, Y. Román-Leshkov, Angew. Chem. 125 (2013) 8180-8183.
[31] H. Huang, C.A. Denard, R. Alamillo, A.J. Crisci, Y. Miao, J.A. Dumesic, S.L. Scott, H. Zhao, ACS Catal. 4 (2014) 2165-2168.
[32] Y. Román-Leshkov, C.J. Barrett, Z.Y. Liu, J.A. Dumesic, Nature 447 (2007) 982-985.
[33] Y. Román-Leshkov, J.N. Chheda, J.A. Dumesic, Science 312 (2006) 1933-1937.
[34] A.I. Torres, P. Daoutidis, M. Tsapatsis, Energy Environ. Sci. 3 (2010) 1560-1572.
[35] J.H. Lunsford, W.P. Rothwell, W. Shen, J. Am. Chem. Soc. 107 (1985) 1540-1547.
[36] J.W. Ward, J. Catal. 11 (1968) 251-258.
[37] R. Huang, W. Qi, R. Su, Z. He, Chem. Commun. 46 (2010) 1115-1117.
[38] H. Zhao, J.E. Holladay, H. Brown, Z.C. Zhang, Science 316 (2007) 1597-1600.
[39] M. Chidambaram, A.T. Bell, Green Chemistry 12 (2010) 1253-1262.
[40] Y. Muslu, Journal of Chemical Technology & Biotechnology 75 (2000) 1151-1159.
[41] C. Tocchi, E. Federici, S. Scargetta, A. D'Annibale, M. Petruccioli, Process Biochemistry 48 (2013) 941-944.
[42] J.J. Conti, P.D. Holtberg, J.R. Diefenderfer, S.A. Napolitano, A.M. Schaal, J.T. Turnure, L.D. Westfall, World energy outlook 2015, Energy Information Administration.
[43] W. Wang, S. Wang, X. Ma, J. Gong, Chem. Soc. Rev. 40 (2011) 3703-3727.
[44] E.A. Quadrelli, G. Centi, J. Duplan, S. Perathoner, ChemSusChem 4 (2011) 1194-1215.
[45] G. Centi, E.A. Quadrelli, S. Perathoner, Energy Environ. Sci. 6 (2013) 1711-1731.
[46] G.A. Olah, G.K.S. Prakash, A. Goeppert, J. Am. Chem. Soc. 133 (2011) 12881-12898.
[47] M. Aresta, Carbon dioxide as chemical feedstock, John Wiley & Sons, 2010.
[48] D. Aaron, C. Tsouris, Separation Science and Technology 40 (2005) 321-348.
[49] H. Patrick, Michel Prud'homme, Fertilizer Outlook 2014-2018, International Fertilizer Industry Association.
[50] M. Aresta, A. Dibenedetto, Dalton Transactions (2007) 2975-2992.
[51] G.A. Olah, A. Goeppert, G.K.S. Prakash, J. Org. Chem. 74 (2008) 487-498.
[52] B. Kumar, M. Llorente, J. Froehlich, T. Dang, A. Sathrum, C.P. Kubiak, Annu. Rev. Phys. Chem. 63 (2012) 541-569.
[53] S. Natesakhawat, J.W. Lekse, J.P. Baltrus, P.R. Ohodnicki, B.H. Howard, X. Deng, C. Matranga, ACS Catal. 2 (2012) 1667-1676.
[54] F. Arena, K. Barbera, G. Italiano, G. Bonura, L. Spadaro, F. Frusteri, J. Catal. 249 (2007) 185-194.
[55] Thermodynamic data acquired from NIST Chemistry WebBook.
[56] C.A. Huff, M.S. Sanford, J. Am. Chem. Soc. 133 (2011) 18122-18125.
[57] P.G. Jessop, T. Ikariya, R. Noyori, Chem. Rev. 95 (1995) 259-272.
[58] E. Balaraman, C. Gunanathan, J. Zhang, L.J. Shimon, D. Milstein, Nat. Chem. 3 (2011) 609-614.
[59] C.A. Huff, J.W. Kampf, M.S. Sanford, Organometallics 31 (2012) 4643-4645.
[60] C.A. Huff, J.W. Kampf, M.S. Sanford, Chem. Commun. 49 (2013) 7147-7149.

[61] S. Wesselbaum, T. vom Stein, J. Klankermayer, W. Leitner, Angew. Chem., Int. Ed. 124 (2012) 7617-7620.
[62] L. Fan, Y. Sakaiya, K. Fujimoto, Appl. Catal., A 180 (1999) L11-L13.

CHAPTER 2

HETEROGENEOUS CATALYSTS FOR ESTER HYDROGENATION

2.1 Introduction

The hydrogenolysis of esters is a key step in the production of fatty alcohols (from natural fatty esters) and other lower alkyl alcohols, such as CH_3OH and ethanol [1-4]. Copper-based catalysts are commonly used because they possess high selectivities for activation of the C-O bonds rather than the C-C bonds [4]. For example, Cu chromite catalysts are well-established for the commercial production of fatty alcohols, although increasing environmental concerns with regard to Cr have resulted in the search for new formulations [5]. Other catalysts containing less toxic materials, such as Cu/SiO_2 [6] and Cu/ZnO [7], have been reported to possess ester hydrogenolysis activities and selectivities that are similar to those for Cu chromite catalysts. Nevertheless, new catalyst formulations are being sought to enhance the performance and sustainability of this process.

Of particular interest here is the low temperature (< 200 ℃), liquid phase hydrogenolysis of esters, a key intermediate step during the low temperature hydrogenation of CO or CO_2 to CH_3OH [8-10]. Christiansen [11] first described a two-step process for converting syngas (CO and H_2) into CH_3OH at 180 ℃ via i) carbonylation of an alcohol to

This chapter has been published in *Catal. Today*, **2016**, *259*, pp 285–291.
DOI:10.1016/j.cattod.2015.08.021

the corresponding ester over a sodium methoxide catalyst and ii) hydrogenolysis (i.e. hydrogenation) of the ester to CH_3OH and the parent alcohol over a reduced Cu oxide catalyst (see Figure 2.1a). Liu et al. explored the use of potassium methoxide and Cu chromite catalysts for syn gas conversion to CH_3OH via methyl formate intermediate at 140-180 ℃ [12]. They suggested the formate hydrogenolysis was rate-limiting due in part to deactivation of the Cu chromite catalyst by CO. Fan et al. [10] reported the liquid phase hydrogenation of CO_2 to CH_3OH over Cu-Zn or Cu-Cr based catalysts at 200 ℃ and proposed that the reaction occurred via a multi-step pathway. The proposed reaction pathway involved i) hydrogenation of CO_2 to formic acid, ii) esterification of formic acid to alkyl formate, and iii) hydrogenolysis of the formate to CH_3OH and the corresponding alcohol (Figure 2.1b). They also suggested that formate hydrogenolysis was the rate-limiting step in the overall reaction system, encouraging the development of more active catalysts for this step. In Chapter 1, we described a homogeneous cascade system developed by Sanford et al. [13]; this system include $(PMe_3)_4Ru(Cl)(OAc)$, $Sc(OTf)_3$, and (PNN)Ru(CO)(H) catalysts, for the hydrogenation of CO_2 through formic acid and formate ester intermediates. A key limitation for this homogeneous cascade system was incompatibility of the ester hydrogenolysis catalyst with other components and reactant species [13, 14]. Using heterogeneous catalysts for ester hydrogenation may provide a solution to improve the material compatibility due to their presence in a difference phase.

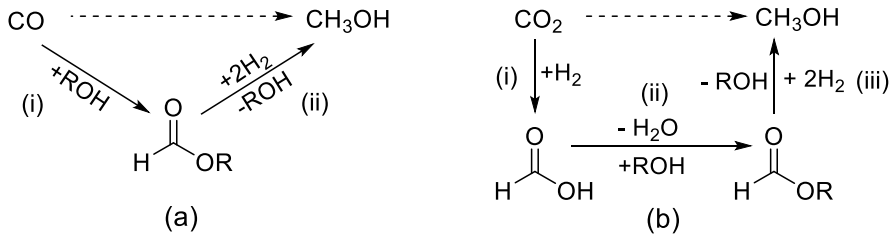

Figure 2.1 Reaction pathways to achieve one-pot CH_3OH synthesis in the presence of alcohol through alkyl formate intermediate, (a) from CO hydrogenation [11], and (b) from CO_2 hydrogenation. Adapted from [10].

A variety of Cu-based catalysts, including Raney Cu [15], Cu/SiO_2 [16], Cu chromite [9, 17, 18], and Cu/ZnO [19], have been reported to be active for the liquid phase hydrogenolysis of alkyl formates at temperatures in the range of 110-200 ℃. Copper chromite catalysts are among the most active; however, their poor tolerance to CO reduces the feasibility of using this type of catalyst in processes where CO or CO_2 is present [15, 20]. A variety of oxide supported Pt and Pd catalysts (including ZnO, Ga_2O_3, In_2O_3, and SiO_2) have also been reported to be active for gas phase methyl formate hydrogenolysis at 150 ℃. The ZnO and In_2O_3 supported catalysts provided the highest selectivities to CH_3OH possibly due to the formation of alloys (e.g. Pt-Zn and Pd-In), although a substantial Pd or Pt loading (10wt%) was required to achieve the best performance [21]. Braca et al. [22] reported that several Re-based heterogeneous catalysts were highly active and selective for the hydrogenolysis of formate at 200 ℃, albeit at high H_2 pressures (~100 bar). The acidity/basicity of the support (SiO_2, TiO_2, Nb_2O_5, and MgO) appeared to have a significant effect on catalytic performance. Homogeneous Re_2O_7 and $Re(CO)_{10}$ catalysts also exhibited high activities initially but suffered from a rapid deactivation due to CO poisoning. Rhenium, however, is relatively expensive, which makes it less attractive for large-scale applications.

In this chapter, results for the low temperature, liquid phase hydrogenolysis of ethyl formate over molybdenum carbide and nitride supported Cu catalysts are described. Molybdenum carbides and nitrides possess catalytic properties that are similar to those for platinum-group-metals [23-26], and catalyze a variety of reactions including Fischer-Tropsch Synthesis (FTS) [27, 28], CO_2 hydrogenation [29, 30], water-gas shift (WGS) [31], alcohol steam reforming [32, 33], and hydrodenitrogenation [34]. Like other early transition metal carbides and nitrides [23, 24], these materials can be synthesized with surface areas exceeding 100 m^2/g [35-37]. The carbides in particular have also been reported to be effective supports, facilitating the production of highly dispersed Pt, Pd, Co and Cu domains, and in some cases, modifying the electronic properties of these metals. [32, 38] This modification can result in superior catalytic performance for carbide supported metals. For example, Schweitzer et al. reported a Pt/Mo_2C catalyst that significantly outperformed oxide supported Pt catalysts for WGS [39]. Lausche et al. described a Pd/W_2C catalyst which demonstrated higher rates and selectivities than those for bulk Pd catalysts during the selective, electrocatalytic hydrogenation of triglycerides [40]. Furthermore, Mo carbides and nitrides, known CO [27, 28] and CO_2 hydrogenation catalysts [30, 41], are naturally tolerant to CO and CO_2. In addition to the supported Cu catalysts, we also synthesized and evaluated a series of Pd/Mo_2C and $Cu\text{-}Pd/Mo_2C$ catalysts, as oxide supported Pd catalysts have been reported to be active and selective for ester hydrogenolysis [21]. Catalytic performance for the Mo carbide and nitride supported catalysts were compared to those for conventional oxide supported Cu catalysts including Al_2O_3, SiO_2, ZnO, and ZrO_2.

2.2 Experimental

2.2.1 Catalyst Preparation and Characterization

The Mo_2C and Mo_2N materials were synthesized from an ammonium molybdate (AM) precursor (Alfa Aesar) using a temperature programmed reaction (TPR) technique. The Mo_2C was prepared by reducing AM in H_2 at 350 °C for 12 h, followed by treatment in 15% CH_4/H_2 at 590 °C for 2h, and the resulting material was then quenched to room temperature. The Mo_2N was synthesized by reacting AM with anhydrous NH_3 as the temperature was linearly heated from room temperature to 350 °C (33 min), then to 450 °C (2.5 h) and finally to 700 °C (2.5 h) followed by a soak at this temperature for 1 h before quenching to room temperature. Other details regarding the synthesis procedures have been described in previous reports [34, 38]. Metals were deposited onto the Mo_2C or Mo_2N supports using a wet impregnation technique. Typically, carbides and nitrides are passivated prior to exposure to air to avoid bulk oxidation of the material [37]. To avoid passivation and deposit metals directly onto the native Mo_2C or Mo_2N surfaces (as opposed to a passivated surface), the freshly-synthesized materials were transferred under an inert gas (CH_4/H_2 or He) into an aqueous solution containing a target concentration of $Cu(NO_3)_2$ or $Pd(NO_3)_2{\cdot}4NH_3$ and then allowed to interact for at least 20 h. Argon was continuously purging through the solutions (during the wet impregnation process) to deaerate and agitate the solution. The synthesized metal/Mo_2C catalysts showed pyrophoric property, indicating the absence of surface passivation on the final materials. Such observation also suggests that neither H_2O nor NO_3^- during the wet impregnation process has passivated/oxidized the catalyst surface. Schweitzer et al. reported that passivation/oxidation with deaerated H_2O did not occur and was not thermodynamically favorable [39]. Our finding on the absence of surface passivation of

Mo_2C catalysts, therefore, is consistent with the literature conclusion. The resulting catalyst slurry was dried at 110 °C for 2 h and reduced in flowing H_2 (400 mL/min) at 300 °C for 4 h to decompose the nitrate and produce the Cu or Pd domains. Preparation of the Cu-Pd/Mo_2C catalysts was achieved sequentially by first depositing Cu onto Mo_2C, followed by transferring the dried Cu/Mo_2C under an inert atmosphere to a deaerated aqueous solution containing the target concentration of $Pd(NO_3)_2 \cdot 4NH_3$. The catalyst was allowed to interact for 5 h and was dried and reduced in a quartz tube reactor using the protocols described earlier.

Properties for the Mo_2C- and Mo_2N-based catalysts were compared to those for bulk and oxide supported Cu catalysts. Nano-Cu (QuantumSphere), Cu/ZnO/Al_2O_3 (Süd-Chemie/Clariant), and Cu/Cr_2CuO_4 (Cu Chromite, Strem Chemicals Inc.) catalysts were acquired from commercial vendors and used after pretreatment (described later). The Cu/ZnO/Al_2O_3 and Cu/Cr_2CuO_4 catalysts are referred to as "Cu-Zn-Al" and "Cu-Cr", respectively. The Cu/γ-Al_2O_3, Cu/SiO_2, and Cu/C catalysts were synthesized via incipient wetness impregnation of γ-Al_2O_3 (Alfa Aesar, 0.4 cm^3/g pore volume), fumed SiO_2 (AEROSIL®, 0.8 cm^3/g pore volume), and carbon black (Fuel Cell Store, Vulcan XC-72R, 0.8 cm^3/g pore volume) with aqueous solutions of $Cu(NO_3)_2$ (5 wt% nominal loading). The supports were pelletized, then ground and sieved to 125-250 μm prior to impregnation with the Cu solution. After impregnation, the catalysts were dried in vacuum at 110 ℃ for 16 h and then annealed under N_2 flow (100 mL/min) at 300 °C for 5 h to decompose the nitrate from $Cu(NO_3)_2$. A Cu/ZrO_2 (referred to as Cu-Zr) catalyst was synthesized via a co-precipitation technique with a 1:1 molar ratio of $Cu(NO_3)_2$ and $Zr(NO_3)_2$ precursors, based on a protocol described elsewhere [42].

Surface areas of the materials were determined from N_2 physisorption isotherms collected using a Micromeritics ASAP 2010 analyzer. The isotherms were analyzed using the Brunauer–Emmett–Teller (BET) method. Prior to the measurements, the catalysts were degassed (< 5 mm Hg) for at least 4 h at elevated temperatures (350 ℃ for the Mo_2C or Mo_2N based catalysts, 200 ℃ for the other Cu-based catalysts). The bulk crystalline structures of the catalysts were characterized using X-ray diffraction performed using a Rigaku Miniflex diffractometer with Cu Kα radiation (λ = 1.5418 Å). The diffraction patterns were obtained by scanning 2θ from 10 to 90 ° at a scan rate of 5 °/min. Inductively coupled plasma (ICP-OES, Varian 710-ES analyzer) was used to determine the metal compositions for the Mo_2C and Mo_2N based catalysts. As appropriate, the metal content is included in the catalyst name; for example, 5 wt% Mo_2C supported Cu is referred to as "5 Cu/Mo_2C".

2.2.2 Activity and Selectivity Measurements

Ethyl formate was selected as the reactant so that CH_3OH produced from other pathways could be distinguished from the parent alcohol of the formate. All of the experiments were performed in a 50 mL autoclave Parr reactor, equipped with a variable-speed impeller. A schematic diagram of this high-pressure, continuously-stirred, semi-batch reactor system is shown in Figure 2.2. A gas chromatograph (Varian 450, equipped with flame ionization and thermal conductivity detectors) was connected directly to the reactor gas outlet for online gas product analysis. A filter was also added to separate the liquid products from the catalyst particles when withdrawing liquid samples; the liquids were analyzed offline using a gas chromatograph (Varian 450) with a flame ionization detector.

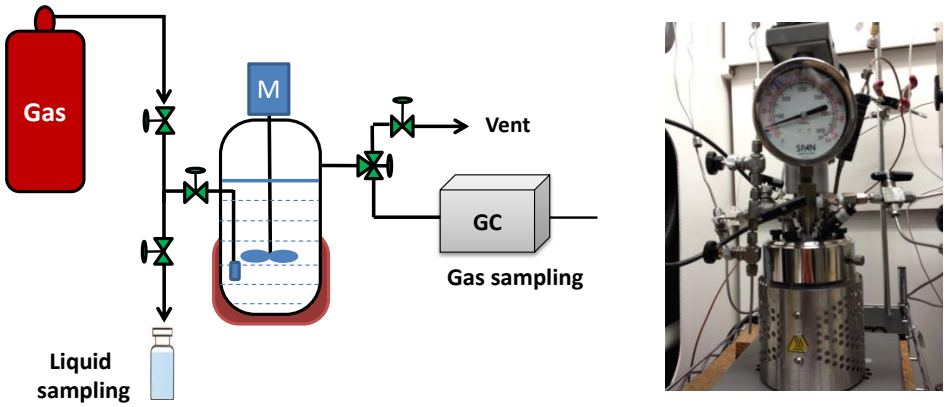

Figure 2.2 Schematic of high pressure, continuously stirred, semi-batch reactor system for liquid phase CO_2 hydrogenation.

All of the Cu-based catalysts were pretreated in 4% H_2/N_2 (100 mL/min) at 200 ℃ for 4 h in the reactor prior to measurement of the rates and selectivities. The Mo_2C or Mo_2N-based catalysts were used as synthesized without passivation. To avoid contact of the materials with air, they were transferred under an inert atmosphere and stored in an Ar filled glovebox. The reactant solution was prepared by adding 0.6 mmol ethyl formate (Acro Organics, 99%) to 37.5 mL 1,4-dioxane (Acro Organics, 99+%, 100 ppm H_2O); decane (10 uL) was introduced as an internal standard for GC analysis. The reactant solution and 200 mg catalyst were loaded into the reactor. The Mo_2C and Mo_2N materials were loaded into the reactor in the glovebox due to their pyrophoricity. After loading the catalysts and the reactant mixture, 30 bar of H_2 was charged into the reactor through a dip tube (immersed in the solvent) to allow sufficient gas dissolution. The solubility of H_2 in 1,4-dioxane is 0.14 M at 135 ℃ and 30 bar H_2 [43]. The reactor was then heated at a rate of 5 ℃/min from room temperature to 135 ℃, and agitated at a constant rate of 300 rpm. The start of the reaction was designated as the time at which the reactor temperature reached 135 ℃. The reactor was maintained at 135 ℃ throughout the reaction. Each experiment was repeated at least twice and the errors

were calculated considering both the standard deviations from replicates and GC analyses. Carbon balances closed to within ± 8 % for all the experiments. The conversion was defined as the percentage of the initial ethyl formate consumed during the reaction, while the selectivity was defined as the molar ratio of a specific product over the total products. The reaction rates were evaluated from temporal variations in the amounts of ethyl formate consumed or CH_3OH formed.

2.3 Results and Discussion

2.3.1 Physical Properties

The surface areas, Cu contents, and Cu crystallite sizes for the supported Cu, Mo_2C and Mo_2N catalysts are listed in Table 2.1. As expected, the Cu/C, Cu/SiO_2 and all of the Mo_2C- and Mo_2N-based catalysts possessed high surface areas (> 100 m^2/g). The reduced surface areas for the Cu/Mo_2C and Cu/Mo_2N catalysts compared to their corresponding support materials is likely a consequence of pore blockage by the Cu nanoparticles. The Cu/γ-Al_2O_3, Cu-Zn-Al, Cu-Cr, and Cu-Zr catalysts exhibited moderate surface areas (45-80 m^2/g), while the Nano-Cu material had a relatively low surface area.

Table 2.1 Physical properties of Cu, Mo_2C, and Mo_2N based catalysts.

Catalysts	Surface Area (m^2/g)	Cu Content (wt%)	Cu Crystallite Size (nm)
Nano-Cu[a]	5.5	100	254
Mo_2C[a]	151	N/A	N/A
Mo_2N	153	N/A	N/A
5 Cu/Mo_2C[a]	135	5.3	34
3 Cu/Mo_2N	141	3.2	N/A[b]
Cu-Zn-Al[a]	60	33	89
Cu-Cr[a]	46	36	163
Cu-Zr	80	34	98
Cu/γ-Al_2O_3	54	5.0	47
Cu/SiO_2	172	5.0	101
Cu/C	169	5.0	58

[a] Values adapted from [39].
[b] Cu crystallite size was not quantified for this catalyst, as the peak at ~ 41 °2θ could not be isolated from that for the γ-Mo_2N support (Figure 2.3).

X-ray diffraction patterns for the catalysts are displayed in Figure 2. The bulk and supported Mo_2C-based catalysts contained a mixture of α-MoC_{1-x} (face centered cubic) and β-Mo_2C (hexagonal close packed); each phase was determined by matching the XRD patterns to the standard spectra reported in the literature [44, 45]. The two phases showed approximately a 1:1 ratio as calculated using the whole pattern fitting Rietveld refinement technique (JADE 7.0). Similar Mo:C ratios (~ 2:1) were measured for α-MoC_{1-x} and β-Mo_2C by the elemental analysis, therefore catalysts containing these materials will be referred to as Mo_2C for simplicity. This composition was also reported by several works in the literature on the same type of Mo_2C material [33, 46]. The Mo_2N-based catalysts contained only γ-Mo_2N phase. Only a weak peak associated with Cu (41 °2θ) was detected for the Cu/Mo_2C catalyst and Cu peaks could not be clearly defined for the Mo_2N supported material. These findings indicated that the Cu dispersion was relatively higher on Mo_2C or Mo_2N compared to that on other supports, although it was possible that the Cu and γ-Mo_2N peaks overlapped

at ~ 41 °2θ. Sharp Cu peaks are observed for the Nano Cu material, indicating that it is phase pure with large crystallites. Copper peaks, as well as peaks for the support oxides, were observed for most of the oxide supported catalysts. Peaks attributable to the oxides were weak or non-existent for the Cu-Cr, Cu-Zr and Cu/SiO_2 catalysts, suggesting that the oxide particles were very small (< 5 nm) or amorphous. In addition, a weak peak was detected for the Cu-Cr catalyst at 54 °2θ. This peak is consistent with the presence of CuO [41]. The Cu crystallite sizes were smallest for the Cu/Mo_2C catalyst; the Cu crystallite size was not quantified for the Cu/Mo_2N catalyst, as the peak at ~ 41 °2θ could not be isolated from that for the γ-Mo_2N support.

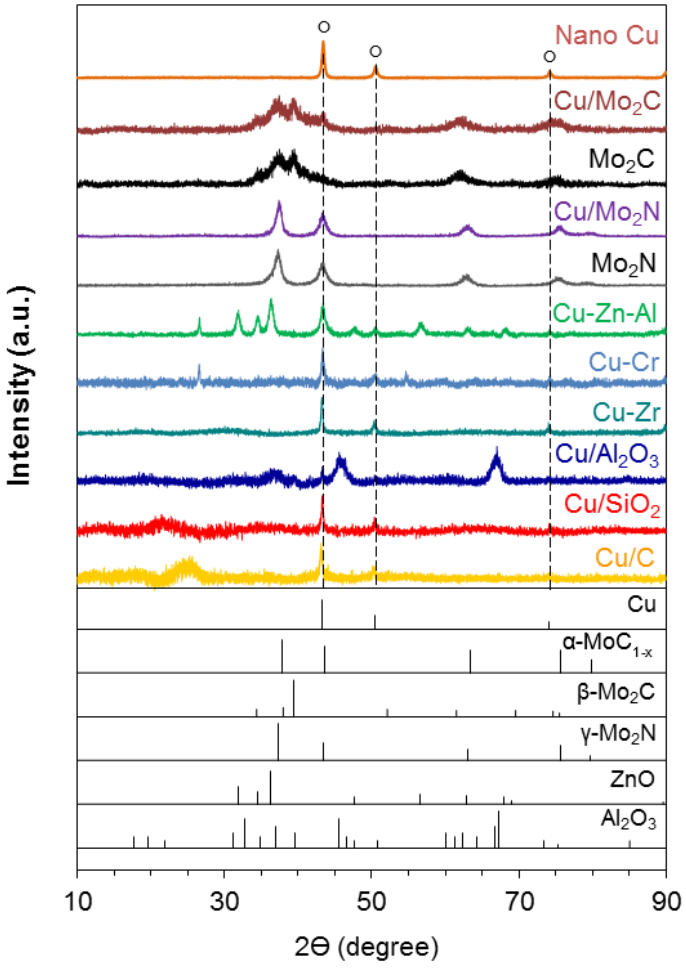

Figure 2.3 X-ray diffraction patterns for the Cu, Mo_2C, and Mo_2N catalysts. The open circle indicates the Cu peaks. The standard patterns on the bottom include Cu (JCPDF 01-085-1326), α-MoC_{1-x} (JCPDF 00-015-0457), β-Mo_2C (JCPDF 00035-0787), γ-Mo_2N (JCPDF 00-025-1366), ZnO (JCPDF 01-080-3004), and Al_2O_3 (JCPDF 00-004-0877).

2.3.2 Catalytic Activities and Selectivities

The ethyl formate hydrogenolysis reaction rates and selectivities over the supported Cu, Mo_2C and Mo_2N catalysts are shown in Table 2.2. Ethyl formate hydrogenolysis generates CH_3OH and C_2H_5OH in an equimolar ratio (Eq. 1), i.e. a 50% selectivity should be expected for each alcohol product. However, we observed that the selectivities to CH_3OH were less than 50% over all of the catalysts, while the selectivities to ethanol were

consistently around 50%. This finding indicated that either CH_3OH was consumed during a secondary reaction or additional ethanol was produced via side reactions. To examine the possibility of CH_3OH consumption, control experiments were conducted with 0.6 mmol CH_3OH as the starting material at 135 ℃ and 30 bar H_2 using 200 mg of each catalyst; these conditions are similar to those used during formate hydrogenolysis. No CH_3OH was consumed during the control trials, indicating that CH_3OH was stable once produced in the reaction system. Interestingly, CO_2 was also observed during the ester hydrogenolysis experiments and its selectivity was comparable to the difference between the CH_3OH and C_2H_5OH selectivities. It is plausible that the excess ethanol was produced via hydrolysis of the formate (Eq. 2.2). H_2O was a contaminant in the 1,4-dioxane solvent according to the product specification (100 ppm H_2O), which resulted in ~ 0.04 mmol of H_2O in the reactor system; while the CO_2 was produced in the amounts of 0.04-0.46 mmol during the ethyl formate hydrogenolysis experiments (Table 2.2). This result suggested that additional H_2O may have come from moisture in the air to balance the amount of CO_2 production. This was not surprising given the hygroscopic nature of 1,4-dioxane. Based on our previous investigations, any formic acid produced during formate hydrolysis would be rapidly converted to CO_2 (Eq. 2.3) under the conditions used in the present work [41]. Meanwhile, the amount of CO_2 is always equivalent to the ethanol produced from the hydrolysis (Eq. 2.2). Therefore, formic acid is most likely the source of CO_2; similar pathway was also suggested by Braca et al [22]. For one reactant (ethyl formate) with two pathways (hydrogenolysis and hydrolysis) to a common product (ethanol), the selectivity for that product should be 50% as was observed for most of the catalysts. Small amounts of CH_4 and methyl formate were also

produced over the Mo_2C-based catalysts, possibly due to formic acid hydrogenation (Eq. 2.4) and/or transesterification (Eq. 2.5), respectively.

$HCOOC_2H_5 + 2H_2 \rightarrow CH_3OH + C_2H_5OH$	$\Delta G° = -38$ kJ/mol	$\Delta H° = -122$ kJ/mol	Eq. 2.1
$HCOOC_2H_5 + H_2O \rightarrow HCOOH + C_2H_5OH$	$\Delta G° = 20$ kJ/mol	$\Delta H° = -6.8$ kJ/mol	Eq. 2.2
$HCOOH \rightarrow CO_2 + H_2$	$\Delta G° = -48$ kJ/mol	$\Delta H° = 16$ kJ/mol	Eq. 2.3
$HCOOC_2H_5 + CH_3OH \rightarrow HCOOCH_3 + C_2H_5OH$	$\Delta G° = -7.1$ kJ/mol	$\Delta H° = -26$ kJ/mol	Eq. 2.4
$HCOOH + 3H_2 \rightarrow CH_4 + 2H_2O$	$\Delta G° = -179$ kJ/mol	$\Delta H° = -237$ kJ/mol	Eq. 2.5

On a gravimetric basis, catalysts containing Mo_2C were the most active, outperforming the oxide supported catalysts, including the Cu-Cr catalyst, by a significant margin. In fact, the bulk Mo_2C catalyst exhibited the highest rate although its selectivity to CH_3OH (27 %) was moderate. The deposition of Cu onto this catalyst improved its selectivity to 41% (the maximum selectivity is 50% based on the reaction stoichiometry). The Cu-Cr, Cu-Zn-Al, Cu-Zr, and Mo_2N catalysts possessed moderate activities, while the other catalysts, including the Nano-Cu catalyst, exhibited low activities. Interesting, the Cu/C catalyst was inactive, possibly due to limited formate adsorption on the carbon support, as was suggested by Braca et al. for a Re/C catalyst [22]. Where possible, the rates were also normalized by the surface areas and Cu loadings in order to define more intrinsic activities. When normalized by their surface areas, rates for the Nano-Cu as well as the Cu-Cr and Cu-Zn-Al catalysts were the highest. The results make sense as the measured total surface areas should be close to the active Cu surface areas for these catalysts, given their relatively high Cu composition. Whereas for the other catalysts with lower Cu loading (~ 5 wt%), the active species surface area may only count for a small portion of the total surface area, therefore, the surface area normalized rates turned out to be smaller. When normalized by the Cu content, all of the supported catalysts yielded rates that are significantly higher than that for

the Nano-Cu catalyst, indicating that Cu is a key active species and its dispersion is critical. The highest rates, when normalized by Cu contents, were achieved for the Mo_2C- and Mo_2N-based catalysts. This result was not unexpected given that Mo_2C and Mo_2N were active without Cu.

Table 2.2 Reaction rates and selectivities for ethyl formate conversion over Cu, Mo_2C, and Mo_2N based catalysts.[a]

Catalysts	Formate Conversion Rate			Selectivity (%)				$k_{obs} \times 10^4$
	(μmol/ g_{catal}/h)	(μmol/ m^2/h)	(mmol/ g_{Cu}/h)	CH_3OH	C_2H_5OH	CO_2	CH_4 +MF[c]	($g_{catal}^{-1} \cdot s^{-1}$)
Nano-Cu[b]	79 ± 4	14.4 ± 0.8	0.08 ±0.04	40 ± 3	51 ± 4	8.9 ± 0.7	0	1.1 ± 0.2
Mo_2C[b]	889 ± 73	5.9 ± 0.6	N/A	27 ± 3	49 ± 5	22 ± 2	1.5	2.8 ± 0.2
Mo_2N	350 ± 42	2.3 ± 0.2	N/A	0	51 ± 4	49 ± 3	0	0
5 Cu/Mo_2C[b]	837 ± 55	6.2 ± 0.5	15.8 ± 2	41 ± 4	49 ± 5	7.5 ± 0.6	2.7	3.6 ± 0.4
3 Cu/Mo_2N	413 ± 37	2.9 ± 0.3	12.9 ± 1	7.2 ± 0.6	51 ± 3	42 ± 2	0	0.04 ± 0.0
Cu-Zn-Al[b]	598 ± 47	10.0 ± 0.6	1.8 ± 0.3	28 ± 2	51 ± 4	21 ± 2	0	1.2 ± 0.1
Cu-Cr[b]	554 ± 32	12.0 ± 0.7	1.5 ± 0.2	27 ± 4	50 ± 6	23 ± 2	0	1.7 ± 0.3
Cu-Zr	567 ± 45	7.1 ± 0.9	1.7 ± 0.2	6.8 ± 0.5	50 ± 5	43 ± 5	0	0.3 ± 0.06
Cu/γ-Al_2O_3	190 ± 14	3.5 ± 0.5	3.8 ± 0.3	5.7 ± 0.5	50 ± 4	44 ± 3	0	0.4 ± 0.1
Cu/SiO_2	78 ± 5	0.5 ± 0.1	1.6 ± 0.1	31 ± 2	50 ± 3	19 ± 1	0	0.6 ± 0.1
Cu/C	0	0	0	0	0	0	0	0

[a] 135 ℃, 30 bar H_2, 0.6 mmol ethyl formate and 37.5 mL 1,4-dioxane, rates calculated at 2 h and selectivities calculated at 8 h.

[b] Rate data are adapted from [39].

[c] MF = methyl formate.

When considering the Cu catalysts, the support appeared to have a significant effect on selectivity, as illustrated by results listed in Table 2.2. The Cu/Mo_2C and Nano-Cu catalysts demonstrated high CH_3OH selectivities (> 40%); selectivities for the Cu-Zn-Al, Cu-Cr, and Cu/SiO_2 catalysts were moderate (~30%) and the Cu/Mo_2N, Cu/ZrO_2, and Cu/γ-Al_2O_3 catalysts yielded relatively low selectivities (< 10 %). Differences in selectivities for these catalysts could be a consequence of the activity or lack of activity for the support. Monti et al. reported, based on results from deuterium labeling studies at ~145 ℃, that methyl formate hydrogenolysis over a Cu/SiO_2 catalyst involved the adsorption of methyl formate on SiO_2 via the carbonyl group and the dissociation of H_2 on the Cu particles [47]. Hydrogen can then be added to the adsorbed formate sequentially to produce CH_3OH as shown in Figure 2.4a. Braca et al. also reported that the SiO_2 supported Re catalyst was more selective to CH_3OH than catalysts produced from more acidic or basic supports [22]. In addition to facilitating the hydrogenolysis reaction, the support could, depending on its acidicity or basicity, catalyze hydrolysis of the formate (see Figure 2.4b) [48, 49]. SiO_2, and Cr_2O_3 tend to be amphoteric and hence their hydrolysis rates should be low. γ-Al_2O_3 is relatively acidic and is known to catalyze hydrolysis reaction [50]. ZrO_2 and ZnO are relatively basic and would facilitate the hydrolysis reaction [51]. The Mo nitrides and carbides have been reported to possess moderate acidity and/or basicity depending on the synthesis and treatment conditions [52, 53] and would also catalyze the hydrolysis of ethyl formate.

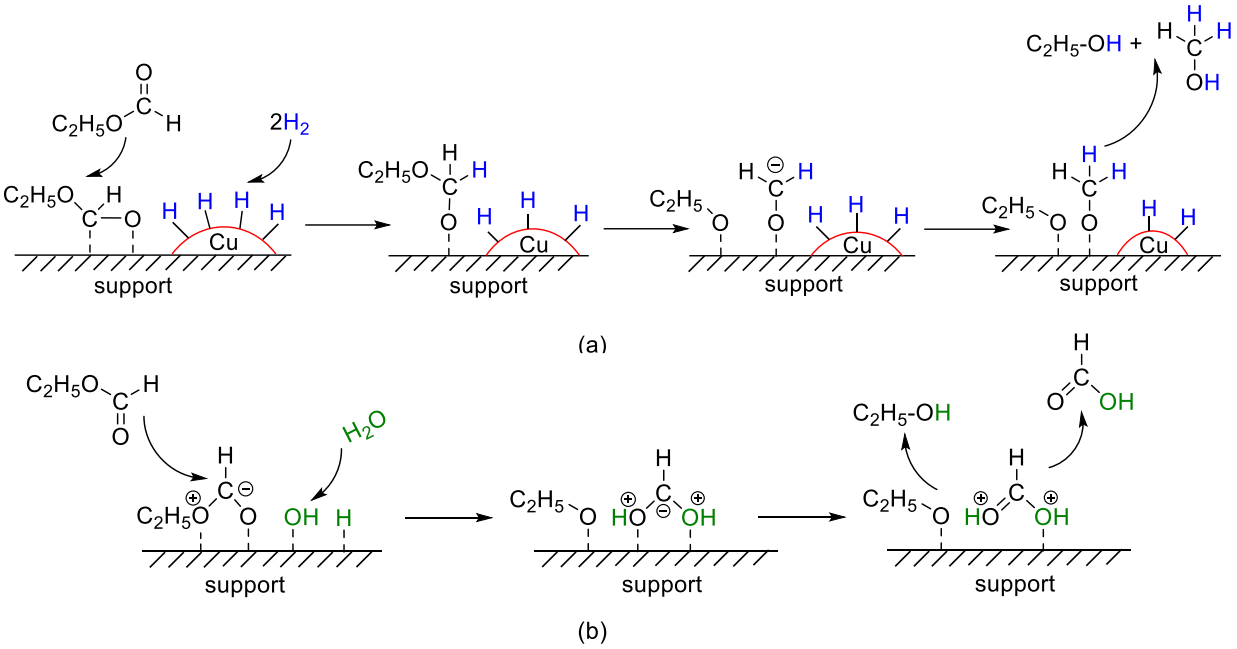

Figure 2.4 Proposed mechanisms for (a) ethyl formate hydrogenolysis over Cu-supported catalysts [43], and (b) ethyl formate hydrolysis.

Temporal variations in the reaction rates were consistent with first order kinetics with respect to ethyl formate ($R^2 \geq 92\%$). The first order dependence on formate is consistent with reports by Monti et al. regarding the kinetics for liquid phase methyl formate hydrogenolysis at 135-200 ℃ [9]. We used the following equation to determine the pseudo first order rate constants, k_{obs}:

$$r_h = k_{obs} \bullet C_{formate} \qquad \text{Eq. 2.6}$$

where r_h = rate of hydrogenolysis [mol/L/g_{catal}/s] based on the formation of CH_3OH, k_{obs} = pseudo first order rate constant [$g_{catal}^{-1} \cdot s^{-1}$] and $C_{formate}$ = the average concentration of formate [mol/L]. Because the concentration of H_2 was in significant excess of stoichiometric (~ 5.3 mmol based on its solubility in 1,4-dioxane at 135 ℃, 30 bar [43]), the H_2 concentration term was embedded in the rate constant. Based on k_{obs}, hydrogenolysis activities for the catalysts

decreased as follows: 5 Cu/Mo_2C > Mo_2C > Cu-Cr > Cu-Zn-Al ≈ Nano-Cu > Cu/SiO_2 ≈ Cu/γ-Al_2O_3 ≈ Cu-Zr > 3 Cu/Mo_2N ≈ Mo_2N ≈ Cu/C = 0 (Table 2.2).

As the Cu/Mo_2C catalyst exhibited the highest reaction rates and selectivities, additional experiments were carried out with this material. Figure 2.5 shows the reactant and product distributions as a function of reaction time and Figure 2.6 shows the Arrhenius plot. The apparent activation energy (E_A) for ethyl formate hydrogenolysis to CH_3OH was 44 ± 3 kJ/mol. Evan et al. reported a value of 48 kJ/mol for a commercial Cu-Cr catalyst in a comparable temperature range (130-170 ℃) [17].

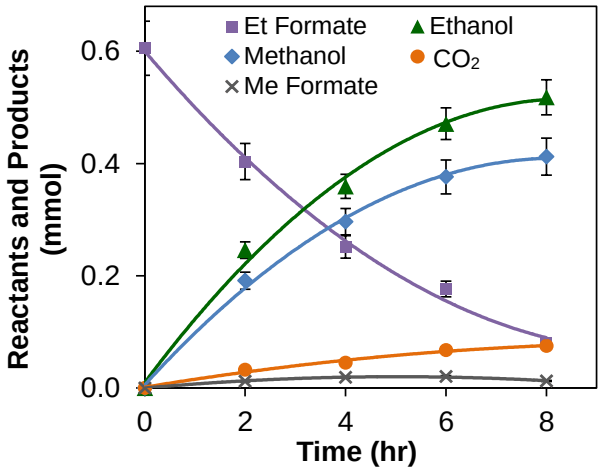

Figure 2.5 Reactant and products plot for ethyl formate hydrogenation over Cu/Mo_2C catalyst (■ Ethyl formate, ▲ Ethanol, ♦ CH_3OH, ● CO_2, × methyl formate). The experiments were performed at 135 ℃, 30 bar H_2, and 37.5 mL 1,4-dioxane.

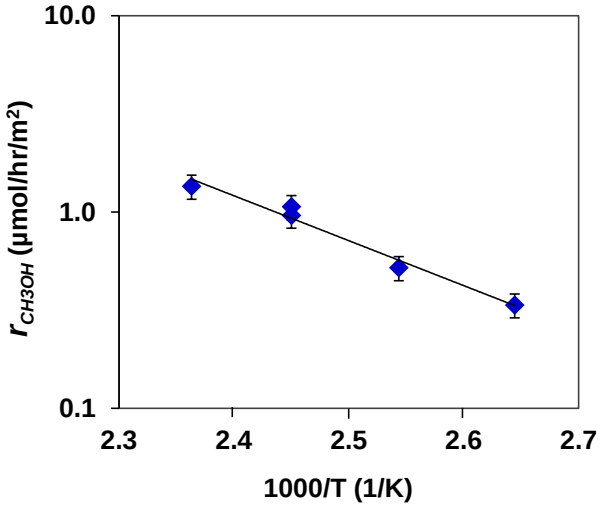

Figure 2.6 Arrhenius plot for ethyl formate hydrogenolysis rate over Cu/Mo_2C. Experiments were performed at 105-150 ℃, 30 bar H_2 and 37.5 mL 1,4-dioxane.

Given results for the Cu/Mo_2C catalysts, we synthesized Mo_2C supported Pd and Pd-Cu catalysts. Palladium has been reported to be active for ester hydrogenolysis [21]. Table 2.3 lists the reaction rates and selectivities for the Mo_2C supported Pd and/or Cu catalysts. Interestingly, the surface area normalized rates for the Mo_2C catalyst and for these metal/Mo_2C catalysts were very similar, ranging from 5.4 and 6.2 µmol/m^2/h at 135 ℃. Given the significant variations in the metal loading, this observation suggested that Pd, Cu and Mo_2C possessed similar intrinsic activities for formate conversion. While the rates were similar, products formed during formate conversion changed significantly when Pd and/or Cu were deposited onto the Mo_2C support. Figure 2.7 compares selectivities for the catalysts after 8 h on stream. The CH_3OH selectivity was lowest for the Mo_2C catalyst and increased with increases in the Pd and/or Cu loading. These results are consistent with Pd and Cu facilitating hydrogenolysis over the Mo_2C catalyst perhaps via a pathway similar to that proposed by Monti et al. for Cu/SiO_2 catalysts (Figure 2.3a) [47]. Mo_2C still differs from other oxide supports in that it is an active species for ester hydrogenolysis itself. As all the

Mo_2C-based materials were synthesized without surface passivation and used in an oxygen-free environment, minimal amount of molybdenum oxide species should be involved in the reaction. In comparing the $5Cu/Mo_2C$ and $5Pd/Mo_2C$ catalysts, one could conclude that Pd is a slightly more effective promoter than Cu. This could be a consequence of differences in the inherent properties of the metals or differences in their dispersions.

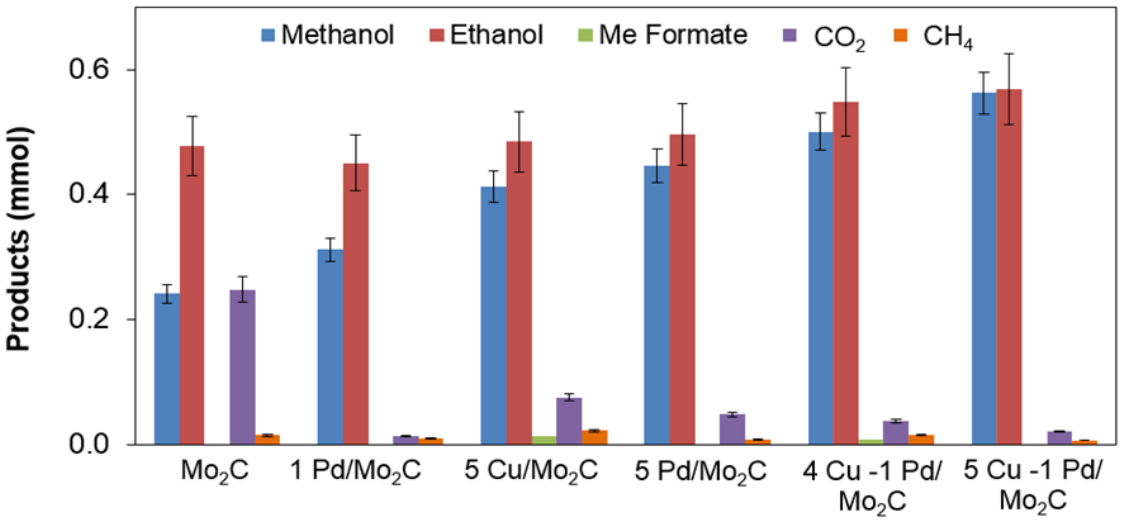

Figure 2.7 Product distributions for ethyl formate hydrogenolysis over the Mo_2C-based catalysts. The experiments were performed at 135 ℃, 30 bar H_2, 8 h, and 37.5 mL 1,4-dioxane**.**

Table 2.3 Reaction activities and selectivities for ethyl formate conversion over Mo_2C supported Cu and/or Pd catalysts.[a]

Catalysts	Properties		Formate Conversion Rate		Selectivity (%)				$k_{obs} \times 10^4$ ($g_{catal}^{-1} \cdot s^{-1}$)
	Surface Area (m^2/g)	Cu or Pd Content (wt%)	(μmol/ g_{catal}/h)	(μmol/ m^2/h)	CH_3OH	C_2H_5OH	CO_2	CH_4 +MF[b]	
1Pd/Mo_2C	143	Pd (1.4)	775 ± 61	5.4 ± 0.3	31 ± 4	50 ± 5	17	1.8	3.2 ± 0.1
5Pd/Mo_2C	138	Pd (5.2)	783 ± 58	5.7 ± 0.4	43 ± 3	50 ± 5	5.8	1.4	3.5 ± 0.3
4Cu-1Pd /Mo_2C	132	Cu (3.8) Pd (1.4)	795 ± 76	6.0 ± 0.7	45 ± 2	50 ± 4	3.4	1.5	4.2 ± 0.4
5Cu-1Pd /Mo_2C	127	Cu (5.2) Pd (1.6)	784 ± 64	6.2 ± 0.6	49 ± 4	49 ± 4	1.8	0.6	4.6 ± 0.4

[a] 135 ℃, 30 bar H_2, 0.6 mmol ethyl formate and 37.5 mL 1,4-dioxane. Rates calculated at 2 h and selectivities calculated at 8 h.

2.4 Conclusions

Research described in this chapter demonstrated that Mo_2C-based catalysts are catalytically active for the low temperature (< 150 ℃) hydrogenolysis of ethyl formate to CH_3OH. This reaction is a key step in the production of alcohols and in the cascade hydrogenation of CO and CO_2 to CH_3OH. Other products, including CO_2 and minor amounts of CH_4 and methyl formate, are also formed, implicating several side reactions (e.g., ethyl formate hydrolysis, formic acid decomposition, and transesterification). The reaction rates were adequately fit to a first order model with respect to ethyl formate; over the best-performing catalyst (1Pd-5Cu/Mo_2C), the rate constant was 4.6×10^{-4} $g_{catal}^{-1}s^{-1}$. The selectivity to CH_3OH appears to be a strong function of the acidity/basicity of the support. The catalysts with amphoteric or weakly acidic/basic supports generally yielded higher CH_3OH selectivities than those for catalysts with strong acidic/basic supports. Materials with strong acid/base sites likely catalyzed the hydrolysis reaction, producing substantial amounts of CO_2. The deposition of nanoscale Cu and/or Pd particles onto the Mo_2C significantly enhanced the catalytic performance, yielding high conversion rates and CH_3OH selectivities approaching 50% (as opposed to 27% for the Mo_2C catalyst). The enhancement in CH_3OH selectivity is likely a consequence of synergy between the metal and support. These catalysts are excellent candidates for use in cascade catalytic systems for the one-pot synthesis of CH_3OH via CO or CO_2 hydrogenation as well as other types of ester hydrogenolysis reactions.

2.5 References

[1] L.G. Hess, H.W. Schulz, US Patent 2782243, 1957.
[2] W.A. Lazier, US Patent 2079414, 1937.
[3] T. Turek, D. Trimm, N. Cant, Catal. Rev. Sci. Eng. 36 (1994) 645-683.
[4] D.S. Brands, E.K. Poels, A. Bliek, Appl. Catal., A 184 (1999) 279-289.
[5] H.B.M. Hoyng, Oleochemicals: Green and Clean, in: T.H. Applewhite, (Ed.), Proceedings: World conference on oleochemicals, The American Oil Chemists Society, Kuala Lumpur, Malaysia, 1991, pp. 211-217.
[6] F.T. van de Scheur, B. van der Linden, M.C. Mittelmeijer-Hazeleger, J.G. Nazloomian, L.H. Staat, Appl. Catal., A 111 (1994) 63-77.
[7] F.T. van de Scheur, L.H. Staal, Appl. Catal., A 108 (1994) 63-83.
[8] J. Evans, P. Casey, M. Wainwright, D. Trimm, N. Cant, Appl. Catal. 7 (1983) 31-41.
[9] D. Monti, M. Kohler, M. Wainwright, D. Trimm, N. Cant, Appl. Catal. 22 (1986) 123-136.
[10] L. Fan, Y. Sakaiya, K. Fujimoto, Appl. Catal., A 180 (1999) L11-L13.
[11] J.A. Christiansen, US Patent 1,302,011, 1919.
[12] Z. Liu, J.W. Tierney, Y.T. Shah, I. Wender, Fuel Process. Technol. 23 (1989) 149-167.
[13] C.A. Huff, M.S. Sanford, J. Am. Chem. Soc. 133 (2011) 18122-18125.
[14] C.A. Huff, J.W. Kampf, M.S. Sanford, Chem. Commun. 49 (2013) 7147-7149.
[15] R. Gormley, V. Rao, Y. Soong, E. Micheli, Appl. Catal., A 87 (1992) 81-101.
[16] A. Agarwal, N. Cant, M. Wainwright, D. Trimm, J. Mol. Catal. 43 (1987) 79-92.
[17] J.W. Evans, P.S. Casey, M.S. Wainwright, D.L. Trimm, N.W. Cant, Appl. Catal. 7 (1983) 31-41.
[18] S. Ohyama, H. Kishida, Appl. Catal., A 172 (1998) 241-247.
[19] G. Braca, A.R. Galletti, N. Laniyonu, G. Sbrana, E. Micheli, M. Di Girolamo, M. Marchionna, Ind. Eng. Chem. Res. 34 (1995) 2358-2363.
[20] Z. Liu, J. Tierney, Y. Shah, I. Wender, Fuel Process. Technol. 18 (1988) 185-199.
[21] N. Iwasa, M. Terashita, M. Arai, N. Takezawa, React. Kinet. Catal. Lett. 74 (2001) 93-98.
[22] G. Braca, A.R. Galletti, G. Sbrana, M. Lami, M. Marchionna, J. Mol. Catal. A: Chem. 95 (1995) 19-26.
[23] S.T. Oyama, The chemistry of transition metal carbides and nitrides, 1st ed., Chapman & Hall USA, New York, 1996.
[24] R.B. Levy, M. Boudart, Science 181 (1973) 547-549.
[25] G. Ranhotra, A. Bell, J. Reimer, J. Catal. 108 (1987) 40-49.
[26] J. Lee, S. Locatelli, S. Oyama, M. Boudart, J. Catal. 125 (1990) 157-170.
[27] P.M. Patterson, T.K. Das, B.H. Davis, Appl. Catal., A 251 (2003) 449-455.
[28] A. Griboval-Constant, J.-M. Giraudon, G. Leclercq, L. Leclercq, Appl. Catal., A 260 (2004) 35-45.
[29] J.-L. Dubois, K. Sayama, H. Arakawa, Chem. Lett. 21 (1992) 5-8.
[30] W. Xu, P. Ramirez, D. Stacchiola, J. Rodriguez, Catal. Lett. 144 (2014) 1-7.
[31] J. Patt, D. Moon, C. Phillips, L. Thompson, Catal. Lett. 65 (2000) 193-195.
[32] W. Setthapun, S. Bej, L. Thompson, Top. Catal. 49 (2008) 73-80.
[33] J.A. Schaidle, A.C. Lausche, L.T. Thompson, J. Catal. 272 (2010) 235-245.
[34] J.-G. Choi, J.R. Brenner, C.W. Colling, B.G. Demczyk, J.L. Dunning, L.T. Thompson, Catal. Today 15 (1992) 201-222.

[35] J.B. Claridge, A.P. York, A.J. Brungs, M.L. Green, Chem. Mater. 12 (2000) 132-142.
[36] M. Ledoux, C. Pham-Huu, Catal. Today 15 (1992) 263-284.
[37] S. Oyama, Catal. Today 15 (1992) 179-200.
[38] J.A. Schaidle, N.M. Schweitzer, O.T. Ajenifujah, L.T. Thompson, J. Catal. 289 (2012) 210-217.
[39] N.M. Schweitzer, J.A. Schaidle, O.K. Ezekoye, X. Pan, S. Linic, L.T. Thompson, J. Am. Chem. Soc. 133 (2011) 2378-2381.
[40] A.C. Lausche, K. Okada, L.T. Thompson, Electrochem. Commun. 15 (2012) 46-49.
[41] Y. Chen, S. Choi, L.T. Thompson, ACS Catal. 5 (2015) 1717-1725
[42] C. Fröhlich, R. Köppel, A. Baiker, M. Kilo, A. Wokaun, Appl. Catal., A 106 (1993) 275-293.
[43] E. Brunner, J. Chem. Eng. Data 30 (1985) 269-273.
[44] S. Nagakura, M. Kikuchi, S. Oketani, Acta Crystallographica 21 (1966) 1009-1010.
[45] J. Schuster, H. Nowotny, Monatshefte für Chemie 110 (1979) 321-333.
[46] T. Hyeon, M. Fang, K.S. Suslick, J. Am. Chem. Soc. 118 (1996) 5492-5493.
[47] D. Monti, N. Cant, D. Trimm, M. Wainwright, J. Catal. 100 (1986) 28-38.
[48] K. Yates, R.A. McClelland, J. Am. Chem. Soc. 89 (1967) 2686-2692.
[49] R. Koster, B. van der Linden, E. Poels, A. Bliek, J. Catal. 204 (2001) 333-338.
[50] A. Fukuoka, P.L. Dhepe, Angew. Chem., Int. Ed. 45 (2006) 5161-5163.
[51] R. Aelion, A. Loebel, F. Eirich, J. Am. Chem. Soc. 72 (1950) 5705-5712.
[52] S.K. Bej, C.A. Bennett, L.T. Thompson, Appl. Catal., A 250 (2003) 197-208.
[53] R.C.V. McGee, S.K. Bej, L.T. Thompson, Appl. Catal., A 284 (2005) 139-146.

CHAPTER 3

COUPLING HOMOGENEOUS AND HETEROGENEOUS CATALYSTS FOR CASCADING CO_2 HYDROGENATION TO CH_3OH

3.1 Introduction

Inspired by photosynthesis, nature's multi-step process for reducing CO_2, a homogeneous cascade system was devised by Huff and Sanford to the convert CO_2 to CH_3OH (see Figure 3.1). The major challenge for this cascade system was the material compatibility; mechanistic studies suggested that the Ru-pincer catalyst was irreversibly inhibited by the $Sc(OTf)_3$, the Lewis acid catalyst needed for esterification, and that the Ru-pincer catalyst was incompatible with CO_2. [1, 2] The incompatibility can be partially addressed by physically separating the Ru-pincer catalyst from the $Sc(OTf)_3$ catalyst; however, performing reactions in separate vessels requires extra purification step to isolate the intermediates, resulting in more effort and cost [3]. Solutions are still being sought to improve the compatibility between the catalyst components in this system.

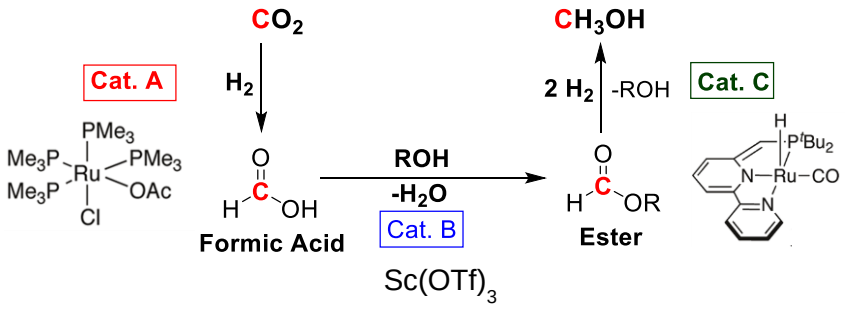

Figure 3.1 Homogeneous cascade system of CO_2 hydrogenation to CH_3OH via formic acid and alkyl formate intermediates. Reaction conditions: 135 ℃, 10 bar CO_2, and 30 bar H_2 for 19 h in 2 ml CH_3OD. Adapted from [4].

Klankermayer and Leitner et al. [5, 6] developed a single Ru-Triphos catalyst to hydrogenate CO_2 to CH_3OH in the presence of $HNTf_2$ (triflimide, a Bronsted acid catalyst) as shown in Figure 3.2. Both Nuclear magnetic resonance (NMR) analysis and density functional theory (DFT) calculation provided evidence that CO_2 hydrogenation occurred through an Ru-Triphos-coordinated formate intermediate (complex **2** in Figure 3.2), activated by $HNTf_2$ and CO_2/H_2 from the Ru-Triphos precursor. This is the first demonstration of a single homogeneous catalyst for the conversion of CO_2 to CH_3OH, where incompatibility issues are not important. The experimental and theoretical studies also provided insightful mechanistic understanding regarding how a Ru-Triphos-coordinated formate was formed as an intermediate and consumed to produce CH_3OH. However, in this work, the operating and catalyst synthesis/activation conditions have to be kept in a narrow window for the best performance of the Ru-Triphos catalyst, making it challenging to develop other viable, cost-effective, and industrially applicable catalytic systems.

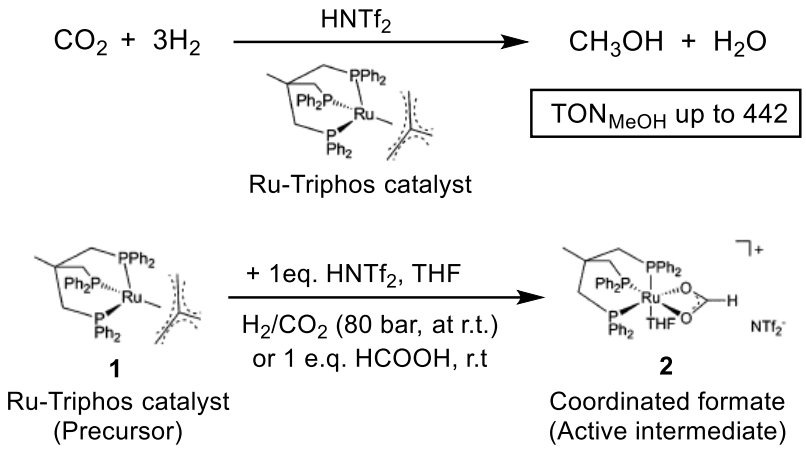

Figure 3.2 Homogeneous CO_2 hydrogenation to CH_3OH using a single Ru-triphos catalyst and the formation of an active formate intermediate (complex 2). 140 ℃, CO_2 20 bar, H_2 60 bar, THF solvent, and 24 h.

Our strategy aims at coupling homo- and hetero-geneous catalysts for the targeted sub-reactions of the cascade sequence from CO_2 to CH_3OH (Figure 3.3). The purpose is to improve the compatibility of cascade systems by introducing heterogeneous active sites that can function at similar conditions to those of the ineffective homogeneous catalysts for specific sub-step(s).

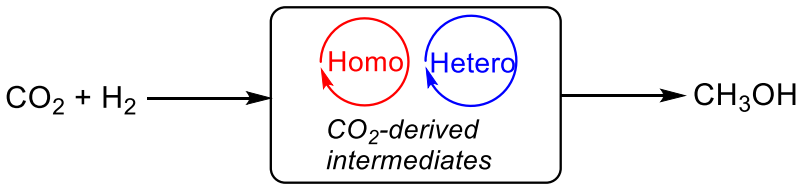

Figure 3.3 A schematic diagram of homogeneous and heterogeneous cascade catalytic system for CO_2 hydrogenation to CH_3OH.

In Chapter 2, results for a series of heterogeneous formate ester hydrogenation catalysts were described. In this chapter, some of the best performing heterogeneous ester hydrogenation catalysts are combined with the homogeneous catalysts to perform the

cascade CO_2 hydrogenation to CH_3OH. In addition to the ester-based pathway, we also investigated other pathways involving formic acid, amide, or alkali formate intermediates under Lewis acidic or basic conditions. The work described in this chapter was performed as part of a collaboration with Danielle Samblanet and Chelsea Huff in the Sanford Group in Chemistry Department at the University of Michigan. Some previous work of this collaboration on the homo-/heterogeneous cascade systems can be found in Dr. Huff's dissertation. [7] This chapter summarizes our techniques and additional key findings on these homo- and hetero-geneous cascade systems.

3.2 Experimental

3.2.1 Catalyst Preparation

Homogeneous catalysts used for this study were either synthesized using the procedures available in the literature (Figure 3.4, A-1 [8], A-2 [6], A-4 [9]) or purchased and used as received (A-3, Strem Chemicals). Catalyst A-1 is a Ru-phosphine catalyst developed by Jessop et al. [1], which catalyzes CO_2 hydrogenation to formate in the presence of an alcohol reagent. Catalyst A-2 is a Ru-triphos complex established by Leitner et al. [6], active for both CO_2 hydrogenation to formate (in the presence of alcohol reagent and acid catalyst) and the subsequent formate hydrogenation to methanol. Catalyst A-3 is a Ru-Macho catalyst, a commercially established catalyst for ester hydrogenation. Catalyst A-4 is a [Cp*Ir(bpy) catalyst (Cp*=pentamethylcyclopentadienyl, bpy=2,2′-bipyridine) developed by Goldberg et al. [11], which effectively activates the carbonyl group in carboxylic acids or esters to produce the corresponding alcohols. These homogeneous catalysts were selected for this

study due to their capability of activating CO_2 and/or C=O group and performing hydrogenation reactions.

The Mo_2C-based catalysts (B-1~B-3) were prepared using protocols described elsewhere in this dissertation (see Section 2.2.1). As Ru/Mo_2C could not be deposited on Mo_2C through wet impregnation due to a poor electronic adsorption based on a previous study [10], an incipient wetness technique was used to achieve the target loading of ~ 5wt%. Briefly, ~ 0.75g of freshly synthesized Mo_2C catalyst and a 97.5 μL aqueous solution containing target concentrations of $RuCl_2$ precursor were transferred under Argon to a water-tolerant oxygen free glovebox filled with N_2. A 10 μL of $RuCl_2$ solution was added to Mo_2C dropwise each time, followed by a thorough stirring of the catalyst after each drop to allow an even deposition of the precursor. The procedure was repeated until all the $RuCl_2$ solution was added. The resulting catalyst slurry was dried on a heating plate for 2 h at 110 ℃ and then transferred to a quartz reactor under N_2. The catalyst was then treated under flowing H_2 at a flow rate of 400 ml/min at 450 ℃ for 4 h. All the freshly-synthesized Mo_2C-based catalysts were transferred to and stored in an H_2O and O_2 free glovebox filled with Ar (MBraun, H_2O <0.1 ppm, O_2 < 5ppm) prior to use to avoid any exposure to O_2.

Homogeneous Catalysts

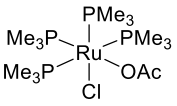

A-1

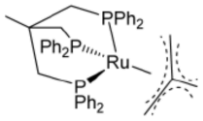

A-2

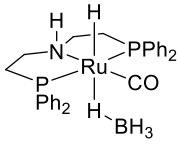

A-3

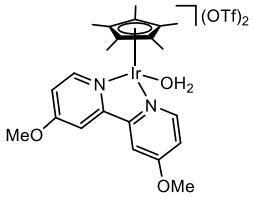

A-4

Heterogeneous Catalysts

Cu/Mo_2C	Ru/Mo_2C	Mo_2C	$Cu/ZnO/Al_2O_3$	Nano Co
B-1	B-2	B-3	B-4	B-5

Figure 3.4 List of homogeneous (A-1~A-4) and heterogeneous (B-1~B-5) catalysts used for this study.

The Cu/Zn/Al (Clariant) and nano Co (QuantumSphere) were acquired commercially and used after pretreatment based on the following protocols. The Cu/Zn/Al was pretreated in 4% H_2/N_2 (200 ml/min) by first heating the material from 25 ℃ to 200 ℃ at a rate of 4 ℃/min and then holding at 200 ℃ for 4 h [11]. The Nano Co was pretreated in 99.99 % H_2 (100 ml/min) by ramping the temperature from 25 ℃ to 450 ℃ at a rate of 4 ℃/min and maintaining at 450 ℃ for 4 h. Both materials were quenched to room temperature after the pretreatment and transferred under Ar to the MBraun glovebox mentioned above. All the Mo_2C-based catalysts were prepared and characterized (using the protocols described in Section 2.2.1 in this dissertation) in the Thompson Lab at the UM Chemical Engineering Department. The catalysts were placed in sample vials and then packed in a secondary container under Ar in order to be transferred (in an oxygen-free environment) to Sanford Lab at UM Chemistry Department for activity measurement. The site densities for Mo_2C-based catalysts and Cu/Zn/Al were

measured by CO and N_2O chemisorption respectively, with experimental details described in section 4.2.2 of this dissertation.

3.2.2 Reaction Set-up

All the reactions were performed in a series of 50 ml autoclave batch reactors (Parr Instrument). Figure 3.5 shows an example of reactor and sample collection setup. A glass liner (customized to fit the reactor dimension) is used for each experiment to allow easy maintenance and avoid contaminations between experiments. The, glass liners, and the heterogeneous catalysts (packed under Ar) were all transferred to a glovebox filled with N_2, where the reactants and catalysts loading (into the reactor) was performed.

Figure 3.5 Reactor vessel and the Schlenk line setup to collect volatile products. Adapted from [4], supporting information.

Heterogeneous catalyst containing ~ 0.01 mmol active sites (based on the site density measurement) was first added to the glass liner. Target amounts of homogeneous complexes (~ 0.01 mmol unless otherwise mentioned) and solvent into the reactor vessel. To properly seal the reactor against high pressure operation, 6 vessel bolts were applied and securely tightened. The following conditions were used for the CO_2 hydrogenation

experiments unless otherwise mentioned: 135 ℃, 10 bar CO_2, 30 bar H_2, and 19 h in 3 mL solvent, ethanol or tetrahydrofuran (THF).

The reactor vessel loaded with catalysts and solvents was then taken out of the glovebox and pressurized with gas reactants, i.e. CO_2 and H_2, using the following protocols. Each vessel was placed into a Parr reactor holder and a customized manifold was used to connect the reactors to the gas cylinders. The manifold was first purged (with both the inlet and outlet open) with CO_2 for approximately 2 minutes at pressures of 11 bar. The inlet of the manifold was then closed with the outlet remaining open to release CO_2 until the pressure dropped to 2 bar. The outlet was then closed and the inlet was open again to pressurize the manifold to 11 bar followed by releasing the pressure to 2 bar. The purging procedure was repeated at least 8 cycles to ensure the manifold was completely filled with CO_2. The reactor vessel inlet was then quickly opened and closed, and the pressure was allowed to equilibrate until the desired pressure level was achieved. Finally, the H_2 gas was introduced to the reactor vessel using the same protocols of introducing the CO_2 gas. The delivering pressure of H_2 to fill the manifold was set to 41 bar in order to achieve the total 40 bar of reactant gases in the reactor. The inlet and outlet valves of the reactor were then closed and the reactor was heated to the desired internal temperature (135 ℃) unless otherwise mentioned. The temperature was monitored using the SpecView (Parr Instrument) software. The reaction start time was recorded once the temperature set point was reached and stabilized.

3.2.3 Reaction Work-up and Product Analysis

Upon finishing the reactions, the vessels were unloaded from the Parr reactor adaptors and transferred to a fume hood. Metering valves were attached to the vessels to

regulate the flow rate of the volatile products as they eluted the reactor. The Schlenk line trap as well at the vessel's small cold trap were cooled using liquid nitrogen before the start of work-up (Figure 3.4). The outlet valve of the reactor vessel was first open followed by opening the metering valve to carefully release excess pressure in the vessel. Once the pressure coming through the trap dropped to approximately 1 atm, the metering valve was closed and the Schlenk line tube was attached to central tube of the trap. Vacuum was then applied to the trap and then closed, before the metering valve was opened all the way and closed. Meanwhile, the trap was allowed to chill for 2 minutes, before opening the Schlenk line again to start the vacuum. This cycle was repeated ~6 times until the reactor vessel reached a complete vacuum, where the pressure did not change significantly when opened to the Schlenk line. The vessels were then transferred to H_2O baths set to 50 ℃. The same procedure of applying vacuum was repeated for 6 times until a complete vacuum was attained.

Immediately after collecting the volatile samples in the cold traps, the tubing to the Schlenk line and metering valve were carefully removed. The cold trap was placed into a beaker to thaw. Dimethylformamide (DMF) of 80 μL was immediately added to the center tube, followed by 0.2 mL of dimethyl sulfoxide-d6 (DMSO-d6) to rinse any residual DMF into the reaction solution. The thawed solution was then added into a 4 mL vial sealed with a Teflon cap. After the solution reached room temperature, an NMR sample was prepared by adding 3-4 drops of the solution to a NMR tube pre-charged with 0.5mL of d-DMSO. The NMR tube was capped and thoroughly shaken to ensure mixing.

The product solution was analyzed by NMR spectroscopy (Varian Inova 500 model) and the spectra were acquired using the following standard settings: relaxation

delay 1.0 s, pulse angle 90 °, acquisition time 5.462 s, 16 repetitions, and Fourier transform size 65536. The integration was performed based on the standard chemical shift (ppm) for each species shown as follows: DMF (7.90-7.96), ethyl formate (8.15-8.18), and CH_3OH (3.12-3.18). The DMF integration was then set to 1.04 mmol (the amount of 80 μL DMF standard added) and the other peaks were normalized to this value to determine the actual amount of each species. The TON was obtained by dividing the mmol of the species by the mmol of catalyst active sites. The turnover frequency (TOF) was calculated by normalizing the TON with reaction time.

3.3 Results and Discussion

Carbon dioxide hydrogenation to CH_3OH was investigated using cascade systems containing homogeneous and heterogeneous catalysts; the systems were tested under both Lewis acidic and basic conditions. The following sections will discuss the findings for this study.

3.3.1 Cascade Systems under Lewis Acidic Conditions

A series of Ru- or Ir- based homogeneous complexes (A-1 to A-4) were used for CO_2 to formic acid step; $Sc(OTf)_3$ catalyst was used for the esterification step; and Cu/Mo_2C catalyst was used for formic acid or ester hydrogenation. Cu/Mo_2C was selected because it exhibited the highest activity and selectivity for ethyl formate hydrogenation to methanol as described in Chapter 2. Previously, Cu/Zn/Al and Cu-Cr were also combined with complex A-1 for the cascade CO_2 hydrogenation; however, their activities appeared to be completely inhibited upon adding the homogeneous complexes. More details regarding these experiments can be found in Huff's dissertation [7]. In this chapter, we will focus on the Mo_2C-based materials as the heterogeneous catalysts for the cascade

CO_2 hydrogenation. Ethyl formate and CH_3OH were the only products detected from the experiments and the TON for each species is shown in Figure 3.6. The Cu/Mo_2C catalyst alone generated 126 TON of CH_3OH and only 8 TON of ethyl formate, indicating that Cu/Mo_2C catalyst itself catalyzed CO_2 hydrogenation to methanol. A control experiment conducted in tetrahydrofuran (THF) without adding ethanol produced a TON of 60 for CH_3OH, suggesting that the addition of ethanol facilitated CO_2 conversion to produce CH_3OH most likely through the ester intermediate. This enhancement may have been achieved by shifting the equilibrium for formic acid production by the subsequent esterification to ethyl formate. Upon adding the homogeneous catalysts, the heterogeneous catalysts suffered different degrees of deactivation, likely a consequence of both site blocking of the heterogeneous catalysts and the surface complexation between the homogeneous and heterogeneous species in the reaction system. The deactivation appeared to be more severe when adding the A-2 or A-4 complexes, suggesting the deactivation pathway was highly dependent on the complex composition and structure. The deactivation upon adding $Sc(OTf)_3$ may be a consequence of $Sc(OTF)_3$ reacting with the basic sites over Mo_2C surface [12] that poisoned the catalyst.

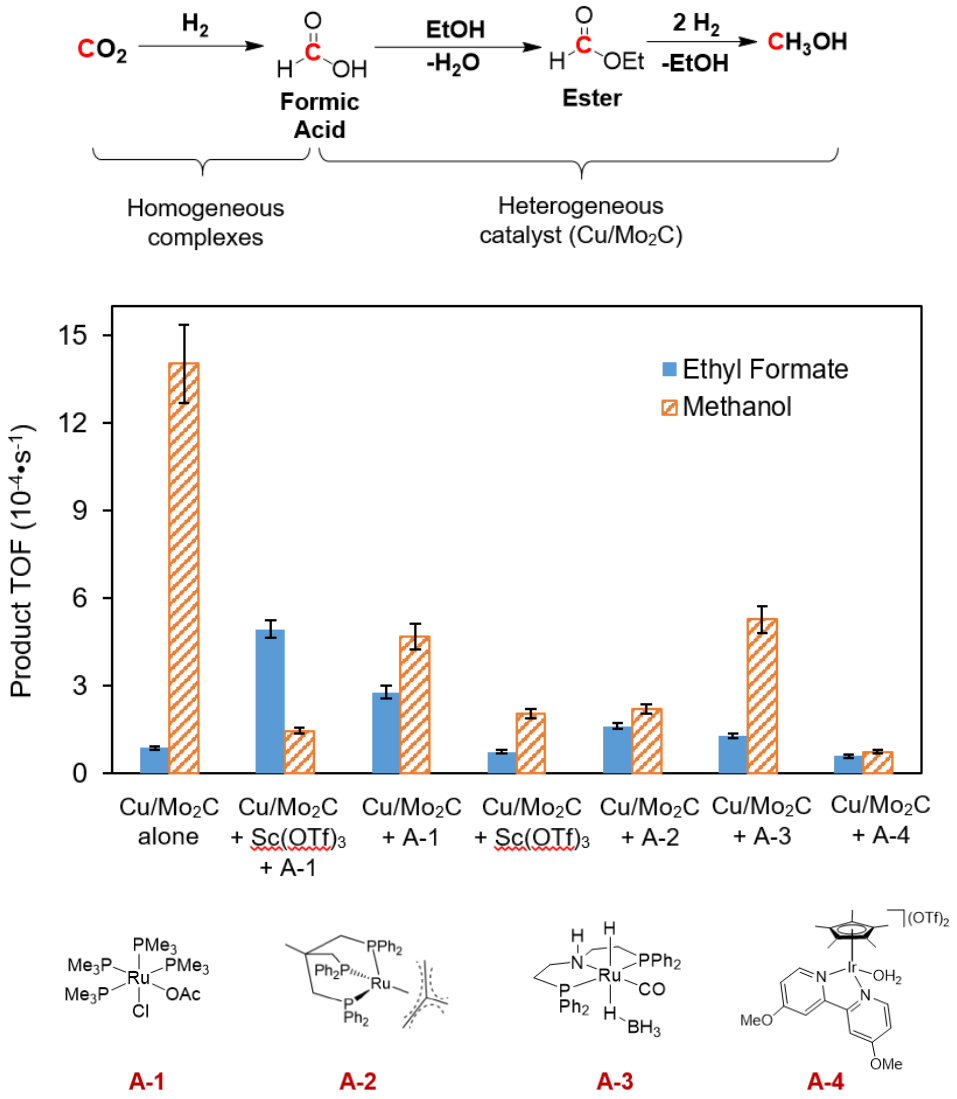

Figure 3.6 Product TONs for CO_2 hydrogenation when combining a series of homogeneous catalysts and Cu/Mo_2C. Experiments were performed at 135 ℃, 10 bar CO_2, 30 bar H_2 in 3 ml ethanol for 19 h, with 0.01 mmol (active sites) of each catalyst added.

To further investigate the deactivation of the Mo_2C-based catalysts when adding the homogeneous catalysts, a series of Mo_2C-based catalysts were studied for CO_2 hydrogenation. The $Ru(PMe_3)_4OAcCl$ complex was used as the representative homogeneous catalyst to convert CO_2 to formic acid; this complex was combined with bulk Mo_2C, Cu/Mo_2C, and Ru/Mo_2C catalysts individually. Their activities for CO_2

hydrogenation are compared in Figure 3.7. When using the Mo_2C and Mo_2C-supported catalysts alone, the activities for CH_3OH production decreased in the following order: $Cu/Mo_2C > Mo_2C > Ru/Mo_2C$. This trend indicated that the addition of Cu facilitated CH_3OH production, while Ru deposition inhibited CH_3OH formation as well as CO_2 conversion. This significant reactivity difference between the Cu/Mo_2C and Ru/Mo_2C catalysts can be attributed to the different types of interaction between the metal and Mo_2C support. Recall that $Cu(NO_3)_2$ and $RuCl_2$ were used as the metal precursors respectively when depositing the metal to Mo_2C support. It was plausible that anion in the precursor can alter the interactions between the metal and Mo_2C support as demonstrated by Schaidle et al. in a previous study [10].

When adding the $Ru(PMe_3)_4OAcCl$ catalyst, all the Mo_2C-based catalysts showed lower activity similar to our previous observation. The rates for Cu/Mo_2C and Mo_2C were comparable after adding the $Ru(PMe_3)_4OAcCl$ complex, which suggested that the promoting effect from Cu for the CH_3OH formation was inhibited and the Mo_2C support was also deactivated by the Ru complex. Interestingly, the Ru/Mo_2C catalyst experienced negligible deactivation upon coupling with $Ru(PMe_3)_4OAcCl$, likely indicating that Ru deposition and contact of $Ru(PMe_3)_4OAcCl$ with Mo_2C followed the same pathway to deactivate Mo_2C catalyst. Ruthenium may have selectively poisoned the sites for CH_3OH production on the Mo_2C surface.

It should be mentioned that over the Mo_2C-based catalysts, CO was also produced in small quantities (4-16% selectivity). To investigate the possibility of CO as an intermediate to produce methanol, CO hydrogenation was performed at 135 ℃, 10 bar CO, and 30 bar H_2, conditions that were similar to CO_2 hydrogenation. The results

showed that methanol produced from CO hydrogenation only accounted for 5-8% of the methanol from CO_2 hydrogenation, suggesting that CO_2 instead of CO was the primary source for methanol. Although Mo_2C-based catalysts exhibit high tolerance for CO, this reactive molecule can irreversibly bind to a number of homogeneous complexes by forming a metal carbonyl bond which deactivates the catalyst. [13]

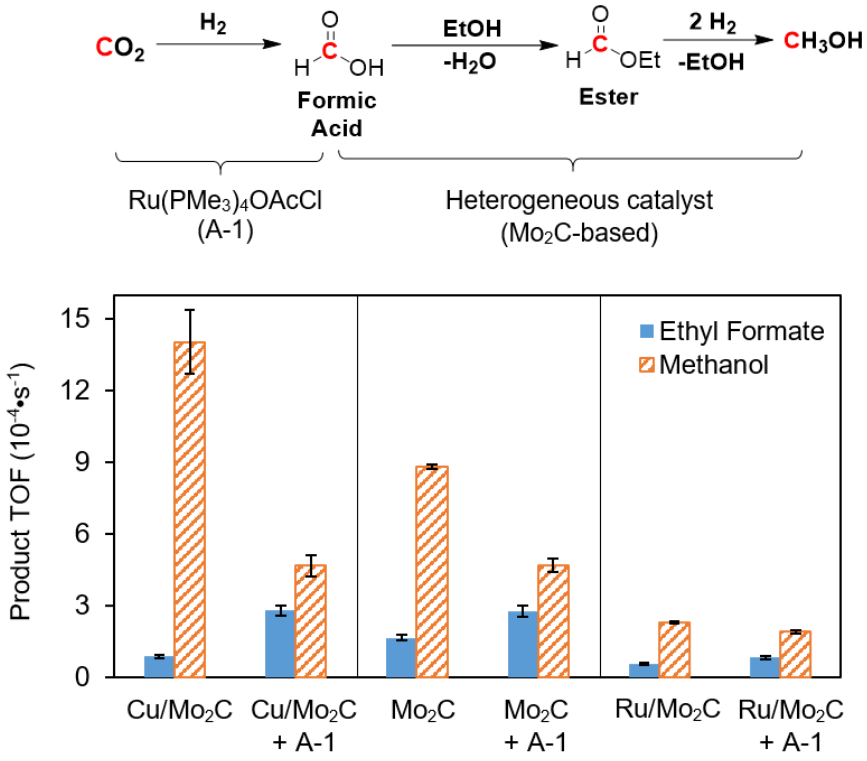

Figure 3.7 Product TONs for CO_2 hydrogenation combining $Ru(PMe_3)_4OAcCl$ catalyst and a series of Mo_2C-based catalysts. Experiments were performed at 135 ℃, 10 bar CO_2, 30 bar H_2 in 3 ml ethanol for 19 h, with 0.01 mmol (active sites) of each catalyst added.

Elemental analysis was also performed on the post-reaction catalyst mixture of $Ru(PMe_3)_4OAcCl$ and Mo_2C to determine the cause of the deactivation. This spent catalyst mixture was recovered and dried under N_2 and washed thoroughly using THF three times to extract/dissolve any Ru-complex that was physically deposited on Mo_2C surface. The amounts of Ru and P (from the phosphine ligand) that remained on the Mo_2C

surface (measured by ICP) are shown in Table 3.1. The results showed a 0.3 wt % Ru and 0.7 wt% P loading on the Mo_2C support, which were equivalent to 11% and 20% of the maximum loadings (assuming the homogeneous complex added to the reactor system was completely deposited). The presence of both Ru and P on the Mo_2C surface suggested the occurrence of chemical deposition/adsorption of Ru species and phosphine ligands onto the Mo_2C surface. Based on the measured site density of 1.6×10^{18} sites/m^2 for Mo_2C, it requires at least 2.7 μmol of active metals and/or ligands (per m^2 of Mo_2C) to completely deactivate Mo_2C (assuming the metal and ligand bind to the Mo_2C active sites at a 1:1 ratio). In this case, the total amount of Ru and phosphine ligand remained on the Mo_2C surface was 2.4 μmol/m^2 Mo_2C, suggesting partial deactivation of Mo_2C. This calculation was consistent with the observation in Figure 3.6. Interestingly, the measured P/Ru ratio was ~7.1, which deviated significantly from the stoichiometric P/Ru ratio of 4 in the $Ru(PMe_3)_4OAcCl$ complex. This deviation suggested phosphine ligand shedding during the reaction.

Table 3.1 Elemental analysis results of post-reaction catalyst mixture of a $Ru(PMe_3)_4OAcCl$ and a Mo_2C catalyst.

Values	Elements on Mo_2C surface	
	Ru	P
wt % (based on Mo_2C)	0.3	0.7
Mol. % (of maximum loading)	11	20
Measured P/Ru molar ratio	7.1 ± 0.4	
Theoretical P/Ru molar ratio	4.0	

3.3.2 Cascade Systems under Lewis Basic Conditions

The cascade system for CO_2 hydrogenation to CH_3OH under basic conditions was recently demonstrated by Rezayee et al. [14] This cascade system involves a series of amide intermediates, with the proposed pathway illustrated in Figure 3.8. This pathway involves a dimethyl amine ($HNMe_2$) cocatalyst and up to three amide intermediates, including dimethyl ammonium dimethylcarbamate (DMC), dimethylformamide (DMF), and dimethyl amine formic acid adduct (DMFA), where DMF is the key intermediate shared by each pathway to produce CH_3OH.

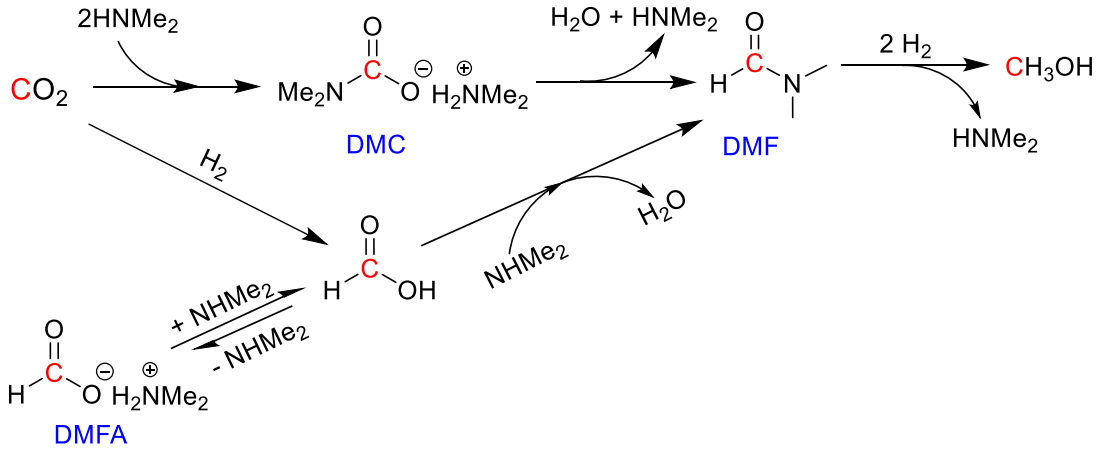

Figure 3.8 Cascade reactions of CO_2 hydrogenation to CH_3OH under basic conditions through amide intermediates. DMC = Dimethylammonium dimethylcabamate, DMF = Dimethyl formamide, and DMFA = Dimethyl amine formic acid adduct. Adapted from [14].

After screening a series of Ru-based complexes for this cascade system, a Ru-Macho catalyst (complex A-3 in Figure 3.3) appeared to be the most active for catalyzing both the formation of amide intermediates and the hydrogenation of DMF to produce CH_3OH. However, a major challenge was that these sub-steps did not share a comparable operating window: The formation of amide intermediates typically required a mild

temperature (< 100 ℃), while the conversion of DMF to CH_3OH needed a higher temperature (> 150 ℃). Therefore, a temperature programmed-process as shown in Figure 3.9 could optimize the yield. The reaction was first performed at 95 ℃ for 18 h and then increased to 155 ℃ for 36 h. The best-performing system afforded a TON of 550 for CH_3OH and a TON of 1870 for the mixture of DMF and DMFA. Given the significant DMF accumulation, it is desirable to consider alternative catalysts to perform the DMF hydrogenation. This need can be potentially fulfilled by introducing heterogeneous catalysts.

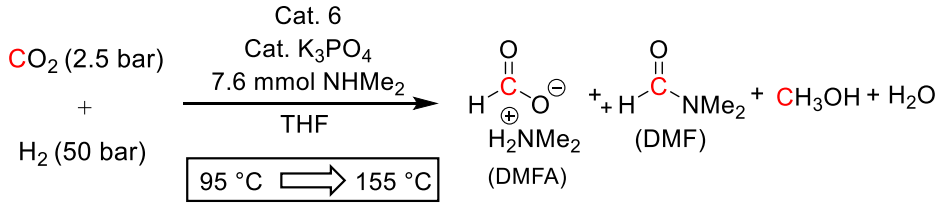

Figure 3.9 A temperature-programmed process for complex A-3/$NHMe_2$-catalyzed hydrogenation of CO_2 to CH_3OH via amide intermediates.

The hydrogenation of DMF was performed over selected heterogeneous catalysts at 135 ℃ and 40 bar H_2, with 0.8 mmol of DMF added as a reactant. The results for CH_3OH production rates and yields are shown in Table 3.2. All the catalysts exhibited activities for DMF hydrogenation to CH_3OH, with the CH_3OH yield ranging from 17-69%. The catalytic activities decreased in the following order: Cu/Zn/Al > Nano Co > Cu/Mo_2C > Ru/Mo_2C (Trial 1-4). This result suggested that Cu and Co were more effective in performing the C-N bond cleavage and hydrogenating the C=O group to produce CH_3OH. However, to be operated under the basic conditions, the heterogeneous catalysts that were active for DMF hydrogenation must also be compatible with the

$HNMe_2$, the cocatalyst required for this pathway. Therefore, one equivalent of $HNMe_2$ (0.8 mmol) was introduced to the DMF hydrogenation to assess its compatibility with the heterogeneous catalysts. The addition of $HNMe_2$ caused severe deactivation of all of the heterogeneous catalysts (Table 3.2, trial 5-8), creating difficulty in introducing these heterogeneous DMF hydrogenation catalysts into amide-based cascade systems unless physical separation is involved. The deactivation pathways and techniques to minimize the deactivation are being explored.

Table 3.2 Dimethyl formamide hydrogenation over a series of heterogeneous catalysts.

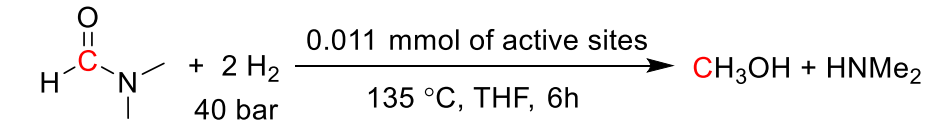

DMF (0.8 mmol)

Trial	Catalysts	Substrate/Additives	CH_3OH TON	CH_3OH Yield (%)
1	Cu/Mo_2C	DMF only	35	49
2	Ru/Mo_2C	DMF only	12	17
3	Nano Co	DMF only	49	69
4	Cu/Zn/Al	DMF only	49	69
5	Cu/Mo_2C	DMF + $HNMe_2$	Trace[a]	0
6	Ru/Mo_2C	DMF + $HNMe_2$	Trace[a]	0
7	Nano Co	DMF + $HNMe_2$	Trace[a]	0
8	Cu/Zn/Al	DMF + $HNMe_2$	9	13

[a] Trace: TON<0.1

Finally, an alternative pathway under basic condition through an alkali formate intermediate was attempted; the pathway is illustrated in Figure 3.10. The strategy is to use a homogeneous catalyst for the hydrogenation of CO_2 to alkali formate, e.g. $HCOO^-K^+$, and a heterogeneous catalyst to hydrogenate $HCOO^-K^+$ to CH_3OH with one equivalent of KOH. Previous work done by Huff et al. [15] has demonstrated that a

Ru(PNN)(CO)(H) catalyst exhibited superior catalytic activity for CO_2 hydrogenation to potassium formate (in the presence of potassium carbonate). The best performing system afforded a total TON of 23,000 at 200 ℃ with 10 bar CO_2 and 30 bar H_2. However, very few studies evaluated the direct hydrogenation of alkali formate to CH_3OH. Dougherty [16] reported the hydrogenation of aqueous sodium formate to CH_3OH with up to a 90% CH_3OH yield using a Co/SiO_2 heterogeneous catalyst at 225 ℃ and 350 bar. This finding encourages the evaluation of other heterogeneous catalysts for the direct hydrogenation of alkali formate.

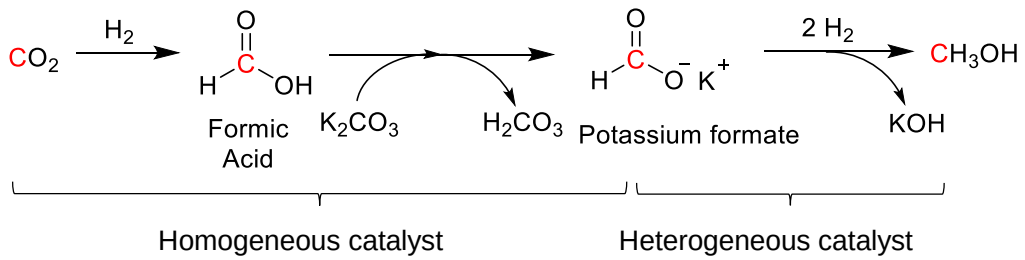

Figure 3.10 Cascade reaction scheme of CO_2 hydrogenation to CH_3OH under basic conditions through an alkali formate intermediate.

A series of heterogeneous catalysts including Cu/Zn/Al, Cu/Mo_2C, and nano Co were tested for the hydrogenation of KOOCH in aqueous solution at 135-200 ℃ with 40 bar H_2, conditions that are comparable with those used for the homogeneous catalysts. However, none of the catalysts exhibited activities for the target reaction. It's possible that the ionic formate possesses a stable C=O group that is difficult to activate at low temperature and H_2 pressure. New catalyst formulations and harsher experimental conditions need to be devised and employed to drive this reaction.

3.4 Factors for Designing Homo-/Heterogeneous Cascade System

The coupled homo-/heterogeneous cascade system has significantly expanded the matrix for catalyst design by utilizing the active sites from both classes of materials; however, the development of this mixed-phase cascade system still requires additional work. One important factor to consider is the compatibility between the homogeneous and heterogeneous materials. For example, we have demonstrated that $Ru(PMe_3)_4OAcCl$ catalyst deactivated Mo_2C, plausibly via chemical deposition, making the cascade system ineffective. However, this deactivation was not identified until the experiments were performed and the results were compared. Protocols for quick screening test could be devised to help identify potential interactions between homogeneous and heterogeneous catalysts. For example, elemental analysis can be performed on the homogeneous and heterogeneous catalyst mixture (washed thoroughly with solvent) to evaluate the significance of interaction between the active species, ligand and the heterogeneous catalyst before performing the more time-consuming activity measurements. Alternatively, this interaction can potentially be removed or minimized by protecting the heterogeneous catalysts via pore size control or anchoring the homogeneous catalysts on a heterogeneous support to physically separate the active species. Anchoring the homogeneous catalysts also improves the recyclability of the catalytic system. Another important factor is to identify a common operating window for each sub-step in the system. In the case of where the optimal thermodynamic conditions for each sub-step are not comparable, reaction conditions (e.g., temperature and pressure) would need to be varied, for example, the temperature-programmed process similar to the one illustrated in Figure 3.8 can be utilized.

3.5 Conclusions

In summary, the study described in this chapter focused on designing homo-/heterogeneous cascade systems for low temperature (≤ 135 °C) CO_2 hydrogenation to CH_3OH. We first targeted a pathway through formic acid and formate ester intermediates under the Lewis acidic condition. The best-performing homogeneous complex, $Ru(PMe_3)_4OAcCl$ (for CO_2 hydrogenation to formic acid), and heterogeneous catalyst Cu/Mo_2C (for formic acid or formate ester hydrogenation to CH_3OH) were combined to form a cascade system. However, the surface interaction between the two materials seemed to cause a severe deactivation on Cu/Mo_2C. We also developed cascade systems under Lewis basic conditions through amide intermediates, including DMC, DMF, and DMFA. Among these intermediates, DMF appeared to be the key one and its hydrogenation would result in enhanced CH_3OH production. We identified several heterogeneous catalysts for the direct hydrogenation of DMF at 135 ℃ and 30 bar H_2, with their activities decreased in the following order: Cu/Zn/Al ≈ Nano Co > Cu/Mo_2C > Ru/Mo_2C. However, these catalysts were not compatible with $HNMe_2$, a cocatalyst required for this pathway and therefore cannot be introduced in designing amide-based cascade systems. Finally, a pathway through the alkali formate intermediate was attempted. However, none of the heterogeneous catalysts studied were viable the for the direct alkali formate hydrogenation to CH_3OH. Future work on identifying new catalysts for alkali formate hydrogenation or modifying reaction conditions are required to enable this reaction.

3.6 References

[1] C.A. Huff, J.W. Kampf, M.S. Sanford, Organometallics 31 (2012) 4643-4645.
[2] C.A. Huff, J.W. Kampf, M.S. Sanford, Chem. Commun. 49 (2013) 7147-7149.
[3] J.M. Lee, Y. Na, H. Han, S. Chang, Chem. Soc. Rev. 33 (2004) 302-312.
[4] C.A. Huff, M.S. Sanford, J. Am. Chem. Soc. 133 (2011) 18122-18125.
[5] S. Wesselbaum, T. vom Stein, J. Klankermayer, W. Leitner, Angew. Chem., Int. Ed. 124 (2012) 7617-7620.
[6] T. vom Stein, T. Weigand, C. Merkens, J. Klankermayer, W. Leitner, ChemCatChem 5 (2013) 439-441.
[7] C.A. Huff, Cascade Hydrogenation of Carbon Dioxide to Methanol, Chemistry, University of Michigan, 2014.
[8] V.V. Mainz, R.A. Andersen, Organometallics 3 (1984) 675-678.
[9] A.J. Miller, D.M. Heinekey, J.M. Mayer, K.I. Goldberg, Angew. Chem., Int. Ed. 52 (2013) 3981-3984.
[10] J.A. Schaidle, N.M. Schweitzer, O.T. Ajenifujah, L.T. Thompson, J. Catal. 289 (2012) 210-217.
[11] J. Patt, D. Moon, C. Phillips, L. Thompson, Catal. Lett. 65 (2000) 193-195.
[12] R.C.V. McGee, S.K. Bej, L.T. Thompson, Appl. Catal., A 284 (2005) 139-146.
[13] J. Falbe, Carbon monoxide in organic synthesis, Springer Science & Business Media, 2013.
[14] N.M. Rezayee, C.A. Huff, M.S. Sanford, J. Am. Chem. Soc. 137 (2015) 1028-1031.
[15] C.A. Huff, M.S. Sanford, ACS Catal. 3 (2013) 2412-2416.
[16] E.F. Dougherty, Hydrogenolysis of formates, 3946563, United States Patent, 1974.

CHAPTER 4

DESIGNING ALL-HETEROGENEOUS CASCADE SYSTEMS FOR CO_2 HYDROGENATION

4.1 Introduction

In Chapter 1, we introduced cascade catalysis as a strategy to advance CO_2 hydrogenation to valuable chemicals. Using CO_2 hydrogenation to CH_3OH as the test reaction, we described several homogeneous and heterogeneous cascade systems; however, the incompatibility among catalysts and reaction species seemed to significantly inhibited the performance. The primary objective of research described in this chapter was to explore the feasibility of low temperature cascade systems for CO_2 hydrogenation to CH_3OH and dimethyl ether (DME) based on heterogeneous catalysts. These all-heterogeneous-based cascade systems hold the promise of providing great compatibility between the catalytic components and easy separation from reactant mixtures.

Conventional processes for CO_2 hydrogenation to CH_3OH are typically carried out in the gas phase over oxide (such as ZnO, ZrO_2, or Al_2O_3) supported Cu catalysts. [1-4] However, these processes are normally carried out at high operating temperatures (230-270 ℃), where CH_3OH production is unfavorable due to the exothermicity of the reaction

Part of this chapter has been published in *ACS Catal.*, **2015**, *5* (3), pp 1717–1725. DOI: 10.1021/cs501656x

(ΔH_{298K} = -49.5 kJ/mol) [2].Lower temperature thermochemical and electro-/photoelectro-chemical methods have also been investigated for the conversion of CO_2 to CH_3OH. Fan et al. employed Cu-based catalysts to hydrogenate CO_2 to CH_3OH through formic acid and ethyl formate intermediates in liquid ethanol at 150-220 ℃.[5] The Cu-Zn oxide catalyst was most active and yielded the maximum CH_3OH selectivity at temperatures near 200 ℃. Yu et al. recently reported the use of a Cu-Zn-Al catalyst for the production of methyl formate from CO_2 in liquid CH_3OH at 150-190 ℃.[6] They proposed that the pathway involved the reaction of a surface formate with CH_3OH to produce methyl formate; however, the conversion of methyl formate to CH_3OH was not reported as the CH_3OH being produced could not be distinguished from the CH_3OH reaction media. A number of electro-/photoelectro-chemical materials, including Cu and carbon nanotube based catalysts, have been developed for CO_2 hydrogenation. [7-11] The electrode nanoarchitecture, cell fabrication and confinement, and material synthesis routes could greatly influence the charge transport and the electrolyte/electrode interactions, which governed the electrochemical catalytic performance. Achieving high selectivities to CH_3OH and high Faradaic efficiencies, however, has proven to be a challenge as reduction potentials for CH_3OH, formic acid, formaldehyde, and H_2 are similar.[12] Semiconductor materials, such as p-type gallium arsenide and p-type indium phosphide have shown promising selectivities to CH_3OH, however, at the expense of high overpotentials. [13, 14]

In this chapter, we targeted several heterogeneous cascade systems to hydrogenate CO_2 through formic acid and/or formate ester intermediates. To design these systems, we evaluated rates and selectivities for the hydrogenation of CO_2, formic acid, and ethyl

formate over several Cu-, Ir-, and Mo_2C-based heterogeneous catalysts. Copper based catalysts have been reported to be active for CO_2 hydrogenation to CH_3OH [2, 15] and are widely used for CH_3OH synthesis from syngas, a mixture of CO and H_2 that often contains small amounts of CO_2 [16]. Dubois et al. [17] and Xu. et al. [18] reported that molybdenum carbides are active for the gas phase hydrogenation of CO_2 at 200-300 ℃, producing mostly CH_4 and CO (~70%), and smaller amounts of CH_3OH (~20%) and other hydrocarbons (up to C_3). More recently, a series of Ir-complexes tethered on high surface area silica support have been reported to be highly active and selective for CO_2 hydrogenation to formic acid [25], making them excellent candidates for the CO_2 to formic acid sub-step catalysts to be included in the cascade system. The results also enabled a prediction of the reaction pathways and key intermediates during CO_2 hydrogenation over the Cu and Mo_2C-based heterogeneous catalysts.

4.2 Experimental

4.2.1 Catalyst Preparation

Several commercially available Cu-based catalysts were acquired and used after pretreatment that is described later. These catalysts included $Cu/ZnO/Al_2O_3$ (Süd-Chemie/Clariant), Cu/Cr_2CuO_4 (Cu Chromite, Strem Chemicals Inc.) and Nano-Cu (QuantumSphere). The $Cu/ZnO/Al_2O_3$ and Cu/Cr_2CuO_4 catalysts will be referred to as the Cu-Zn-Al and Cu-Cr catalysts throughout this chapter. The Nano-Cu catalyst was included to explore the importance of a support material. The high surface area Mo_2C was synthesized using a temperature programmed reaction (TPR) technique. Prior to the synthesis, ~1.3g of ammonium molybdate (AM) precursor, $(NH_4)_6MO_7O_{24}•4H_2O$ (Alfa Aesar) was sieved to 125-250 μm and then loaded into a quartz tube reactor. The AM

was first reduced in H_2 flowing at 400 mL/min, as the temperature was increased from 25 to 350 ℃ in 70 min. Subsequently the material was held at 350 ℃ for 12 h. The reaction gas was then switched to 15% CH_4/H_2 flowing at 400 mL/min; the temperature was increased to 590 ℃ in 1.5 h and maintained at 590 ℃ for 2 h before quenching to room temperature. The Cu/Mo_2C catalyst was prepared using a wet-impregnation method; the protocol for synthesizing this and other carbide supported metals has been described in detail elsewhere.[26] Briefly, the freshly-synthesized Mo_2C was transferred under 15% CH_4/H_2 gas into a beaker containing 70 mL deaerated H_2O (to avoid the oxidation of Mo_2C) with 4.4 mg/L of $Cu(NO_3)_2$ and allowed to interact for 20 h. This method enabled the metal precursor to directly interact with the native Mo_2C surface (as opposed to a passivated material). The resulting catalyst slurry was dried and reduced *in-situ* in the reactor to decompose the nitrate and produce dispersed Cu domains.

4.2.2 Catalyst Characterization

Surface areas of the materials were measured using a Micromeritics ASAP 2010 analyzer based on N_2 physisorption. All of the catalysts were degassed (< 5 mm Hg) at elevated temperatures (Cu-based catalysts at 200 ℃ and Mo_2C-based catalysts at 350 ℃) for 4 h prior to the surface area measurements. The bulk crystalline structures were characterized using X-ray diffraction (Rigaku Miniflex 600) with 2θ ranging from 10 °to 90 ° and a scan rate of 5 °/min. Crystallite sizes were estimated via line broadening analysis using the Scherrer equation.[27] Metal compositions for the Cu/Mo_2C catalyst were determined by inductively coupled plasma optical emission spectrometry (ICP-OES) using a Varian 710-ES analyzer. Solutions for the ICP measurements were prepared by dissolving 15 mg of catalyst in 1.5 mL of aqua regia, consisting of 1.125 mL of HCl

(Fisher Scientific) and 0.375 mL of HNO_3 (70%, Fisher Scientific). The solution was sonicated for 10 mins and left for 10 h to allow complete dissolution. The resulting solution was diluted by a factor of 14 using ultra pure H_2O (18MΩ•cm, Millipore Hilli-Q Advantage A10) to achieve concentrations appropriate for the ICP analysis.

The surface site densities for Mo_2C-based catalysts were determined via CO chemisorption. Prior to the measurements, the Mo_2C and Cu/Mo_2C catalysts were pretreated in 15% CH_4/H_2 for 4 h at 590 ℃, then degassed in He at 600 ℃ for 1 h. The catalysts were cooled to 25 ℃ and repeatedly dosed with 5% CO/He (5 mL loop) until reaching saturation. To quantify the surface site densities for the other Cu-containing catalysts, N_2O decomposition technique was used. The Cu-Zn-Al and Cu-Cr catalysts were reduced in 10% H_2/Ar at 200 ℃ for 4 h, then degassed in He at 210 ℃ for 1 h. The catalysts were then cooled to 60 ℃ and exposed to a flowing mixture of 10% N_2O/He for 2 h. Followed by the N_2O treatment, the sample was purged with He and cooled to 25 ℃. A H_2 temperature-programmed reduction (TPR) was then performed by increasing the temperature from 25 to 400 ℃ in 10% H_2/Ar at 5 ℃/min. The surface site density was determined by quantifying the H_2 consumed during TPR. [28] It should be mentioned that these chemisorbates (N_2O and CO) cannot be used to independently determine the sites for Cu and Mo_2C over the Cu/Mo_2C surface, because N_2O and CO adsorb to both Cu and Mo_2C. However, the use of CO chemisorption will underestimate the active sites of Cu as demonstrated by Evans et al. [29], and slightly overestimate the turnover frequencies over Cu/Mo_2C. Nevertheless, as Cu only accounts for 5.8 wt% (based on ICP analysis) for this catalyst, CO chemisorption still provide the reasonable estimate of the site density.

4.2.3 Reaction Rate and Selectivity Measurements

All of the reactions were performed in a 50 mL Parr Instruments reactor (Micro 5500). The reactor system was equipped with a programmable temperature controller and a magnetic drive for the impeller. The gas phase reactor effluent was analyzed using gas chromatography (Varian 450 with flame ionization and thermal conductivity detectors). Liquid samples (0.4 mL) were periodically withdrawn during the reaction using a dip tube, which was equipped with a 20 μm filter to separate the liquid from the solid catalyst particles. These liquid samples were analyzed offline using gas chromatography (Varian 450 with flame ionization detector). As gas chromatography (GC) showed low responses for formic acid, we utilized an indirect measurement by derivatizing formic acid to ethyl formate, so that it can be easily quantified by GC-FID. The derivatization was performed by combining 0.4 mL product sample and 2 mL solution of 1% p-toluenesulfonic (Sigma Aldrich) acid in 2 mL ethanol in a 20 mL sample vial. The mixture was heated and stirred at 60 ℃ in a silicon oil bath for 6 h to allow the reaction to go to equilibrium. In this case, the p-toluenesulfonic acid could catalyze the esterification to convert formic acid to ethyl formate with ethanol in excess amount. Measurement performed after the derivatization indicated a recovery of 92 ± 7 % of formic acid to ethyl formate.

Prior to the reactions, the commercial Cu-based catalysts were reduced in the reactor vessel at 200 ℃ for 4 h under a flowing mixture of 4% H_2/N_2 (50 mL/min). Due to the pyrophoricity of Mo_2C catalysts, the materials were first treated with deaerated H_2O to form a slurry to avoid bulk oxidation of the materials. The slurry was then quickly transferred to the reactor vessel, where it was dried in H_2 (50 mL/min) at 110 ℃ for 2 h. The dried catalyst was then heated to 300 ℃ at a rate of 4.2 ℃/min and reduced at 300

℃ under H_2 flowing at 100 mL/min for 4 h. The amount of catalyst loaded into the reactor was 200 mg unless otherwise noted.

Solvents for the reactions contained 37.5 mL 1,4-dioxane (anhydrous, Acro Organics) and 10 μL n-decane (Acro Organics) as an internal standard. In this study, 1,4-dioxane was selected as the solvent given its solubility for CH_3OH, relatively high boiling point (101 ℃) and stability/inertness during the reaction. Due to the thermal expansion of the 1,4-doxane solvent [30], the actual solvent volumes during the reaction were estimated to be 39 and 42 ml respectively at 135 and 200 ℃, corresponding to 4% and 12% volume expansion compared to the 37.5 mL solvent loaded at room temperature. The extent of thermal expansion caused by dissolved CO_2 was negligible and did not cause any increase to the total solvent volume [31]. Other solvents including toluene and tetrahydrofuran (THF) were considered but were not utilized due to their low solubility for CH_3OH (0.1 g CH_3OH/100g Toluene) and poor separation for GC analysis. While ethanol was used as the solvent by Fan et al. [5], a major limitation was that ethanol altered the reaction pathway, making it difficult to distinguish the CH_3OH produced from CO_2 or via formate intermediate. Note that we carried out a series of experiments to identify the facilitating effect of ethanol on reaction pathways by adding a small amount of ethanol to the 1,4-dioxane solvent as described later.

For the CO_2 hydrogenation experiments, the reactor was charged with 10 bar CO_2 and 30 bar H_2 through a dip tube after purging the solvents with H_2 for 15 min to remove dissolved oxygen. As we are also interested in combining heterogeneous and homogeneous catalysts to generate a cascade system for CO_2 hydrogenation, the reactions were carried out at 135 ℃, a temperature where the homogeneous catalysts reported by

Huff et al. were active [32]. Under these conditions, solubilities for CO_2 and H_2 are approximately 1.5 and 0.14 mol/L, respectively. [33, 34] For selected reactions, 2 mL ethanol was added to 35.5 mL 1,4-dioxane. For the formic acid and ethyl formate hydrogenation experiments, 3 mmol formic acid (98%, Alfa Aesar) or 0.6 mmol ethyl formate (99.9%, Acro Organics) was added to the solvent. The reactant mixture was purged with 99.9% H_2 (for 15 mins) to remove any oxygen and was then charged with 30 bar H_2. The reactor was heated at a rate of 5 ℃/min from room temperature to 135 ℃, and then agitated at a constant rate of 300 rpm, which indicated the start of the reaction. The reactor was maintained at 135 ℃ through the reaction. Reaction rates for CO_2, formic acid, and ethyl formate hydrogenation were calculated based on formation rates for the products (on a C_1 basis) or consumption rates for the reactants. Carbon balances closed to within ±8% for all the experiments. The turnover frequencies (TOF) were determined by normalizing the rates by the surface site densities. The selectivity is defined as the molar ratio of a specific product over the total products.

4.3 Results

4.3.1 Surface and Physical Properties

The surface area, surface site density, Cu content, and Cu crystallite size for the catalysts are listed in Table 4.1. The Mo_2C and Cu/Mo_2C catalysts had surface areas in excess of 100 m^2/g; the commercial Cu-Zn-Al and Cu-Cr catalysts possessed moderate surface areas; and the Nano-Cu material had a relatively low surface area, as expected. The decreased surface area for the Cu/Mo_2C catalyst (135 m^2/g) compared to the Mo_2C catalyst (150 m^2/g) was likely due to partial blocking of pores in the Mo_2C by Cu nanoparticles. Nevertheless, the surface area for the Cu/Mo_2C catalyst was comparable

to those reported for other Mo_2C supported metals synthesized using similar conditions (e.g., Pt/Mo_2C with 133 m^2/g [23]). The surface site densities for all of the materials were in the range of 1.3-2.4×10^{18} sites/m^2 or 13-24% surface coverage assuming 10^{19} total sites/m^2.

Table 4.1 Surface and physical properties for the Cu and Mo_2C-based catalysts.

Catalysts	Surface Area (m^2/g)	Surface Site Density (μmol/g)	Cu Content (wt %)[a]	Average Cu Crystallite Size (nm)
Nano-Cu	5.5	--	100	254
Cu-Zu-Al	60	192[b]	33	89
Cu-Cr	46	184	36	163
Mo_2C	151	406	0	NA
Cu/Mo_2C	135	298	5.8	34

[a] Cu contents for the Cu-Zn-Al, Cu-Cr and Nano-Cu catalysts were obtained from vendor specifications.
[b] From Ref [29].

Diffraction patterns for the catalysts are illustrated in Figure 4.2. The pattern for the Cu-Zn-Al catalyst clearly indicated the presence of Cu and ZnO crystallites, while the Al_2O_3 phase was amorphous by X-ray diffraction. The XRD pattern for the Cu-Cr catalyst contained peaks for Cu; there was also a peak at $54^\circ 2\theta$ that was consistent with the presence of CuO within the Cu-Cr (Cu/Cr_2CuO_4) catalyst. The pattern for the Nano-Cu material showed intense Cu peaks and confirmed its phase purity. As expected, the Cu crystallite sizes for the Nano-Cu material were the largest among the other Cu containing catalysts due to the lack of Cu dispersion. The bulk Mo_2C and Cu/Mo_2C materials exhibited peaks for β-Mo_2C and α-MoC_{1-x},[28] with similar proportions of each phase based on the relative peak areas. Since the overall Mo to C ratio approaches two, these materials will be referred to as "Mo_2C". No peaks were observed for molybdenum oxides

(MoO_2 or MoO_3) in patterns for the carbides, indicating complete carburization during the synthesis. For the Cu/Mo_2C material, there was a broad peak at 41 °2θ corresponding to Cu (111). This result was consistent with a high degree of dispersion for the Cu crystallites on the Mo_2C surface. Table 4.1 lists crystallite sizes for all of the catalysts.

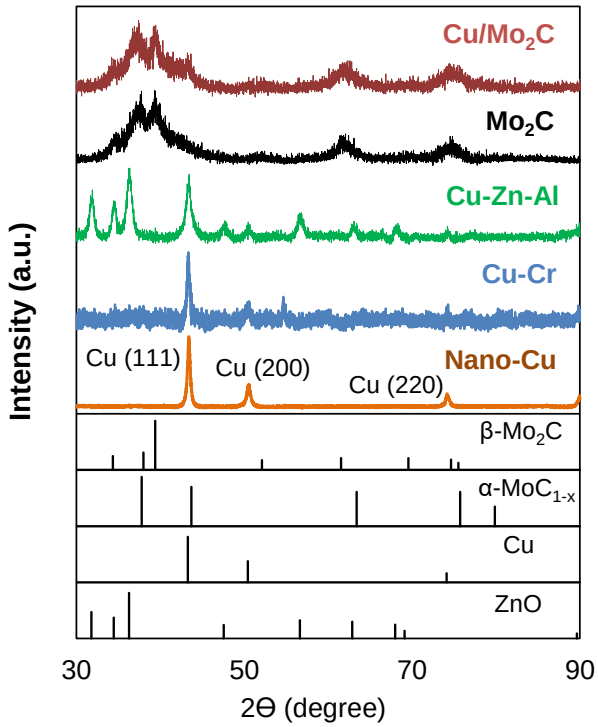

Figure 4.1 X-ray diffraction patterns for the Cu and Mo_2C-based catalysts. β-Mo_2C (JCPDF 00035-0787), α-MoC1-x (JCPDF 00-015-0457), Cu (JCPDF 01-085-1326), ZnO (JCPDF 01-080-3004).

4.3.2 Reaction Rates and Selectivities

4.3.2.1 CO_2 Hydrogenation

With the exception of the Nano-Cu catalyst, all of the materials were active for the conversion of CO_2. The rates and selectivities after 2 h of reaction are listed in Table 4.2. The Cu-Zn-Al and Cu/Mo_2C catalysts possessed the highest rates, CH_3OH selectivities, and CH_3OH production TOFs. Given the system detection limits (5 ppm), products from

the Nano-Cu catalyst would have easily been detected if rates per surface area for this material were of the same order as those for the other catalysts. The lack of activity could be a consequence of support effects. [15, 35, 36] There is significant literature suggesting the need for an oxide to function synergistically with Cu. [1, 3, 37] The importance of the support is also reflected in the different TOFs for the Cu-Zn-Al, Cu-Cr, and Cu/Mo_2C catalysts. The Mo_2C catalyst was slightly more active than the Cu-Cr catalyst but was much less active and selective than the Cu-Zn-Al and Cu/Mo_2C catalysts, producing significant amounts of CO and some CH_4. In comparing the Mo_2C and Cu/Mo_2C catalysts, we observed that the addition of Cu to Mo_2C resulted in a significant increase in activity and a reduction in the CO and CH_4 selectivities.

Table 4.2 CO_2 hydrogenation over Cu and Mo_2C-based catalysts.[a]

Catalysts	CO_2 Conv. Rate		Selectivity %			CH_3OH Production Rate ($\mu mol/m^2/h$)	CH_3OH Production TOF ($s^{-1} \bullet 10^4$)
	($\mu mol/g_{cat}/h$)	($\mu mol/m^2/h$)	CH_3OH	CH_4	CO		
Nano-Cu	--	--	--	--	--	--	--
Cu-Zn-Al	168	2.8	100	0	0	2.8	2.4
Cu-Cr	29	0.6	88	0	12	0.54	0.38
Mo_2C	83	0.5	79	5.3	16	0.43	0.44
Cu/Mo_2C	225	1.7	93	2.6	4.1	1.6	2.0

[a] 135 °C, 10 bar CO_2, 30 bar H_2, 37.5 mL 1,4-dioxane, rates calculated at 2 h.

To investigate the potential of formic acid and formate ester intermediates, a series of experiments were carried out where ethanol (to facilitate esterification of formic acid to ethyl formate), formic acid, or ethyl formate were added to the CO_2/H_2 reactant. Ethyl formate was used instead of methyl formate to allow easy distinction of CH_3OH produced during CO_2 hydrogenation from that produced during formate hydrogenation. The

introduction of 50 mmol of ethanol (2 mL) to the CO_2 and H_2 reactants resulted in the formation of ethyl formate and CH_3OH for all of the catalysts as shown in Table 4.3. The overall CO_2 conversion rates were significantly enhanced after adding ethanol. The increase in the CO_2 conversion rate was greatest for the Cu-Cr catalyst, which exhibited high selectivity and formation rate to ethyl formate. This finding suggested that formate hydrogenation to CH_3OH was rate limiting for this catalyst. For the other catalysts, the introduction of ethanol caused a significant increase in the CH_3OH formation rate. The increased CH_3OH formation rates on the addition of ethanol are consistent with formic acid formation being the rate limiting step. Indeed, as shown in Figure 4.2, the addition of formic acid (3 mmol) caused a significant increase in the CH_3OH production rate for the Cu/Mo_2C catalyst. Finally, we note that the addition of ethyl formate (2.5 mmol) also caused an increase in the CH_3OH production rate, although the increase was not as substantial as when formic acid was added to the CO_2/H_2 reactant; ethanol was also observed confirming ethyl formate hydrogenation.

Table 4.3 CO_2 hydrogenation in the presence of ethanol over Cu and Mo_2C-based catalysts.[a]

Catalysts	CO_2 Conv. Rate		Selectivity %			HCO_2Et[b] Production		CH_3OH Production	
	(μmol/ g_{cat}/h)	(μmol /m^2/h)	HCO_2Et[b]	CH_3OH	CH_4 +CO	Rate (μmol /m^2/h)	TOF (s^{-1}•10^4)	Rate (μmol /m^2/h)	TOF (s^{-1}•10^4)
Cu-Zn-Al	325	5.4	36	61	3.5	1.9	1.7	3.3	2.9
Cu-Cr	269	5.8	97	3.0	0	5.7	3.9	0.18	0.12
Cu/Mo_2C	458	3.4	29	66	4.8	1.0	1.2	2.2	2.8

[a] 135 °C, 10 bar CO_2, 30 bar H_2, 2mL ethanol, 35.5 mL 1,4-dioxane, rates calculated at 2h.
[b] HCO_2Et = ethyl formate.

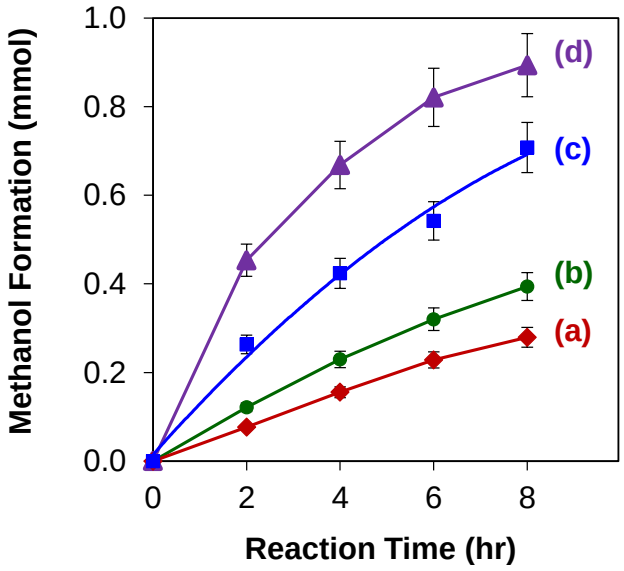

Figure 4.2 Methanol formation during CO_2 hydrogenation over the Cu/Mo_2C catalyst with (a) CO_2 and H_2, (b) CO_2 and H_2 with 50 mmol ethanol, (c) CO_2 and H_2 with 2.5 mmol ethyl formate, and (d) CO_2 and H_2 with 3 mmol formic acid. The experiments were carried out at 135 ℃ with 10 bar CO_2, 30 bar H_2, and 35.5-37.5 mL 1,4-dioxane.

Since the introduction of formic acid during the CO_2 hydrogenation resulted in a substantial increase in CH_3OH formation over the Cu/Mo_2C catalyst, it is desirable to identify a catalyst that selectively converts CO_2 to formic acid that can be combined with Cu/Mo_2C to further enhance the CH_3OH production. In identifying such catalyst, we collaborated with Hicks Group at University of Notre Dame, Chemical Engineering. The Hicks Group examined a series of Ir complexes tethered on high surface area silica support, e.g. SBA-15 for the CO_2 hydrogenation to formic acid at low temperatures as shown in Figure 4.3. The best performance was attained using a bidentate Ir-PN/SBA-15 (complex D-2 in Figure 4.3), reaching a TOF of 3.3 s^{-1} for formic acid formation at 20 bar H_2, 20 bar CO_2, 20 mL H_2O and 2 mL NEt_3 (triethyl amine), with a 10 μmol Ir loading [25]. This is by far the most active system reported in the literature for CO_2 hydrogenation

to formic acid over heterogeneous catalysts. This high activity appears to be attributed to both the phosphine ligand, which activates CO_2, and the amine group, which stabilizes CO_2, in the bidentate structure of this catalyst.

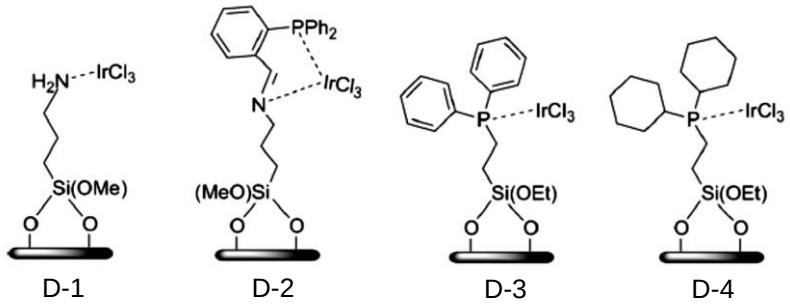

Figure 4.3 Structures of Ir-complexes tethered on SBA-15 support studied for CO_2 hydrogenation to formic acid. Taken from [25].

We obtained the high-performing Ir-PN/SBA-15 catalyst from Hicks Group and evaluated its activity at 10 bar CO_2, 30 bar H_2, 115 ℃ and 37.5 mL 1,4-dioxane, the comparable conditions used for the CO_2 hydrogenation in our reaction system. The Ir-PN/SBA-15 catalyst exhibited a total TOF of 5.2×10^4 s^{-1} and a selectivity of 100% to formic acid. The formic acid production as a function of reaction time can be found in Figure 4.4a. Note that the TOF achieved at the current condition is about 3 orders of magnitude lower compared to the TOF obtained in the aqueous environment with the addition of NEt_3 at 20 bar CO_2 and 20 bar H_2 as reported by Xu et. al [25]. We believe the presence of NEt_3 played a significant role in driving the equilibrium of CO_2 conversion to formic acid by forming a HCOOH• NEt_3 adduct [38], which enhanced the overall the formic acid formation rate. The differences in CO_2 or H_2 solubilities in each solvent (H_2O vs. 1,4-dioxane) can also contribute to the difference in the catalytic performance.

4.3.2.2 Formic Acid Hydrogenation

All of the catalysts were active for the conversion of formic acid, although CO_2 was the principal product. Rates and selectivities after 2 h of reaction are listed in Table 4.4. The highest surface area specific rate was observed for the Nano-Cu catalyst but the formic acid was almost exclusively converted to CO_2. The conversion of formic acid to CO_2 ($\Delta G_{135\,℃}$ = -72 kJ/mol) is thermodynamically more favorable than the production of CH_3OH ($\Delta G_{135\,℃}$ = -46.3 kJ/mol) under the reaction conditions that were employed.[39] Activities for the Cu/Mo_2C and Cu-Zn-Al catalysts were similar; the CH_3OH selectivity for the Cu/Mo_2C catalyst was slightly higher than that for the Cu-Zn-Al catalyst. As anticipated, the Mo_2C catalyst was less active and less selective towards CH_3OH production compared to the Cu/Mo_2C catalyst. Both of these catalysts produced methyl formate, CH_4, and CO. The enhanced CH_3OH selectivity for the Cu/Mo_2C catalyst compared to the Mo_2C and Nano-Cu catalysts individually suggested a synergy between the Mo_2C and Cu. The Cu-Cr catalyst was the least active and selective for CH_3OH production from formic acid.

Table 4.4 Formic acid hydrogenation over Cu and Mo_2C-based catalysts.[a]

Catalysts	Formic Acid Conv. Rate		Selectivity %					CH_3OH Production Rate ($\mu mol/m^2/h$)	CH_3OH Production TOF ($s^{-1} \bullet 10^4$)
	(mmol/g_{cat}/h)	($\mu mol/m^2/h$)	CH_3OH	HCO_2Me[b]	CH_4	CO	CO_2		
Nano-Cu	1.7	300	4.6	0.0	0.0	0.0	95	14	--
Cu-Zn-Al	2.1	36	27	0.0	0.0	0.0	73	9.7	8.4
Cu-Cr	3.8	84	1.8	0.0	0.0	0.3	98	1.5	1.0
Mo_2C	3.4	22	15	5.2	0.8	2.7	77	3.3	3.4
Cu/Mo_2C	3.7	28	30	8.2	0.5	1.9	59	8.3	11

[a] 135 °C, 30 bar H_2, 3 mmol formic acid, 37.5 mL 1,4-dioxane, rates calculated at 2h.
[b] HCO_2Me = methyl formate.

4.3.2.3 Ethyl Formate Hydrogenation

With the exception of the Nano-Cu catalyst, all of the other catalysts were similarly active. The reaction rates and selectivities after 2 h of reaction are shown in Table 4.5. Again we used ethyl formate instead of methyl formate to allow easy distinction of the products. It is interesting to note that the Cu-Cr catalyst was nearly as active as the other supported Cu catalysts. Recall that the Cu-Cr catalyst was highly active for ethyl formate formation from CO_2 in the presence of ethanol but was relatively inactive for CH_3OH formation from CO_2 (with and without ethanol) or formic acid hydrogenation. These results suggested that CO_2 inhibited the conversion of ethyl formate to CH_3OH over the Cu-Cr catalyst. This finding will be considered in the selection of catalysts for the cascade system.

Table 4.5 Ethyl formate hydrogenation over Cu and Mo_2C-based catalysts.[a]

Catalysts	Ethyl Formate Conv. Rate		Selectivity %				CH_3OH Production Rate ($\mu mol/m^2/h$)	CH_3OH Production TOF ($s^{-1} \bullet 10^4$)
	($\mu mol/g_{cat}/h$)	($\mu mol/m^2/h$)	CH_3OH	C_2H_5OH	CH_4	CO_2		
Nano-Cu	79	14	37	54	0	9.2	10	--
Cu-Zn-Al	598	10	25	55	0	20	4.4	3.8
Cu-Cr	554	12	27	52	0	21	6.0	4.1
Mo_2C	889	5.9	21	53	1.9	24	2.3	2.3
Cu/Mo_2C	837	6.2	33	51	0.6	16	3.7	4.6

[a]135 °C, 30 bar H_2, 0.6 mmol ethyl formate, 37.5 mL 1,4-dioxane, rates calculated at 2h.

Stoichiometrically, the hydrogenation of ethyl formate should produce equal amounts of CH_3OH and ethanol. CH_3OH to ethanol ratios for the catalysts ranged from 0.4-0.7, lower than the stoichiometric value of unity. These results indicated that side reactions occurred. A plausible source for the excess ethanol is the hydrolysis of ethyl formate. This reaction would produce ethanol and formic acid, a likely source of the CO_2

produced by most of the catalysts. In fact, the excess ethanol was comparable to the amount of CO_2 produced. In addition to CH_3OH, ethanol and CO_2, small amounts of CH_4 were produced over the Mo_2C containing catalysts. CH_4 formation was also observed for these catalysts during CO_2 and formic acid hydrogenation. A more thorough analysis and the performance of other catalysts for ethyl formate hydrogenation are detailed in Chapter 2 of this dissertation.

4.3.2.4 Cascade CO_2 Hydrogenation

Our primary objective is to design cascade systems for the hydrogenation of CO_2 based on heterogeneous catalysts. To this end, we identified catalysts that would facilitate the production of formic acid and ethyl formate from CO_2 as well as the catalysts that would perform the subsequent formic acid or ethyl formate hydrogenation to CH_3OH. The following paragraphs will discuss the results of combining the promising catalysts identified from each sub-step for the cascade CO_2 hydrogenation.

(i) CO_2 hydrogenation to CH_3OH through formic acid intermediate

We aim to first demonstrate the feasibility of an all-heterogeneous cascade system through a two-step pathway via formic acid intermediate for the CO_2 to CH_3OH. Based on the catalyst screening results in section 4.3.2, we selected an Ir-PN/SBA-15 catalyst for the conversion of CO_2 to formic acid and a Cu/Mo_2C catalyst for the hydrogenation of formic acid to CH_3OH. Catalyst loadings of 50 mg Ir-PN/SBA-15 and 85 mg of Cu/Mo_2C catalysts were used to match the rate of formic acid formation and consumption from each step. The experiments were performed at 115 ℃, as the Ir-PN/SBA catalyst was found to decompose (with black Ir particle formation) at temperatures > 120 ℃. The product TOF of the reactants and products over each individual catalytic system and the cascade system are

shown in Table 4.6. The Ir-PN/SBA-15 alone only produced formic acid, suggesting it is a single site catalyst. The Cu/Mo_2C catalyst produced mainly CH_3OH and a small quantify of CH_4, consistent with product distribution shown in Section 4.3.2.1 (Table 4.2). The catalyst mixture of Ir-PN/SBA-15 and Cu/Mo_2C produced formic acid (42%) and CH_3OH (58%) and minor amount of CH_4. The main purpose of creating this cascade system is to produce CH_3OH more efficiently. From Table 4.6, the CH_3OH production rate from the cascade system is ~ 4.1 times of that from the mathematical additive of each individual catalytic system, indicating the two catalysts work cooperatively through the formic acid intermediate to produce CH_3OH from CO_2. Interestingly, the overall CO_2 conversion TOF has also improved slightly by ~10% over the cascade system compared to each single catalytic system. This finding indicated that the immediate consumption of formic acid by Cu/Mo_2C to produce CH_3OH helped drive the equilibrium of formic acid formation from CO_2, therefore enhancing the overall CO_2 conversion rate.

Table 4.6 Product TOFs for CO_2 hydrogenation over Ir-PN/SBA-15 and Cu/Mo_2C catalysts.[a]

Catalysts	TOF (10^{-4}•s^{-1})				Selectivity (%)		
	CO_2	HCOOH	CH_3OH	CH_4	HCOOH	CH_3OH	CH_4
Ir-PN/SBA-15	5.2	5.2	0.00	0.00	100	0	0
Cu/Mo_2C	0.9	0.00	0.9	0.01	0.0	98.7	1.3
Ir-PN/SBA-15 + Cu/Mo_2C	6.8	3.0	3.7	0.04	44.5	54.9	0.6

[a] 115 ℃, 10 bar of CO_2, 30 bar of H_2, 37.5 mL of 1,4-dioxane, TOF calculated at 2 h.

The product profiles as a function of time over each individual and cascade catalytic systems are shown in Figure 4.4. Over the cascade system, the products clearly exhibited the profiles of formic acid being consumed as an intermediate and additional CH_3OH being produced with enhanced rate. This observation further confirmed that Ir-PN/SBA-15 and

Cu/Mo_2C work in concert through formic acid intermediate to promote the cascade CO_2 hydrogenation to CH_3OH. Running this cascade system at longer time (> 8h) or increasing the Cu/Mo_2C loading should result in a complete consumption of formic acid, increasing the overall methanol yield.

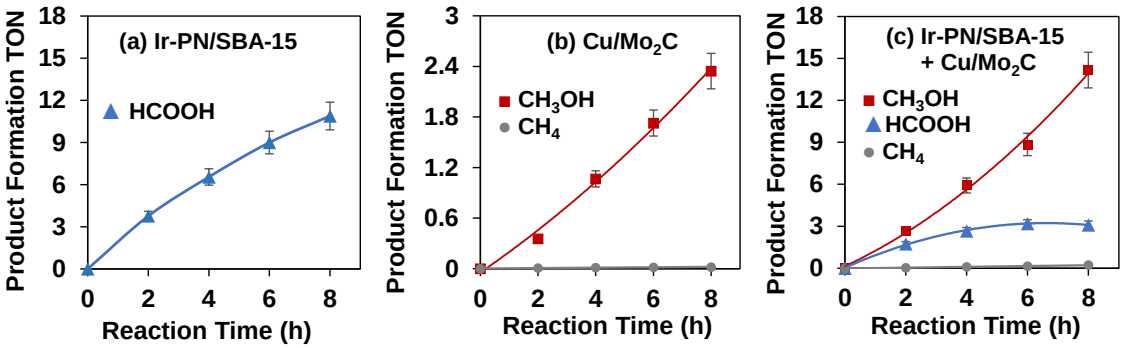

Figure 4.4 Products formation (▲formic acid, ■ CH_3OH, ● methane) during CO_2 hydrogenation over (a) Ir-PN/SBA-15, (b) Cu/Mo_2C, and (c) a mixture of the Ir-PN/SBA-15 and Cu/Mo_2C catalysts. The experiments were carried out at 115 ℃ with 10 bar CO_2, 30 bar H_2, 30 bar H_2, and 37.5 mL 1,4-dioxane with catalysts loadings of 50 mg Ir-PN/SBA-15 and 85 mg Cu/Mo_2C.

(ii) CO_2 hydrogenation to CH_3OH through ethyl formate intermediate

Based on the activity measurement in Section 4.3.2.1, the addition of ethanol reagent seemed to alter the reaction pathway by forming an ethyl formate intermediate via the esterification step. These results encouraged us to design another heterogeneous-based cascade system via the ethyl formate intermediate for producing CH_3OH from CO_2. In the presence of ethanol, the Cu-Cr catalyst was highly active and selective for CO_2 hydrogenation to ethyl formate. This catalyst was not, however, active for ethyl formate hydrogenation in the presence of ethanol. Several of the catalysts were active for the hydrogenation of ethyl formate in the presence of ethanol, and we selected the Cu/Mo_2C catalyst due to its high rate and selectivity to CH_3OH. Equal masses of the Cu-Cr and

Cu/Mo_2C catalysts were used for the cascade system given their similar rates for the hydrogenation of CO_2 to ethyl formate and ethyl formate to CH_3OH, respectively.

The CH_3OH and ethyl formate produced as a function of time for the individual Cu-Cr and Cu/Mo_2C catalysts and the mixture of the two in the presence of ethanol are illustrated in Figure 4.5. Over the Cu/Mo_2C catalyst (Figure 4.5a), CH_3OH was the major product (~74% selectivity), accompanied by a smaller amount of ethyl formate (~20%). The improved CH_3OH formation rate (after introducing ethanol) indicated that ethyl formate was an intermediate. In contrast, for the Cu-Cr catalyst (Figure 4.5b), ethyl formate was the principal product (~ 97% selectivity), and its subsequent hydrogenation to CH_3OH was inhibited. For a mixture of the Cu/Mo_2C and Cu-Cr catalysts (Figure 4.5c), CH_3OH production has enhanced by ~60%, while the formation of ethyl formate decreased by a similar amount, compared to the combined amounts for the individual catalysts. These results suggested that the Cu/Mo_2C and Cu-Cr catalysts worked cooperatively to hydrogenate CO_2 to CH_3OH via the ethyl formate intermediate. The cascade system achieved a CO_2 conversion rate of 416 $\mu mol/g_{cat}/h$, and CH_3OH and ethyl formate selectivities of 77% and 20% respectively after 24 h of reaction. The corresponding CH_3OH TOF (calculated at 2 h) for the system is 4.7×10^{-4} s^{-1}.

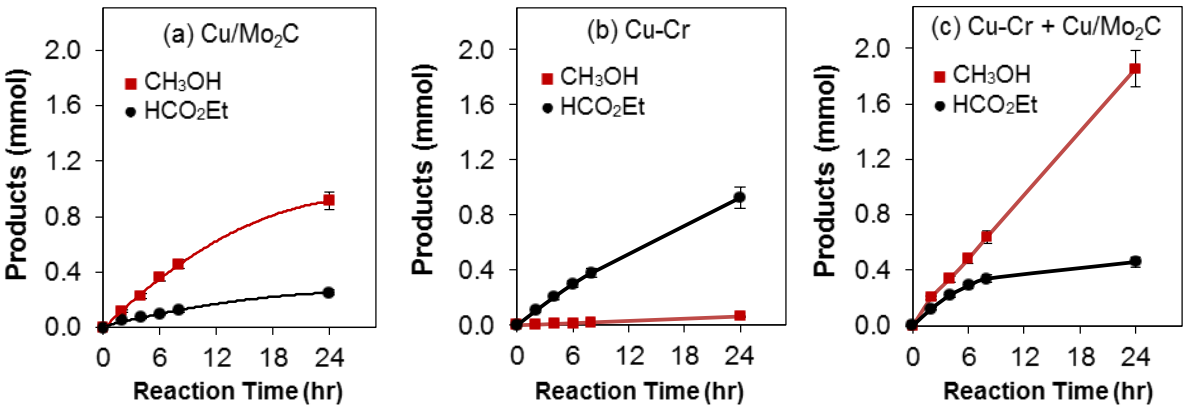

Figure 4.5 Products formation (■ CH_3OH, ● Ethyl formate) during CO_2 hydrogenation in the presence of ethanol (2 mL) over the (a) Cu-Cr, (b) Cu/Mo_2C, and (c) a mixture of the Cu-Cr and Cu/Mo_2C catalysts. The experiments were carried out at 135 ℃ with 10 bar CO_2, 30 bar H_2, and 35.5 mL 1,4-dioxane.

The demonstration of low temperature (135 ℃) Cu-Cr: Cu/Mo_2C heterogeneous cascade system for CO_2 hydrogenation inspired the investigation of a similar system at higher temperature. Therefore, we performed CO_2 hydrogenation at 200 ℃ in the presence of ethanol over Cu-Cr and Cu/Mo_2C catalysts (200 mg each) both individually and over the catalyst mixture to examine how temperature influences the reactivity and the cooperation between the catalysts. The product distribution as a function of time is displayed in Figure 4.6. Clearly, over the Cu/Mo_2C catalyst, CH_3OH was the predominant product; while ethyl formate was an insignificant intermediate and was almost completely consumed after 24 h. Meanwhile, the addition of ethanol reagent only resulted in a slight increase in CH_3OH formation compared to the CH_3OH formation in a control run where no ethanol was introduced (shown as red dash line in Figure 4.6a). These results suggested that for Cu/Mo_2C catalyst, the dominant reaction pathway was likely through the formic acid or a surface formate intermediate, where the ester intermediate did not contribute much to the CH_3OH formation. In contrast, over the Cu-Cr catalyst, CH_3OH and ethyl

formate were first produced in comparable amounts; the CH_3OH formation kept increasing while the ethyl formate was gradually consumed as the reaction time increased. We also observed that by adding ethanol, the amount of CH_3OH formation rate increased by ~100%; this result suggested that CO_2 hydrogenation to CH_3OH proceeded both with and without ethyl formate intermediate, and each pathway contributed almost equally to produce CH_3OH. Recall that ethyl formate hydrogenation was inhibited in the presence of CO_2 over the Cu-Cr catalyst at 135 ℃; this finding likely suggested that this inhibition became less significant at 200 ℃. The cascade system containing both Cu/Mo_2C and Cu-Cr exhibited a CH_3OH production rate that was 30% higher than the additive from each individual catalytic system, indicating the two catalysts still worked cooperatively through the ethyl formate intermediate. However, as ethyl formate could be consumed over each catalyst individually, the enhancement by utilizing cascade system at 200 ℃ (30%) was not as significant as that at 135 ℃ (60%).

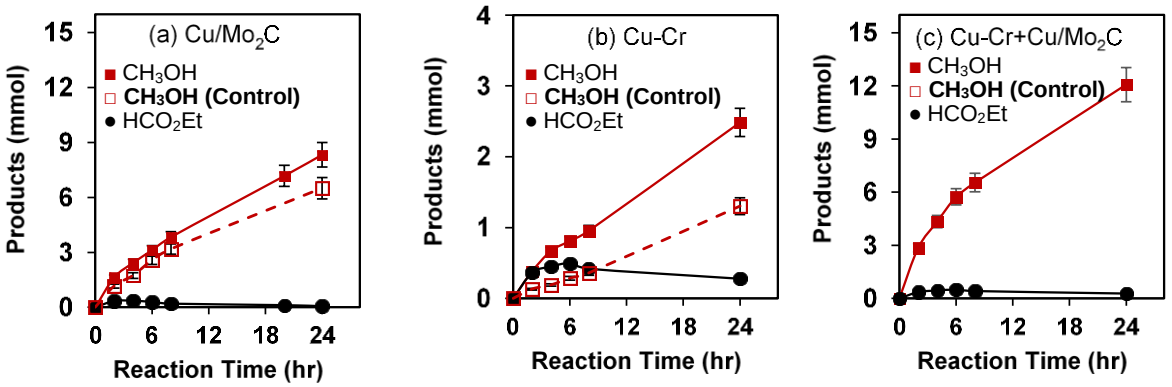

Figure 4.6 Products formation (■ CH_3OH in the presence of ethanol, □ CH_3OH in the absence of ethanol ● Ethyl formate) during CO_2 hydrogenation over (a) Cu-Cr, (b) Cu/Mo_2C, and (c) a mixture of the Cu-Cr and Cu/Mo_2C catalysts. The experiments were carried out at 200 ℃ with 10 bar CO_2, 30 bar H_2, and 35.5 mL 1,4-dioxane with 200 mg of each catalyst.

The CO_2 conversion TOF and the product selectivity are summarized in Table 4.7 for the Cu-Cr and/or Cu/Mo_2C individually and as a mixture. By increasing the temperature from 135 ℃ to 200 ℃, the overall CO_2 TOF has increased by ~ 12 times, which corresponded to an activation energy ($E_{A,\ app}$) of 63.7 kJ/mol. This value was comparable with the E_A reported in the literature for a gas phase CO_2 hydrogenation at 220 – 280 ℃ [1]. In addition to CH_3OH and ethyl formate, we also observed the formation of C_2-C_4 hydrocarbons whenever Cu/Mo_2C was present at 200 ℃. Recall that only small amount of CH_4 was produced at 135 ℃.

Table 4.7 CO_2 hydrogenation over Cu-Cr and/or Cu/Mo_2C catalysts in the presence of ethanol.

Catalysts	Temp (℃)	CO_2 TOF (10^{-4}•s^{-1})	Selectivity (%)[b]						
			EF	MeOH	CO	CH_4	C_2	C_3	C_4
Cu-Cr	200	36.4	36.4	38.1	25.4	0.1	0.0	0.0	0.0
Cu/Mo_2C	200	65.2	15.0	70.9	5.6	5.3	2.1	0.8	0.3
Cu-Cr + Cu/Mo_2C	200	106.7	8.4	75.9	4.4	7.2	2.8	0.9	0.3
Cu-Cr + Cu/Mo_2C	135	8.1	36.6	61.1	1.3	1.0	0.0	0.0	0.0

[a] 10 bar CO_2, 30 bar H_2, 35.5 mL 1,4-dioxane, rates calculated at 2h.
[b] EF = Ethyl formate, MeOH = CH_3OH, C_2 = C_2H_4 + C_2H_6, C_3 = C_3H_6 + C_3H_8, C_4 = C_4H_8 + C_4H_{10}

The distribution of only CO and hydrocarbons over the Cu-Cr and/or Cu/Mo_2C catalysts individually and as a mixture are compared in Figure 4.7a. The Cu-Cr catalyst produced primarily CO with negligible amounts of hydrocarbons. By contrast, the Cu/Mo_2C catalyst produced less CO compared to Cu-Cr and a series of hydrocarbons ranging from C_1-C_4 in comparable amounts. Interestingly, the hydrocarbon formation over the catalyst mixture was more significant than that from a single Cu/Mo_2C catalyst. We hypothesize that this enhancement in hydrocarbon formation was a consequence of CO

acting as an intermediate to C_1-C_4 hydrocarbons, where the substantial amount of CO produced over Cu-Cr could be converted by Cu/Mo_2C to give rise to higher hydrocarbon formation. The product profile in Figure 4.7b also clearly showed the trend of CO being consumed as an intermediate while the production of C_1-C_4 kept increasing over the reaction time. The possibility of CO acting as the intermediate to C_1-C_4 hydrocarbons were evaluated experimentally in Chapter 5.

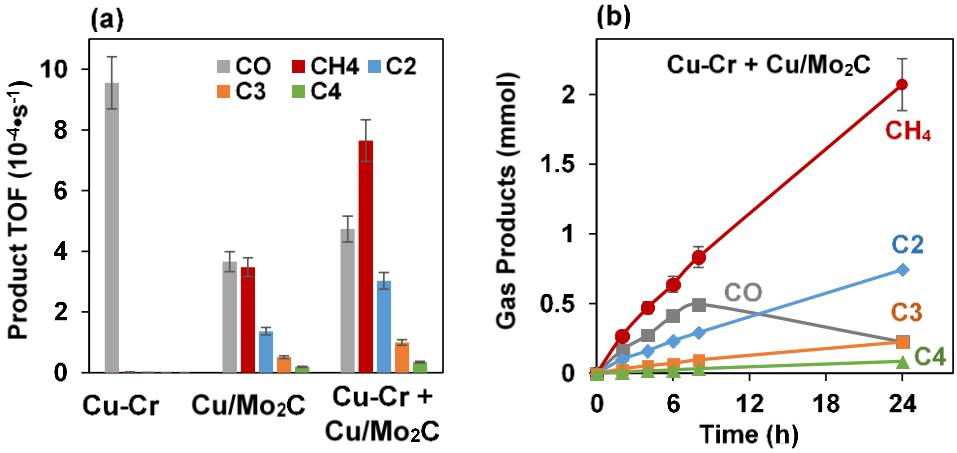

Figure 4.7 CO and hydrocarbon formation (■ CO, ■ CH_4, ■ C_2H_4 + C_2H_6, ■ C_3H_6 + C_3H_8, ■ C_4H_8 + C_4H_{10}) during CO_2 hydrogenation in the presence of ethanol (2 mL). (a) Comparison of product distributions over Cu-Cr, Cu/Mo_2C, and the mixture, (b) product profiles as a function of reaction time over Cu-Cr and Cu/Mo_2C mixture. The experiments were carried out at 200 ℃ with 10 bar CO_2, 30 bar H_2, and 35.5 mL 1,4-dioxane.

(iii) CO_2 hydrogenation to dimethyl ether through CH_3OH

Given the CH_3OH formation rates for some of the catalysts, we also considered a cascade system to convert CO_2 to dimethyl ether via CH_3OH intermediate. The Cu-Zn-Al and Cu/Mo_2C catalysts were most active for the hydrogenation of CO_2 to CH_3OH. Zeolitic catalysts such as HZSM-5 are known to dehydrate CH_3OH to dimethyl ether and at high temperatures to hydrocarbons via the CH_3OH to olefins (MTO) process or CH_3OH to gasoline (MTG) [40, 41]. Figure 4.8 illustrates the CH_3OH and dimethyl ether formed as a

function of time for the individual Cu/Mo_2C and HZSM-5 catalysts as well as the mixture. The results suggested that the Cu/Mo_2C and HZSM-5 catalysts worked in concert to produce dimethyl ether from CO_2 via CH_3OH intermediate.

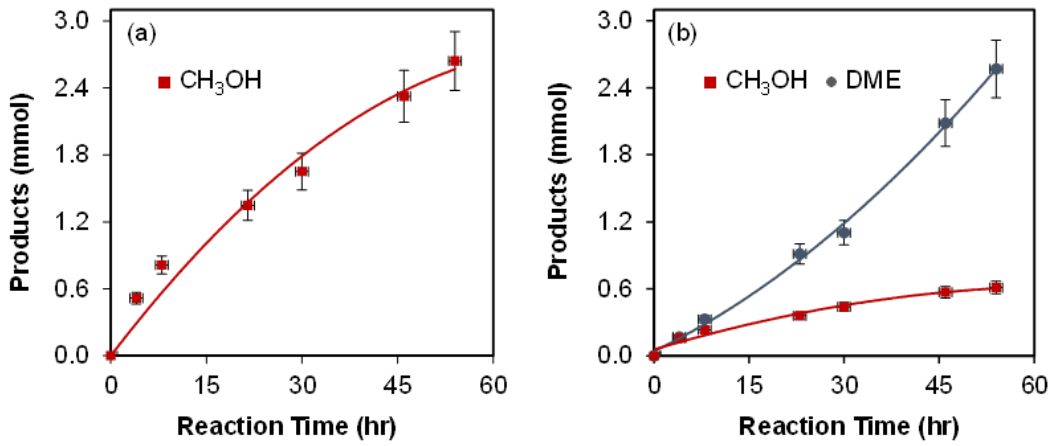

Figure 4.8 CH_3OH and dimethyl ether (DME) production from CO_2 hydrogenation over (a) Cu/Mo_2C catalyst (600 mg) and (b) a mixture of Cu/Mo_2C and HZSM-5 catalysts (600 mg each).The experiments were carried out at 135 ℃ with 10 bar CO_2, 30 bar H_2, 37.5 mL 1,4-dioxane, 54 h. The HZSM-5 catalyst alone was not active under these conditions.

4.4 Discussion

Results for the Cu-Zn-Al and Cu-Cr catalysts are somewhat different from those reported by Fan et al. [5] They did not observe CH_3OH production at temperatures below ~150 ℃; the only products were ethyl formate and CO. The CH_3OH selectivity was maximum (~60%) at 200 ℃. We observed relatively high selectivities (> 75%) for all of the catalysts at 135 ℃ (Table 2). There were several plausible explanations for differences between our results and those reported by Fan et al.[5] Their experiments were carried out with ethanol as the solvent; we used 1,4-dioxane. While H_2 solubilities for these solvents are similar (0.16 and 0.13 mol/L for ethanol[42] and 1,4-dioxane[33], respectively), the CO_2 solubilities are very different (0.14 and 1.5 mol/L, respectively [34, 43]). In addition,

their use of ethanol would facilitate the esterification reaction and could accelerate CH_3OH production. Finally, it is possible that the catalysts were in different states of reduction. Our protocol included a step to pretreat the catalysts prior to measurement of their rates and selectivities. The protocol described by Fan et al.[5] did not include a pretreatment step. It has been reported that Cu^0 is the active species for CH_3OH synthesis [2, 15]; therefore, one would expect lower activities for the untreated oxide catalysts.

Turnover frequency is a measure of the intrinsic activity of a catalyst. There are no reported TOFs that can be compared directly with our results, however, at 220-240 ℃ and 10-80 bar, TOFs for CH_3OH production have been reported in the range of 0.002-0.021 s^{-1} for Cu-based catalysts [44-46]. To better compare our results with the literature examples for CO_2 hydrogenation to methanol, we extrapolated the methanol TOFs reported in the literature to 200 ℃ and 40 bar, the similar conditions for this study. This extrapolation was achieved using an activation energy of 70 kJ/mol [47] and a rate law correlating the partial pressures of CO_2 and H_2 (Eq. 4.1-4.2) [48]. A summary of methanol TOF comparing the literature study and our work is shown in Table 4.8. Our work showed a methanol TOF ranging from 0.001 – 0.008 s^{-1} over a series of Cu-based catalysts (Entries 8-11, Table 4.8). These TOF values were comparable with the results reported by Fan et al. (0.004 – 0.007 s^{-1}) for liquid phase CO_2 hydrogenation in ethanol (Entries 6-7, Table 4.8), while at the lower end of the TOF values of 0.003 – 0.021 s^{-1} for the gas phase CO_2 hydrogenation. The concentrations for CO_2 and H_2 are 1.0, 0.18 M in 1,4-dioxane (based on the solubilities) and 0.3, 0.9 M in gas phase (based on ideal gas law). This difference of gas concentrations made the overall gas phase pressure (i.e. $p_{CO2}pH_2$ in Eq. 4.2) slightly higher than that in

1,4-dioxane (by 30%), which partially explained the relatively higher methanol TOFs for the gas phase CO_2 hydrogenation.

$$r_{CH_3OH} = \frac{Kp_{CO2}p_{H2}[1-\left(\frac{1}{K'}\right)\left(\frac{p_{H2O}p_{CH3OH}}{p_{H2}^3 p_{CO2}}\right)]}{[1+\left(\frac{K_{H2O}}{K_2}\right)\left(\frac{p_{H2O}}{p_{H2}}\right)+\sqrt{K_{H2}p_{H2}}+K_{H2O}p_{H2O}]} \quad \text{Eq. 4.1}$$

$$r_{CH_3OH} \propto p_{CO2}p_{H2} \quad \text{Eq. 4.2}$$

Where K, KH_{2O}, K', KH_{2O}, K_2, and KH_2 denote the rate constants for the elementary steps in the overall reaction; p_{CO2}, pH_2, pH_{2O}, and pCH_3OH represent the partial pressure of the corresponding species. The rate law in Eq. 4.1 can be simplified as Eq. 4.2 by setting $pH_{2O} = 0$. This simplification was valid as the amount of H_2O present in the system was two orders of magnitude smaller compared to that of CO_2 and H_2.

Table 4.8 Comparing methanol TOF on Cu-based catalysts between the literature and this study.[a]

Catalysts	T/P (℃/bar)	Methanol TOF(10^{-4}•s^{-1})	Phase	Methanol TOF at 200 ℃/40 bar (Extrapolated)	Refs
Cu-Zn-Zr	220/80	212	Gas	26	[44]
Cu-Zr	240/20	210	Gas	210	[2]
Cu-Zn-Zr	240/20	170	Gas	170	[2]
Cu-Zn-Zr-Ga-Y	240/20	120	Gas	120	[2]
Cu-Zn	220/20	26	Gas	51	[46]
Cu-Zn	200/30	40	Liquid[a]	71	[5]
Cu-Cr	200/30	23	Liquid[a]	41	[5]
Cu-Zn-Al	200/40	58	Liquid[b]	N/A	This work
Cu/Mo_2C	200/40	46	Liquid[b]	N/A	This work
Cu-Cr	200/40	0.01	Liquid[b]	N/A	This work
Cu/Mo_2C + Cu-Cr	200/40	0.08	Liquid[b]	N/A	This work

[a] The liquid contained 10 ml ethanol (solvent and alcohol reagent).
[b] The liquid contained 35.5 ml 1,4-dioxane (solvent) and 2 ml ethanol (alcohol reagent).

The estimated TOF for the Cu-Cr:Cu/Mo_2C cascade system was 4.7×10^{-4} s^{-1}. Huff et al. reported a CH_3OH production turnover number of 2.5 at 135 ℃ after 16 h for a homogeneous cascade system incorporating $(PMe_3)_4$Ru-(Cl)(OAc), $Sc(OTf)_3$, and (PNN)Ru(CO)(H) complexes; the corresponding TOF would be 4.3×10^{-5} s^{-1}.[32]

Interestingly, they reported a CH_3OH turnover number that would be equivalent to a TOF of 3.6×10^{-4} s^{-1} for a cascade system where CO_2 hydrogenation to formic acid and formic acid esterification were carried out at 75 ℃ then the formate was hydrogenated at 135 ℃ in a separate reactor (without the first two catalysts). This TOF was similar in magnitude to that achieved for the heterogeneous catalysts described in this chapter.

By comparing the CH_3OH production rates from the hydrogenation of CO_2 and suspected intermediates (formic acid and ethyl formate), we were able to further interrogate the reaction pathways reported by Fan et al.[5] and propose rate-limiting steps. Figure 4.9 illustrates reaction pathways that are most consistent with our results. In the absence of ethanol, formic acid is likely the principal intermediate. In the presence of ethanol, the pathway from CO_2 to CH_3OH seemed to include formic acid and formate intermediates. Our results are consistent with the hydrogenation of CO_2 to formic acid being the rate-limiting step for most of the Cu and Mo_2C-based catalysts.

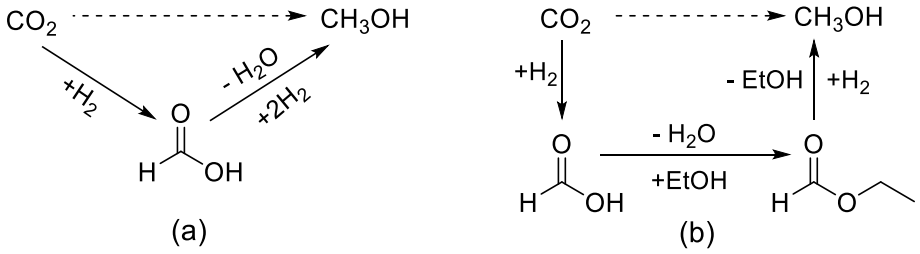

Figure 4.9 Summary of reaction pathways for CO_2 hydrogenation over the Cu and Mo_2C based catalysts (a) in the absence of ethanol and (b) in the presence of ethanol.

The primary goal through these cascade systems is to maximize the production of CH_3OH while minimizing the accumulation of the intermediates such as formic acid and ethyl formate by converting them through subsequent reactions. However, the selective formation of ethyl formate on Cu-Cr catalyst at 135 ℃ may provide opportunities to

develop processes with the formate ester as the target product. These processes are especially attractive given that ester is a more value-added product compared to CH_3OH; the unit price for ethyl formate and CH_3OH are ~ 12 [49] and 0.4 K$/Mton [50] based on the current market. It should also be noted that the market demand for ester is at least three orders of magnitude smaller than that for CH_3OH. The scale of the production has to be considered when comparing the economic viability for producing CH_3OH and formate from CO_2. Yu et al. first reported the production of methyl formate from CO_2 hydrogenation over a Cu-Zn-Al catalyst using CH_3OH solvent, which afforded a total conversion rate of 0.05 $\mu mol_{CO2} \bullet m^{-2} \bullet s^{-1}$, with selectivities of 79% and 21% to methyl formate and CO respectively at 150 ℃, 20 bar H_2, and 140 bar CO_2. In contrast, our study using Cu-Cr yielded a lower rate (0.002 $\mu mol_{CO2} \bullet m^{-2} \bullet s^{-1}$) but a higher selectivity to formate (ethyl formate: 97% and CO: 3%) at 135 ℃, 30 bar H_2, and 10 bar CO_2. These differences in activities/selectivites were expected given the different operating conditions. Nevertheless, these results are promising and provide useful knowledge for the optimization and scale-up for the process of formate ester production from CO_2.

Results for the Mo_2C and Cu/Mo_2C catalysts suggested a synergy between Cu and Mo_2C. We expect that the Cu was zero-valent based on prior investigations.[26] Vidal et al. reported evidence of synergy between Cu or Au and TiC (support) during gas phase CO_2 hydrogenation to CH_3OH. [51] These metals are effective sites for hydrogen dissociation. Synergistic effects between the metal and carbide have also been reported for Pt/Mo_2C catalysts during water-gas-shift [23] and Pd/WC catalysts during the selective hydrogenation of triglycerides[52]. It is plausible that Cu particles on the Cu/Mo_2C catalyst enhanced the hydrogen surface coverage, thereby facilitating the hydrogenation of CO_2.

We also note that the synergy has been reported between Cu and oxides, such as ZnO, in the associated catalysts [1, 3, 37].

By combining a CH_3OH synthesis catalyst (Cu/Mo_2C) and a MTO/MTG catalyst (HZSM-5), we were able to establish a cascade system that converted CO_2 to DME. It should be mentioned that DME has also been proposed to be a key intermediate to produce hydrocarbons during the MTO/MTG processes [40]. The general mechanisms for "CH_3OH to hydrocarbon" can be briefly described by three key steps: 1) ether formation, 2) initial C-C bond formation, and 3) chain propagation and aromatization [53] as shown in Figure 4.10a. Specifically, the hydrocarbon formation was considered to occur through a "rake" mechanism [54], where condensation of ethers occurred on the catalyst surface, followed by dehydration and H^+ transfer (Figure 4.10b). The chain propagation was achieved by the sequential insertion of a carbene ($:CH_2$), produced from CH_3OH dehydration, to DME to produce longer chain ethers, such as methyl ethyl and methyl propyl ethers, which served as the intermediates to produce ethylene and propylene respectively.

In the Cu/Mo_2C:HZSM-5 cascade system at 135 ℃ (Section 4.3.2.4), no other CH_3OH derived product was measured except for DME, suggesting that the subsequent conversion of DME to hydrocarbons did not occur. According to a surface reactivity study by Salvador et al. [55] over an H-Y type zeolite, the CH_3OH to DME conversion typically started to occur at 120 ℃ and reached maximum at 210 ℃; however, the formation of hydrocarbons did not occur until 250 ℃. These findings are consistent with our observation on the absence of hydrocarbons at 135 ℃. Most of the CH_3OH to hydrocarbon processes are performed in gas phase at temperatures greater than 300 ℃ and atmospheric pressure, the conditions where hydrocarbon formation are favored [56].

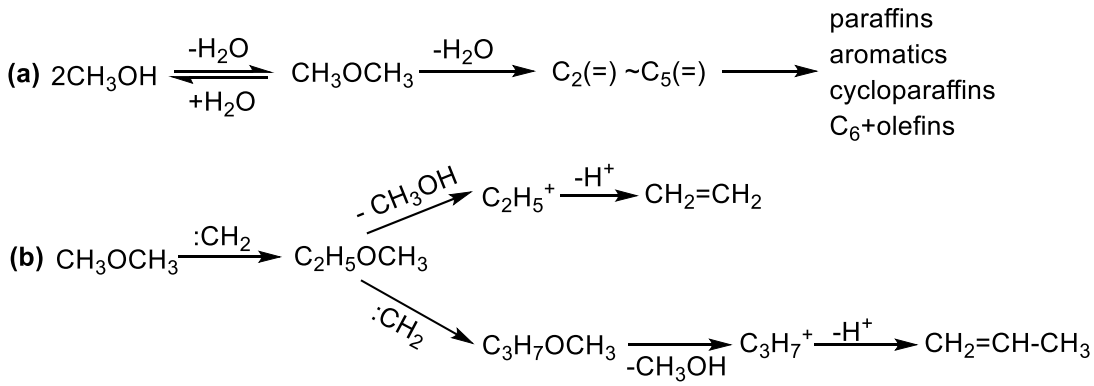

Figure 4.10 Scheme of reaction mechanisms for CH_3OH to hydrocarbon process: (a) General mechanisms over a HZSM-5 catalyst, taken from [53] and (b) proposed pathways for ethylene and propylene production from DME.

Although the mechanistic study of CH_3OH to hydrocarbon conversion is beyond the scope of this dissertation, it is important to notice that the one-pot conversion of CO_2 to hydrocarbon through CH_3OH intermediate is challenging. This challenge was due to two major sub-steps in this cascade sequence are not favored at the same operating window. In particular, CH_3OH synthesis from CO_2 hydrogenation is favored at low temperature and high pressure [2], while the subsequent CH_3OH to hydrocarbon conversion is favored at high temperature and low pressure [56]. Performing the reactions in two separate vessels or introducing new catalyst to promote DME to hydrocarbon conversion at comparable conditions with CH_3OH synthesis process are two possible solutions.

We also evaluated the product yield from each cascade system described in this chapter and the results are shown in Table 4.9. All the product yields achieved at 115-135 ℃ were at least an order of magnitude lower than the theoretical yield, suggesting they still possess great potentials to be optimized. For the Cu-Cr:Cu/Mo_2C cascade system, increasing the temperature from 135 to 200 ℃ has significantly improved the product yield

from 4.3 to 34% respectively, making it closer to the equilibrium yield. A systematic study on reaction parameters are required to rationally optimize these cascade systems, which will also be helpful in evaluating the feasibility of scaling up these systems for commercial applications.

Table 4.9 Product yields (%) for all the heterogeneous cascade systems for CO_2 hydrogenation.[a]

Cascade Systems	T(℃)	Time (h)	Yield (%)[b]	Equilibrium Yield(%)[c]
Ir-PN/SBA-15 + Cu/Mo_2C	115	8	0.4	53
Cu-Cr + Cu/Mo_2C[d]	135	24	4.3	48
Cu-Cr + Cu/Mo_2C[d]	200	24	34	58
Cu/Mo_2C + HZSM-5	135	54	5.9	67

[a] Experiments performed at 10 bar CO_2, 30 bar H_2 in 37.5 ml 1,4-dioxane.
[b] Yield = total amount of products on C1 basis (mmol)/CO_2 feed (mmol).
[c] Calculated using the thermodynamic parameters and model from [57].
[d] Performed in the presence of ethanol.

The heterogeneous-based cascade systems described in this chapter (see Figure 4.11) are the first demonstrations for liquid phase CO_2 hydrogenation at relatively mild reaction conditions. The commercial CH_3OH production rate (from syngas) typically ranged from 0.4-1.0 kg/(l•h) at 250-300 ℃ and 50-100 bar. In this study, our best performing Cu-Cr:Cu/Mo_2C cascade system exhibited a CH_3OH production rate of 0.01 kg/(l•h), about two orders of magnitude lower than the commercial rates, albeit at milder reaction conditions at 200 ℃ and 40 bar. Future work should investigate key reaction parameters, e.g. temperatures, pressures, solvents, and ratio of catalyst components to further optimize the reaction performance for these cascade systems.

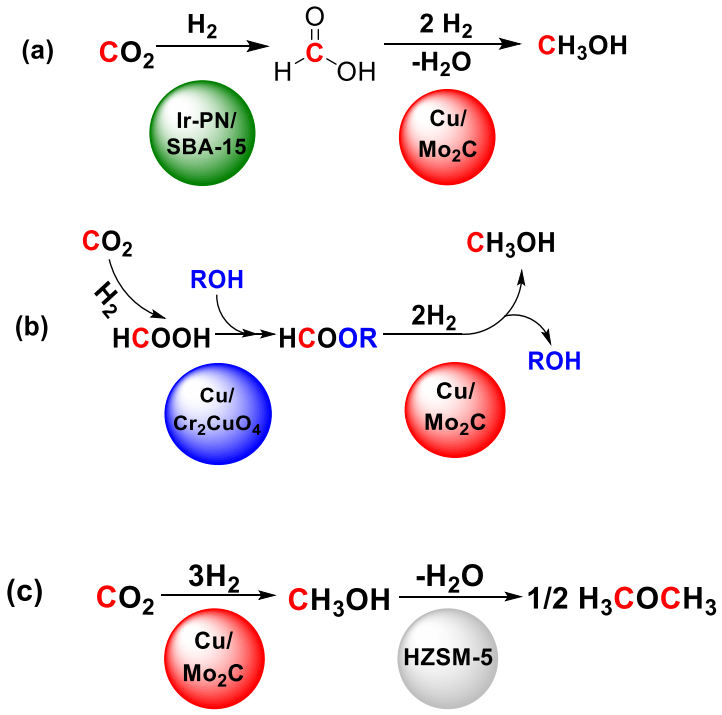

Figure 4.11 Schematic of proposed reaction pathways for (a) Ir-PN/SBA-15: Cu/Mo_2C cascade system, (b) Cu-Cr:Cu/Mo_2C cascade system, and (c) Cu/Mo_2C:HZSM-5 cascade system.

4.5 Conclusions

In this chapter we described two novel heterogeneous cascade systems for the hydrogenation of CO_2 to CH_3OH through formic acid or formate intermediates. One system coupled Ir-PN/SBA-15 and Cu/Mo_2C catalysts, affording a total TOF of 3.7×10^{-4} s^{-1} for CH_3OH production at 115 ℃, 10 bar CO_2, and 30 bar H_2. The other system combined Cu-Cr and Cu/Mo_2C catalysts and yielded a TOF of 4.7×10^{-4} s^{-1} for CH_3OH production at 135 ℃, 10 bar CO_2, and 30 bar H_2. The results encouraged the development of other cascade systems of this type. We also observed that a Cu/Mo_2C catalyst was active for CO_2 hydrogenation to CH_3OH. The deposition of Cu onto the Mo_2C surface enhanced the

CH_3OH formation rates. These Mo_2C-based materials were also active for formic acid and formate ester hydrogenation. The introduction of ethanol during CO_2 hydrogenation resulted in improved CH_3OH production rates over the Cu/Mo_2C and Cu-Zn-Al catalysts. We attributed this to the accelerated formation of ethyl formate and its subsequent hydrogenation to CH_3OH. In contrast, the Cu-Cr catalyst was selective for the production of ethyl formate; its subsequent conversion to CH_3OH was inhibited by CO_2. The production of dimethyl ether from CO_2 was also demonstrated over a Cu/Mo_2C:HZSM-5 cascade system, where CO_2 was hydrogenated to CH_3OH over Cu/Mo_2C and CH_3OH was further converted to dimethyl ether by HZSM-5.

4.6 References

[1] Y. Choi, K. Futagami, T. Fujitani, J. Nakamura, Appl. Catal., A 208 (2001) 163-167.
[2] S. Natesakhawat, J.W. Lekse, J.P. Baltrus, P.R. Ohodnicki, B.H. Howard, X. Deng, C. Matranga, ACS Catal. 2 (2012) 1667-1676.
[3] M. Kurtz, N. Bauer, C. Büscher, H. Wilmer, O. Hinrichsen, R. Becker, S. Rabe, K. Merz, M. Driess, R.A. Fischer, Catal. Lett. 92 (2004) 49-52.
[4] W. Wang, S. Wang, X. Ma, J. Gong, Chem. Soc. Rev. 40 (2011) 3703-3727.
[5] L. Fan, Y. Sakaiya, K. Fujimoto, Appl. Catal., A 180 (1999) L11-L13.
[6] K.K.M. Yu, S.C. Tsang, Catal. Lett. 141 (2011) 259-265.
[7] T. Inoue, A. Fujishima, S. Konishi, K. Honda, Nature 277 (1979) 637-638.
[8] S. Kuwabata, K. Nishida, R. Tsuda, H. Inoue, H. Yoneyama, J. Electrochem. Soc. 141 (1994) 1498-1503.
[9] E.E. Barton, D.M. Rampulla, A.B. Bocarsly, J. Am. Chem. Soc. 130 (2008) 6342-6344.
[10] Y. Hori, Electrochemical CO_2 Reduction on Metal Electrodes, Modern Aspects of Electrochemistry, Springer, 2008, pp. 89-189.
[11] G. Centi, S. Perathoner, Catal. Today 150 (2010) 151-162.
[12] B. Kumar, M. Llorente, J. Froehlich, T. Dang, A. Sathrum, C.P. Kubiak, Annu. Rev. Phys. Chem. 63 (2012) 541-569.
[13] D. Canfield, K. Frese Jr, J. Electrochem. Soc. 130 (1983) 1772-1773.
[14] M. Tomkiewicz, J.M. Woodall, Science 196 (1977) 990-991.
[15] M. Behrens, F. Studt, I. Kasatkin, S. Kühl, M. Hävecker, F. Abild-Pedersen, S. Zander, F. Girgsdies, P. Kurr, B.-L. Kniep, M. Tovar, R.W. Fischer, J.K. Nørskov, R. Schlögl, Science 336 (2012) 893-897.
[16] C. Yang, Z. Ma, N. Zhao, W. Wei, T. Hu, Y. Sun, Catal. Today 115 (2006) 222-227.
[17] J.-L. Dubois, K. Sayama, H. Arakawa, Chem. Lett. 21 (1992) 5-8.
[18] W. Xu, P. Ramirez, D. Stacchiola, J. Rodriguez, Catal. Lett. 144 (2014) 1-7.
[19] D.-V.N. Vo, A.A. Adesina, Appl. Catal., A 399 (2011) 221-232.

[20] M. Xiang, D. Li, H. Xiao, J. Zhang, H. Qi, W. Li, B. Zhong, Y. Sun, Fuel 87 (2008) 599-603.
[21] P.M. Patterson, T.K. Das, B.H. Davis, Appl. Catal., A 251 (2003) 449-455.
[22] J. Patt, D. Moon, C. Phillips, L. Thompson, Catal. Lett. 65 (2000) 193-195.
[23] N.M. Schweitzer, J.A. Schaidle, O.K. Ezekoye, X. Pan, S. Linic, L.T. Thompson, J. Am. Chem. Soc. 133 (2011) 2378-2381.
[24] H. Ren, W. Yu, M. Salciccioli, Y. Chen, Y. Huang, K. Xiong, D.G. Vlachos, J.G. Chen, ChemSusChem 6 (2013) 798-801.
[25] Z. Xu, N.D. McNamara, G.T. Neumann, W.F. Schneider, J.C. Hicks, ChemCatChem 5 (2013) 1769-1771.
[26] J.A. Schaidle, N.M. Schweitzer, O.T. Ajenifujah, L.T. Thompson, J. Catal. 289 (2012) 210-217.
[27] H.P. Klug, L.E. Alexander, X-Ray Diffraction Procedures: For Polycrystalline and Amorphous Materials, 2nd ed., Wiley-VCH, 1974.
[28] J.A. Schaidle, A.C. Lausche, L.T. Thompson, J. Catal. 272 (2010) 235-245.
[29] J. Evans, M. Wainwright, A. Bridgewater, D. Young, Appl. Catal. 7 (1983) 75-83.
[30] Thermal expansion data for the solvents are obtained from the handbook provided by Parr Instrument Co.
[31] G.C. Kennedy, Amer. J. Sci 252 (1954).
[32] C.A. Huff, M.S. Sanford, J. Am. Chem. Soc. 133 (2011) 18122-18125.
[33] E. Brunner, J. Chem. Eng. Data 30 (1985) 269-273.
[34] D. Kassim, H. Zainel, S. Al-Asaf, E. Talib, Fluid Phase Equilib. 41 (1988) 287-294.
[35] M.M. Günter, T. Ressler, R.E. Jentoft, B. Bems, J. Catal. 203 (2001) 133-149.
[36] I. Kasatkin, P. Kurr, B. Kniep, A. Trunschke, R. Schlögl, Angew. Chem. 119 (2007) 7465-7468.
[37] T. Fujitani, J. Nakamura, Appl. Catal., A 191 (2000) 111-129.
[38] P.G. Jessop, T. Ikariya, R. Noyori, Chem. Rev. 95 (1995) 259-272.
[39] Thermodynamic calculations are based on standard values from NIST Chemistry WebBook.
[40] F.J. Keil, Microporous Mesoporous Mater. 29 (1999) 49-66.
[41] G. Centi, G. Iaquaniello, S. Perathoner, ChemSusChem 4 (2011) 1265-1273.
[42] Purwanto, R. Deshpande, R. Chaudhari, H. Delmas, J. Chem. Eng. Data 41 (1996) 1414-1417.
[43] I. Dalmolin, E. Skovroinski, A. Biasi, M. Corazza, C. Dariva, J.V. Oliveira, Fluid Phase Equilib. 245 (2006) 193-200.
[44] J. Słoczyński, R. Grabowski, A. Kozłowska, P. Olszewski, J. Stoch, J. Skrzypek, M. Lachowska, Appl. Catal., A 278 (2004) 11-23.
[45] F. Arena, K. Barbera, G. Italiano, G. Bonura, L. Spadaro, F. Frusteri, J. Catal. 249 (2007) 185-194.
[46] Q. Sun, Y.-L. Zhang, H.-Y. Chen, J.-F. Deng, D. Wu, S.-Y. Chen, J. Catal. 167 (1997) 92-105.
[47] P.B. Rasmussen, P.M. Holmblad, T. Askgaard, C.V. Ovesen, P. Stoltze, J.K. Nørskov, I. Chorkendorff, Catal. Lett. 26 (1994) 373-381.
[48] K.M.V. Bussche, G.F. Froment, J. Catal. 161 (1996) 1-10.
[49] Ethyl formate pricing from Vigon International. Information available at http://www.vigon.com/ethylformate.aspx.

[50] ICIS Pricing for Methanol, updated on Jan. 10, 2014. Information avaialble at www.icispricing.com.
[51] A.B. Vidal, L. Feria, J. Evans, Y. Takahashi, P. Liu, K. Nakamura, F. Illas, J.A. Rodriguez, J. Phys. Chem. Lett. 3 (2012) 2275-2280.
[52] A.C. Lausche, K. Okada, L.T. Thompson, Electrochem. Commun. 15 (2012) 46-49.
[53] C.D. Chang, A.J. Silvestri, J. Catal. 47 (1977) 249-259.
[54] F. Cormerais, J. Chem. Research(S) 362 (1980).
[55] P. Salvador, W. Kladnig, Journal of the Chemical Society, Faraday Transactions 1: Physical Chemistry in Condensed Phases 73 (1977) 1153-1168.
[56] M. Stöcker, Microporous Mesoporous Mater. 29 (1999) 3-48.
[57] J.G.v. Bennekom, J.G.M. Winkelman, R.H. Venderbosch, S.D.G.B. Nieland, H.J. Heeres, Ind. Eng. Chem. Res. 51 (2012) 12233-12243.

CHAPTER 5

CO_2 HYDROGENATION OVER METAL/MO_2C CATALYSTS

5.1 Introduction

In previous chapters, we investigated the use of Mo_2C-based catalysts for the hydrogenation of CO_2 and the subsequent intermediates, including formic acid and ester formate, for methanol synthesis using cascade systems. In addition of being an active catalyst for CO_2 hydrogenation, Mo_2C was also proved to be an effective support [1], capable of modifying the electronic properties of the deposited metals that sometimes resulted in superior performance compared to the bulk Mo_2C material [2]. Dubio et al. reported that the addition of Cu to the Mo_2C and Fe_3C catalysts resulted in comparable activities for CO_2 conversion but substantial enhancements in the CH_3OH selectivities by more than 50%. Similar enhancements were described by Vidal et al. [3], using Cu or Au promoted TiC (001) to produce CH_3OH from CO_2 hydrogenation at 250 – 320 ℃. The Cu/TiC (001) material exhibited a CH_3OH production rate that was an order of magnitude higher than that for the pure TiC (001) material. They suggested the improved rate for methanol synthesis was a consequence of a charge polarization on the TiC surface upon the deposition of Cu or Au nanoparticles, making the TiC surface more effective for activating CO_2. More recently, Porosoff et al. [4] reported that a bulk Mo_2C catalyst outperformed CeO_2 supported Pt or Pd catalysts for CO_2 hydrogenation, producing

primarily CO (~93% selectivity) at 300 ℃ and 1 atm via the reverse water-gas shift (RWGS) reaction. They also showed that the addition of Co onto Mo_2C resulted in a moderate increase in the CO selectivity, likely attributing to the capability of Co/Mo_2C to dissociate CH_4 to C and H_2 that decreased the selectivity to CH_4 side product.

In this chapter, we further evaluate nanostructured Mo_2C supported metal catalysts, including Cu, Pd, Co, and Fe, for CO_2 hydrogenation in liquid solvents and at temperatures higher than 135 ℃. We also investigated the reaction pathways by probing the systems with possible intermediates, including CO and CH_3OH. The use of liquid solvents as opposed to reactions in gas phase, can impact catalyst stability [5], i.e. the capability of maintaining same activities over the total reaction time on stream. For example, Verhoef et al. [6] reported that MCM-41 supported heteropoly acid catalysts were susceptible to severe deactivation during liquid phase esterifications compared to carrying out these reactions in the gas phase. This deactivation was primarily due to the presence of H_2O which enhanced the mobility of the heteropoly acid species and caused catalyst sintering [6]. Therefore, we also investigated stabilities of the M/Mo_2C catalysts by comparing the surface and bulk, physical and chemical properties before and after reaction. The findings will enhance our understanding of Mo_2C-supported metal catalysts for low temperature CO_2 hydrogenation and provide a scientific basis for their rational design for other related applications.

5.2 Materials and Methods

5.2.1 Catalyst Preparation

The bulk Mo_2C catalyst was prepared using a temperature programmed reaction (TPR) technique starting from an ammonium molybdate (AM) precursor,

$(NH_4)_6MO_7O_{24}•4H_2O$ (Alfa Aesar). Approximately 1.3g of AM was sieved to 125-250 μm and then loaded into a quartz tube reactor. The AM was treated in H_2 flowing at 400 mL/min for 70 min, as the temperature was increased from 25 to 350 ℃ and held at 350 ℃ for 12 h. The reaction gas was then switched to 15% CH_4/H_2 (400 mL/min) while the temperature was increased to 590 ℃ in 1.5 h and maintained at 590 ℃ for 2 h; the reactor was then immediately quenched to room temperature. The Cu/Mo_2C and Pd/Mo_2C catalysts were prepared using a wet impregnation method described elsewhere [12]. Briefly, the freshly-synthesized Mo_2C was transferred under 15% CH_4/H_2 gas into a beaker containing 70 mL deaerated H_2O (to avoid the oxidation of Mo_2C) with target amounts of $Cu(NO_3)_2$ and $Pd(NO_3)_2{\cdot}4NH_3$ and allowed to interact for 20 h to achieve the 5 wt% nominal metal loading. Argon was continuously purged through the solutions during the wet impregnation process to deaerate and agitate the solution. This method enabled the metal precursor to directly interact with the native Mo_2C surface (as opposed to a passivated material). A recently study by Wyvratt et al. reported that deposition of active metal onto the native Mo_2C produced nanoscale metal domains that were better-dispersed than those deposited onto a passivated Mo_2C surface, resulting in superior catalytic performance for the WGS reaction [13]. It has also been suggested by Schaidle et al. that Cu and Pd are deposited onto the Mo_2C via electrostatic adsorption and both metals are reduced in-situ by the Mo_2C support during the wet impregnation process [12]. The resulting catalyst slurry was dried at 110 °C for 2 h and reduced in flowing H_2 (400 mL/min) at 300 °C for 4 h to decompose the nitrate and produce the Cu or Pd domains. The Co/Mo_2C and Fe/Mo_2C catalysts were synthesized using the incipient wetness impregnation. The impregnation was performed using an aqueous solution containing

target amount of $Co(NO_3)_2$ or $Fe(NO_3)_3$, on the Mo_2C support with a pore volume of 0.13 cm^3/g (measured by N_2 physisorption). The incipient wetness was applied because only small amounts of Co and Fe (< 2 wt%) could be deposited via electrostatic adsorption [12]. The freshly synthesized Mo_2C was transferred under Argon to a H_2O-tolerant, oxygen free glovebox filled with N_2 to avoid any bulk or surface oxidation of Mo_2C. The resulting catalysts were dried in the glovebox on a heating plate at 110 ℃ for 2 h and then transferred under Argon into a quartz reactor where they were reduced in flowing H_2 (400 ml/min) for 4 h at 450 °C to produce the Fe and Co domains.

5.2.2 Catalyst Characterization

Surface areas of the materials were measured using a Micromeritics ASAP 2010 analyzer based on N_2 physisorption. All of the Mo_2C-based catalysts were degassed (< 5 mm Hg) at 350 ℃ for 4 h prior to the surface area measurements. The bulk crystalline structures were characterized using X-ray diffraction (Rigaku Miniflex 600) with 2θ ranging from 10 °to 90 °and a scan rate of 5 °/min. Crystallite sizes were estimated via line broadening analysis using the Scherrer equation [14]. Scanning electron microscopy (SEM) for select catalysts were performed using FEI Nova Nanolab Dualbeam (FIB/SEM). To enhance the conductivity, the materials were gold sputter coated prior to imaging. Elemental analyses were carried out using Energy Dispersive X-ray Spectroscopy (EDX). All the materials were passivated in 1% O_2/He for 5 h before performing SEM in order to be loaded into the sample chamber without bulk oxidation. Metal compositions for the M/Mo_2C catalysts were determined by inductively coupled plasma (ICP-OES) using a Varian 710-ES analyzer.

The surface site densities for Mo_2C-based catalysts were determined via CO chemisorption using a Micromeritics AutoChem II 2920 system with a thermal conductivity detector. The Mo_2C-based catalysts were passivated in order to be loaded into the reactor chamber equipped with the AutoChem II 2920 system. Prior to the measurements, the catalysts were recarburized in 15% CH_4/H_2 for 4 h at 590 ℃, then degassed in He at 600 ℃ for 1 h. The catalysts were then cooled to 25 ℃ and repeatedly dosed with 5% CO/He (5 mL sample loop) until reaching saturation. Deconvolution of contributions from the metal and Mo_2C is desired, however, it is difficult because CO can adsorb to both the metal and Mo_2C. Nevertheless, as Mo_2C accounts for 95 wt% of the catalyst, the CO chemisorption uptakes should provide reasonable estimates of site densities. The catalyst surface coverage were estimated by assuming a 10^{19} active sites/m^2 for the Mo_2C support [4]. The H_2 temperature-programmed reduction (H_2-TPR) was also carried out using the Micromeritics AutoChem II 2920 system. The passivated M/Mo_2C catalysts were first purged with He with a flow rate of 70 ml/min at 200 ℃ for 2 h and then were cooled to room temperature. The H_2-TPR was then conducted in 10% H_2/Ar by increasing the temperature from room temperature to 800 ℃ at a heating rate of 4 ℃/min, where the H_2 consumption was recorded as a function of temperature.

5.2.3 Reaction Rates and Selectivities

The activity measurements were performed in a 50 mL Parr Instruments reactor (Micro 5500). The reactor system was equipped with a programmable temperature controller and a magnetic drive for the impeller. The gas phase reactor effluent was analyzed using gas chromatography (Varian 450 with flame ionization and thermal conductivity detectors). Liquid samples (0.4 mL) were periodically withdrawn during the

reaction using a dip tube, which was equipped with a 20 μm filter to separate the liquid from the solid catalyst particles. The liquid samples were analyzed offline using gas chromatography (Varian 450 with flame ionization detector).

The Mo_2C-based catalysts were used as synthesized without passivation. To avoid contact of the materials with air, they were transferred under an inert atmosphere and stored in an Ar filled glovebox (Mbraun UNIlab, H_2O < 0.1 ppm, O_2 < 5ppm). Solvents for the reactions contained 37.5 mL 1,4-dioxane (anhydrous, Acros Organics) and 10 μL n-decane (Acros Organics) as an internal standard. For the CO_2 hydrogenation experiments, the reactors were charged with 10 bar CO_2 and 30 bar H_2 through a dip tube after purging the solvents with H_2 for 15 min to remove dissolved oxygen at temperatures of 135-200 °C. Under these conditions, the solubilities for CO_2 and H_2 are approximately 0.15 and 0.14 mol/L at 135 °C and 0.10 and 0.18 mol/L [15, 16] at 200 °C, respectively, in 1,4-dioxane. The CO_2 reaction rates were calculated based on formation rates for the products (on a C_1 basis) after 2 h. Carbon balances closed to within ± 8% for the experiments. The turnover frequency (TOF) was determined by normalizing the rate by the CO uptakes. The selectivity is defined as the molar ratio of a specific product over the total products on a C_1 basis.

For select catalysts, CO hydrogenation and CH_3OH hydrogenation were performed at 200 °C to investigate the reaction pathways. For CO hydrogenation the reactant was 10 bar CO and 30 bar H_2 in 37.5 ml 1,4-dioxane. The CH_3OH hydrogenation experiments were performed using 7 mmol (~0.3 ml) CH_3OH, 10 bar N_2 (used as an inert gas to balance the pressure) and 30 bar H_2 in 37.2 ml 1,4-dioxane. A catalyst loading of 200 mg was used for each experiment unless stated otherwise. The reactor was heated at a rate of 5 °C/min

from room temperature to the target reaction temperature, and then agitated at a constant rate of 300 rpm, which indicated the start of the reaction.

Several of the spent catalysts were recovered for characterization. To avoid contact with air, the materials were removed from the reactor (as catalyst slurry) in the Ar-filled glovebox and dried in vacuum for 2 h at room temperature in the glovebox antechamber. The dried catalysts were collected and stored in the glovebox before they were characterized. Similar weights were measured for the recovered catalysts, suggesting minimal catalyst loss during the reaction.

5.3 Results

5.3.1 Pre-Reaction Catalyst Properties

The metal contents, surface areas, site densities, and corresponding theoretical surface coverages for all of the catalysts are listed in Table 5.1. Metal contents for each of the M/Mo_2C catalysts were ~5 wt%, the target loading. The deposition of metals onto Mo_2C caused a slight decrease in the surface areas, possibly due to pore blocking by the metal particles. Site densities for the M/Mo_2C materials were lower than that for the bulk Mo_2C (~1.6 $molecules_{CO}/nm^2$) with the Pd/Mo_2C catalyst possessing the highest site density and lowest nominal surface coverage owing perhaps to the high atomic mass of Pd. For comparison, site densities for Cu [19] , Pd [17, 18], Co [20, 21], and Fe [22, 23] have been reported to be 4.9, 6.6, 7.4 and 12.1 $molecules_{CO}/nm^2$, respectively. The lower site densities for the M/Mo_2C catalysts suggest that metal-Mo_2C interactions suppressed CO adsorption on the metals. Similar reductions in CO adsorption capacities have been reported a Pt/Mo_2C catalyst prepared using methods similar to those described in our chapter [12].

Table 5.1 Physical properties of the M/Mo_2C catalysts.[a]

Catalysts	Metal Content (wt%)	Surface Area (m^2/g)	Site Density (μmol/g)	Surface Coverage (ML%)[a]
Mo_2C	N/A	151	406	N/A
Cu/Mo_2C	5.3	135	298	35.1
Pd/Mo_2C	5.2	138	346	20.6
Co/Mo_2C	5.5	124	305	39.4
Fe/Mo_2C	5.1	118	306	38.4

[a] Calculated assuming 10^{19} sites/m^2 of Mo_2C support.

X-ray diffraction patterns for the catalysts are shown in Figure 5.1. The Mo_2C support contained a mixture of α-MoC_{1-x} (x ~0.5) and β-Mo_2C in approximately equal amounts (quantified by Whole Pattern Fitting Rietveld Refinement) and there was no evidence of Mo oxides. This finding indicated a complete carburization of Mo oxide precursor during the synthesis process. Given the Mo:C ratio for the material, we will refer to the Mo carbide as Mo_2C. Diffraction patterns for the M/Mo_2C catalysts resembled that for the bulk Mo_2C with no discernable peaks for the supported metals. This observation was likely a consequence of the small dimensions of the metal crystallites, although in some cases, the most significant peaks associated with the metals overlapped with the Mo_2C peaks (Figure. A1). For example, the Cu (111) peak at ~43 ° and Pd (111) peak at ~40 ° are located near the most intense peaks for α-MoC_{1-x} and β-Mo_2C, respectively. The XRD detection limit is approximately 5 nm.

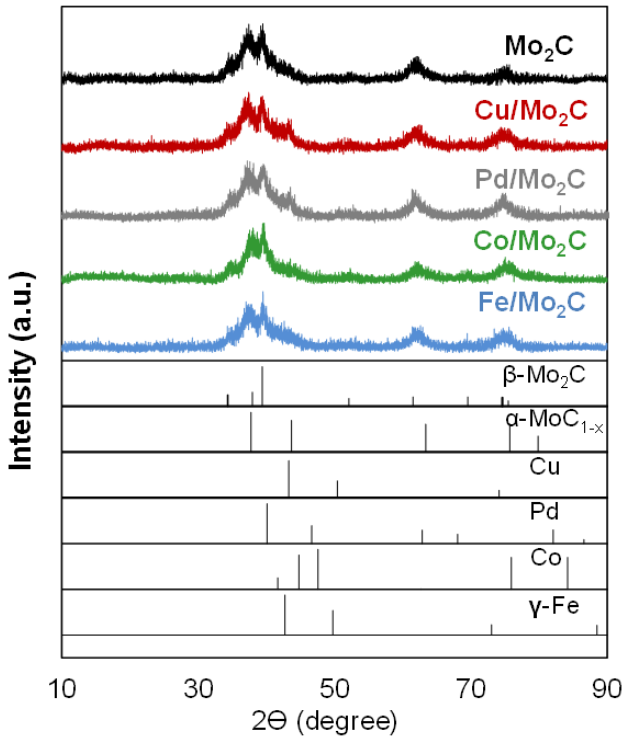

Figure 5.1 X-ray diffraction patterns for Mo_2C, M/Mo_2C, and standards.

5.3.2 CO_2 Hydrogenation

The CO_2 hydrogenation reaction rates and selectivities for the Mo_2C and M/Mo_2C catalysts are summarized in Table 5.2. At 135 ℃, CH_3OH was the major product with selectivities in excess of 79%, while CO and CH_4 were produced in small quantities. The deposited metals moderately enhanced the CO_2 conversion rates and CH_3OH selectivities. Very small but measurable amounts of C_2H_6 and C_3H_8 were observed for the Co/Mo_2C and Fe/Mo_2C catalysts. When the temperature was increased to 200 ℃, the CO_2 conversion rate increased by more than an order of magnitude. We also observed a significant shift in product distributions with C_1-C_4 hydrocarbons produced over all of the catalysts. There was also a concomitant decrease in the selectivity to CH_3OH on increasing the temperature

to 200 ℃ (50-70%) compared to that at 135 ℃ (80-95%). This reduction in selectivity was anticipated as CH_3OH synthesis is a highly exothermic reaction ($\Delta H_{25\,℃}$ = -49.5 kJ/mol).

Table 5.2 CO_2 hydrogenation rates and selectivities over Mo_2C and M/Mo_2C catalysts.[a]

Catalysts	T_{rxn} (℃)	CO_2 Conv. Rate/TOF[b]		Selectivity (%)[c,d]						
		umol/m^2 /s•10^4	s^{-1}•10^4	MeOH	EtOH	CO	CH_4	C_2H_4	C_2H_6	C_{3+}
Mo_2C	135[e]	1.7	0.6	79	0	16	5.3	0	0	0
	200	55	20	53	16	4.9	17	0.8	5.0	3.0
Cu/Mo_2C	135[e]	4.6	2.1	93	0	4.1	2.6	0	0	0
	200	90	41	63	14	8.6	9.8	0.3	3.7	1.9
Pd/Mo_2C	135	5.9	2.3	95	0	3.6	1.6	0	0	0
	200	97	39	68	11	9.6	7.6	0.3	2.5	1.3
Co/Mo_2C	135	4.8	1.9	84	0	5.7	9.4	0	1.1	0.1
	200	86	35	46	25	9.5	9.5	0.6	5.6	1.4
Fe/Mo_2C	135	3.9	1.5	87	0	4.1	7.2	0	1.2	0.6
	200	99	38	58	16	6.8	8.1	0.4	6.3	3.8

[a]10 bar CO_2, 30 bar H_2, 37.5 ml 1,4-dioxane and 200 mg catalyst.
[b]Calculated at 2 h.
[c]Calculated at ~ 1.0 % CO_2 conversion at 135 ℃ and ~ 10% CO_2 conversion at 200 ℃. The selectivities are calculated on a C_1 basis.
[d]C_3 contains C_3H_6 and C_3H_8, C_4 contains C_4H_8 and C_4H_{10}.
[e]Rate data taken from [33].

Figure 5.2 compares TOFs for alcohol formation over the M/Mo_2C catalysts at 135 and 200 ℃. The CH_3OH TOFs at 135 ℃ decreased in the following order: Pd/Mo_2C > $Cu/Mo_2C \approx Co/Mo_2C$ > $Fe/Mo_2C \approx Mo_2C$ (Figure 5.2a). At 200 ℃, the order was slightly different: $Cu/Mo_2C \approx Pd/Mo_2C$ > Fe/Mo_2C > Co/Mo_2C > Mo_2C. These differences indicated the importance of the deposited metals. In addition to CH_3OH, C_2H_5OH was produced at 200 ℃. Interestingly, when taken together, the CH_3OH and C_2H_5OH TOFs for all of the M/Mo_2C catalysts were similar (26-30 $\times 10^{-4}$ s^{-1}). A potential pathway to C_2H_5OH and roles of the metals will be discussed in later sections.

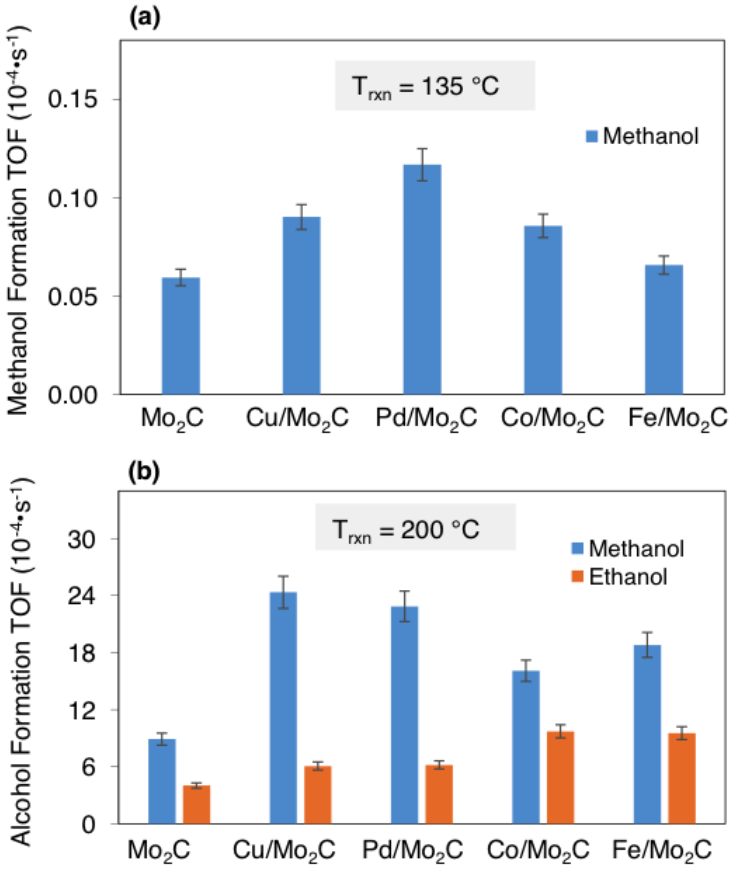

Figure 5.2 Turnover frequencies of CH_3OH and ethanol formation at (a) 135 ℃ and (b) 200 ℃ on M/Mo_2C catalysts. Experiments were performed at 10 bar CO_2, 30 bar H_2 and 37.5 ml 1,4-dioxane.

Figure 5.3 compares TOFs for CO and hydrocarbon formation at 135 and 200 ℃. At 135 ℃, the addition of Cu or Pd to Mo_2C had very small effects on the CO and hydrocarbon formation rates, while the addition of Fe and Co resulted in a decrease in CO formation and increase in hydrocarbon formation; mostly CH_4 and small amounts of C_2H_6 and C_3H_8. Similarly, at 200 ℃, Cu and Pd had very small effects on the production of CO and hydrocarbon compared to that for bulk Mo_2C catalyst, suggesting these metals were not active for the production of hydrocarbons. In contrast, the deposition of Fe and Co onto Mo_2C significantly enhanced the production of C_2-C_4 hydrocarbons, while decreasing the

selectivity to CO. The hydrocarbons were primarily paraffins, with an olefin/paraffin ratio of 0.08 – 0.35 (see Figure. A2). Such low olefin/paraffin ratios have also been reported for other Mo_2C-based materials [6, 24]; this observation is also consistent with the high hydrogenation activities associated with Mo_2C. Addition of the metal did not significantly affect the olefin/paraffin ratios.

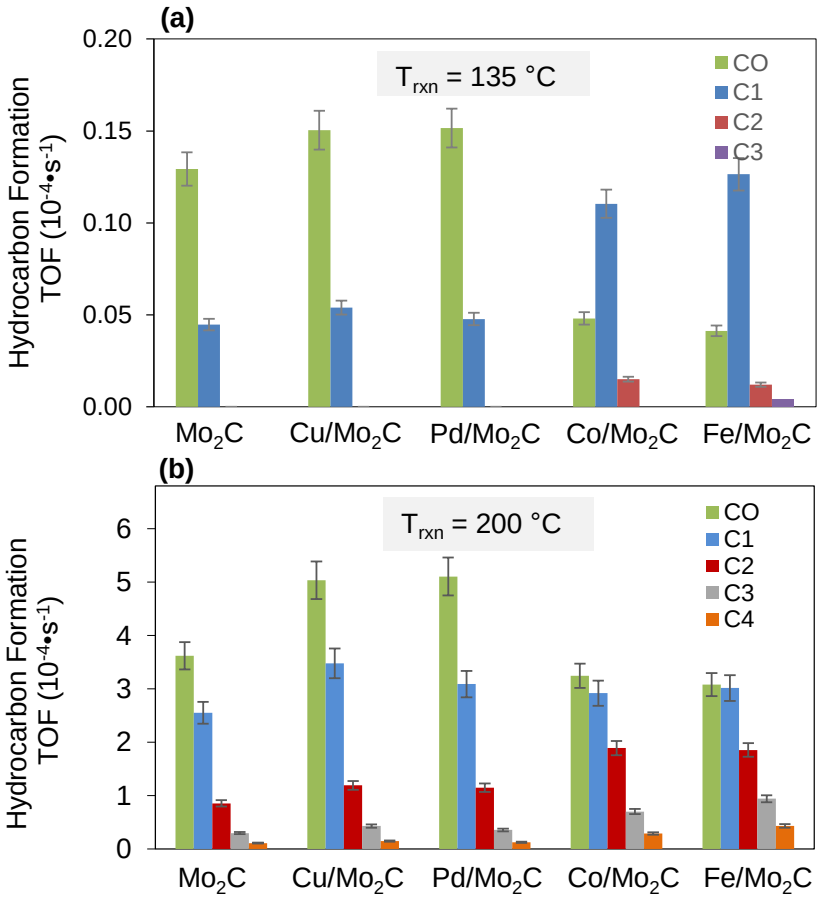

Figure 5.3 Turnover frequencies of CO and hydrocarbon formation at (a) 135 ℃ and (b) 200 ℃ on M/Mo_2C catalysts. Experiments were performed at 10 bar CO_2, 30 bar H_2 and 37.5 ml 1,4-dioxane.

5.3.3 Reaction Pathway Investigation

There are multiple pathways to the products described in the last section. The CO_2 hydrogenation products could be the result of CO produced via the RWGS reaction. Mo_2C

catalysts have been reported to be highly active for RWGS [25]. Alcohols and hydrocarbons could be produced from CO. Alternately the alcohols and hydrocarbons may have been produced directly from CO_2. Apparent activation energies for individual products often provide useful insights regarding the reaction pathways. We also used CO and CH_3OH as the reactants to interrogate the reaction pathways. Based on the activities and selectivities presented in Section 5.3.2, we selected the Cu/Mo_2C (selective for CH_3OH) and Fe/Mo_2C (selective for C_2-C_4 hydrocarbon) catalysts for the reaction pathway investigations.

Arrhenius plots for the formation of CH_3OH and hydrocarbons for the Cu/Mo_2C and Fe/Mo_2C catalysts are illustrated in Figure 5.4. The corresponding apparent activation energies, $E_{a,App}$, are listed in Table 5.3. Activation energies for hydrocarbon formation were very different and much higher than those for CH_3OH formation. This suggested that the rate determining steps involved different intermediates and perhaps different active sites. In comparing $E_{a,\,App}$ values for Mo_2C with those for the supported metal catalysts, we note a slight reduction consistent with the metal facilitating conversion. These trends are consistent with our previous findings that Cu facilitates CH_3OH production while Fe enhances hydrocarbon formation over Mo_2C surface.

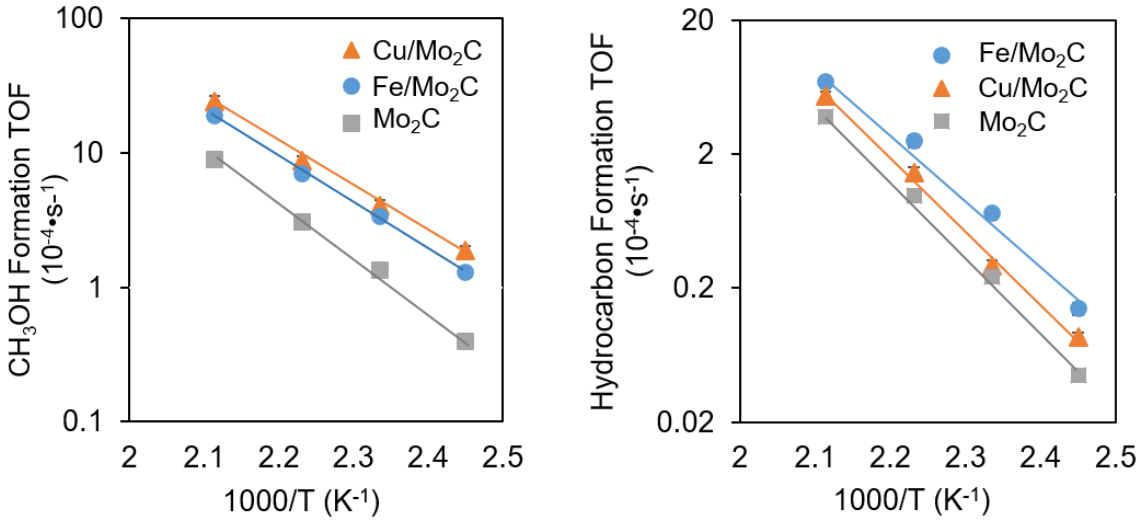

Figure 5.4 Arrhenius plots for the formation of (a) CH_3OH and (b) hydrocarbons from CO_2 hydrogenation at temperatures of 135-200 ℃ on Mo_2C, Cu/Mo_2C, and Fe/Mo_2C. The experiments were performed at temperatures of 135, 155, 175, 200 ℃, 10 bar CO_2 and 30 bar H_2 in 1,4-dioxane.

Table 5.3 Apparent activation energies for the Mo_2C and M/Mo_2C catalysts.

Catalysts	$E_{a,App}$ (kJ/mol)[a]	
	CH_3OH Formation	Hydrocarbon Formation
Mo_2C	76 ±7	110 ±8
Cu/Mo_2C	60 ±5	105 ±8
Fe/Mo_2C	65 ±4	96 ±7

[a] $E_{a,App}$ was calculated based on the reaction rates at 135-200 ℃

5.3.3.1 CO Hydrogenation

The hydrogenation of CO was performed at 200 ℃ using 10 bar CO, 30 bar H_2 over Cu/Mo_2C and Fe/Mo_2C catalysts. The product formation TOFs are shown in Figure 5.5. For both the Cu/Mo_2C and Fe/Mo_2C catalysts, CH_3OH and C_2H_5OH were observed. The CH_3OH produced during CO hydrogenation was only 7.7 and 3.2% of that produced during CO_2 hydrogenation over these catalysts, respectively. This result suggested that most of the CH_3OH produced during CO_2 hydrogenation was directly from CO_2. The

hydrocarbon formation TOFs from CO were 3-4 times higher than those from CO_2 hydrogenation, perhaps due to a higher CO concentration (by about a factor of 4) compared to the CO_2 concentration. Interestingly, when normalized by the CO concentrations, the hydrocarbon formation rates were comparable (within ±12%) for CO and CO_2 hydrogenation, again suggesting that the hydrocarbons were primarily produced via CO hydrogenation. In addition, the dominant product was CO_2 for both catalysts, suggesting the significance of WGS at these conditions. We will compare the chain propagation properties in the discussion section.

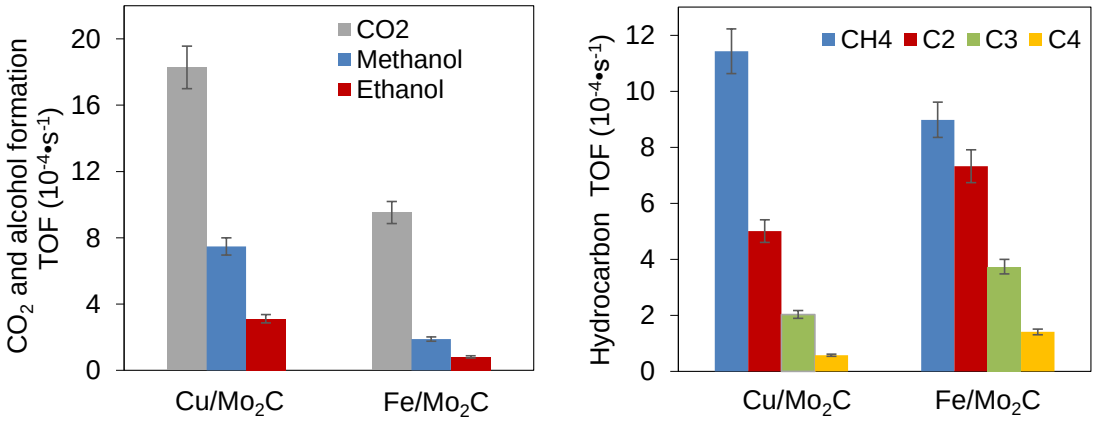

Figure 5.5 Product TOFs for CO hydrogenation over Cu/Mo_2C and Fe/Mo_2C catalysts. (a) CO_2 and alcohol TOF (b) hydrocarbon TOF. Experiments were performed at 200 ℃, 10 bar CO, 30 bar H_2 and 37.5 ml 1,4-dioxane.

5.3.3.2 CH_3OH Hydrogenation

The CH_3OH hydrogenation experiments were performed at 200 ℃ with 7 mmol of CH_3OH, 30 bar H_2, and 10 bar N_2 over the Cu/Mo_2C and Fe/Mo_2C catalysts. The only detectable product was CH_4 (See Figure. A3 in the Appendix A), a consequence of CH_3OH hydrodeoxygenation (HDO) as shown in Eq. (1).

$$CH_3OH + H_2 \rightarrow CH_4 + H_2O, \quad \Delta G_{200°C} = -106\, kJ/mol \qquad \text{Eq. 5.1}$$

Early transition metal carbides including Mo_2C are known to be highly active HDO catalysts [26]. Although CH_3OH HDO is thermodynamically favorable, it is an undesirable side reaction, as CH_4 and H_2O are less valuable than CH_3OH and H_2. The normalized CH_3OH consumption rate only accounted for 3~5% of CH_3OH produced during CO_2 hydrogenation, suggesting that only a small portion of the CH_3OH was lost via HDO. The Cu/Mo_2C was twice as active as the Fe/Mo_2C catalyst (Figure. A3) for CH_3OH HDO with Cu being more effective in producing CH_4. The results also indicated that CH_3OH was not an intermediate for the production of C_2-C_4 hydrocarbons. The amount of CH_4 produced from CH_3OH HDO was negligible (0.7-1%) compared to the total CH_4 formation during the CO_2 hydrogenation. Neither CO nor CO_2 were observed, indicating that CH_3OH steam reforming was insignificant under the conditions employed. The absence of CH_3OH steam reforming was likely a consequence of the high hydrogen content and the lack of H_2O, although anhydrous 1,4-dioxane, the solvent used in our experiments, can contain up to ~100 ppm H_2O.

5.3.4 Post-Reaction Catalyst Properties

To evaluate the stabilities of M/Mo_2C catalysts, several physical and surface properties were characterized before (pre-reaction) and after (post-reaction) use for CO_2 hydrogenation. Again, the Cu/Mo_2C and Fe/Mo_2C catalysts were characterized. There were negligible differences in the surface areas and metal contents before and after reaction (Table 5.4). Diffraction patterns for the pre- and post-reaction Cu/Mo_2C and Fe/Mo_2C catalysts (Figure. A6) were similar although the post-reaction Cu/Mo_2C catalyst exhibited

a slightly sharper peak at 43 °, corresponding to Cu (111). This result suggested a small degree of sintering for the Cu/Mo_2C catalyst. Nevertheless, the results indicated the robustness of the Cu/Mo_2C and Fe/Mo_2C catalysts.

Table 5.4 Surface areas and metal contents for pre- and post-reaction Cu/Mo_2C and Fe/Mo_2C catalysts.

Catalysts	Surface Area (m^2/g)		Metal Contents (%)	
	pre-reaction	post-reaction	pre-reaction	post-reaction
Cu/Mo_2C	135 ±4	129 ±3	5.3 ±0.4	5.5 ±0.7
Fe/Mo_2C	118 ±3	116 ±2	5.1 ±0.5	5.2 ±0.4

Micrographs of the passivated, pre- and post-reaction Cu/Mo_2C and Fe/Mo_2C catalysts are illustrated in Figure 5.6. For the pre-reaction Cu/Mo_2C catalyst (Figure 5.6a), Cu was dispersed unevenly over the Mo_2C surface with particle sizes ranging from 30-500 nm. For the post-reaction Cu/Mo_2C catalyst, slightly larger Cu particles were observed ranging from 50-750 nm. This result is consistent with the diffraction results and confirmed some degree of sintering for the Cu particles during CO_2 hydrogenation at 200 ℃. In contrast, the Fe/Mo_2C catalyst contained relatively large patches of Fe (3-10 μm). These patches are likely the cause for the decrease in the surface area by ~20% (Table 5.1). There was no significant change in the surface morphology when comparing the pre- and post-reaction Fe/Mo_2C catalysts. Interestingly, despite the substantial Fe particles observed in the micrographs, no discernable Fe peaks were observed in the diffraction patterns. A plausible explanation is that Fe is part of either γ-Fe or Fe_2O_3, where their most significant peaks overlap with the major peaks of Mo_2C at ~41 ° and 37 ° respectively, making phase deconvolution difficult (Figure. A1). It has been reported that during the FTS, the active phase for the Fe-based catalyst is an iron carbide [27-29]. No obvious iron carbides were

observed from the XRD, although one of the major Fe_2C peaks also overlaps with the Mo_2C peak at 43 ° (Figure. A1). From the EDX data (see Figure. A4), the carbon and iron were not co-located suggesting that Fe_2C was not present. Interestingly, oxygen and iron were co-located, which implicated the presence of Fe_2O_3 at least at the surface for the passivated materials.

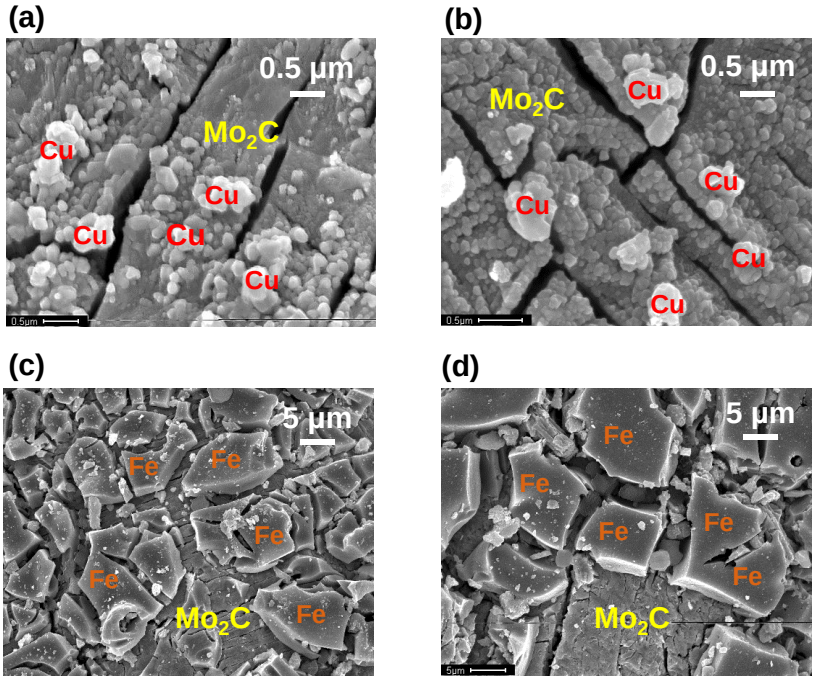

Figure 5.6 Scanning electron micrographs for (a) pre-reaction Cu/Mo_2C, (b) post-reaction Cu/Mo_2C, (c) pre-reaction Fe/Mo_2C, and (d) post-reaction Fe/Mo_2C catalysts.

The H_2-TPR profiles for passivated pre- and post-reaction Cu/Mo_2C and Fe/Mo_2C catalysts are shown in Figure 5.7. The bulk Mo_2C catalyst produced two major peaks: one at low temperature ~ 210 ℃ that we attributed to reduction of the passivation layer [30], and a high temperature peak at ~ 700 ℃ which corresponds to decomposition of the Mo_2C, as observed previously [3]. The addition of Cu and Fe caused a shift in the lower temperature peak from 210 ℃ to 170 and 140 ℃, respectively. A similar shift has been

reported for Pt/Mo_2C catalysts prepared using methods similar to those described in this chapter [31]. This was likely due to H_2 activation over the supported metal; subsequently this hydrogen could be used to reduce the passivated Mo_2C [32, 33]. The presence of the supported metals did not appear to affect decomposition of the Mo_2C (~700 ℃). Similar H_2-TPR profiles were observed for the pre- and post-reaction catalysts, indicating that exposure to the reactants and solvent during the reaction did not alter surface chemistries of the M/Mo_2C catalysts.

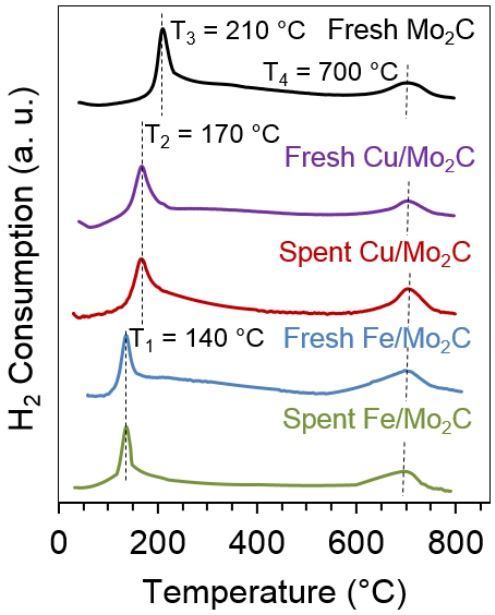

Figure 5.7 H_2 consumption during the H_2-TPR experiment for the M/Mo_2C pre- and post-reaction catalysts. Conditions: 10% H_2/Ar, 4 ℃/min heating rate.

We also characterized the post-reaction catalysts by rerunning the CO_2 hydrogenation experiments. These experiments also provided an assessment of the recyclabilites of the catalysts. The results for the Cu/Mo_2C and Fe/Mo_2C catalysts are shown in Figure 5.8. The slight decrease in CH_3OH production over the Cu/Mo_2C catalyst is consistent with the Cu sintering observed by XRD and SEM. The Fe/Mo_2C activity remained fairly constant on re-use.

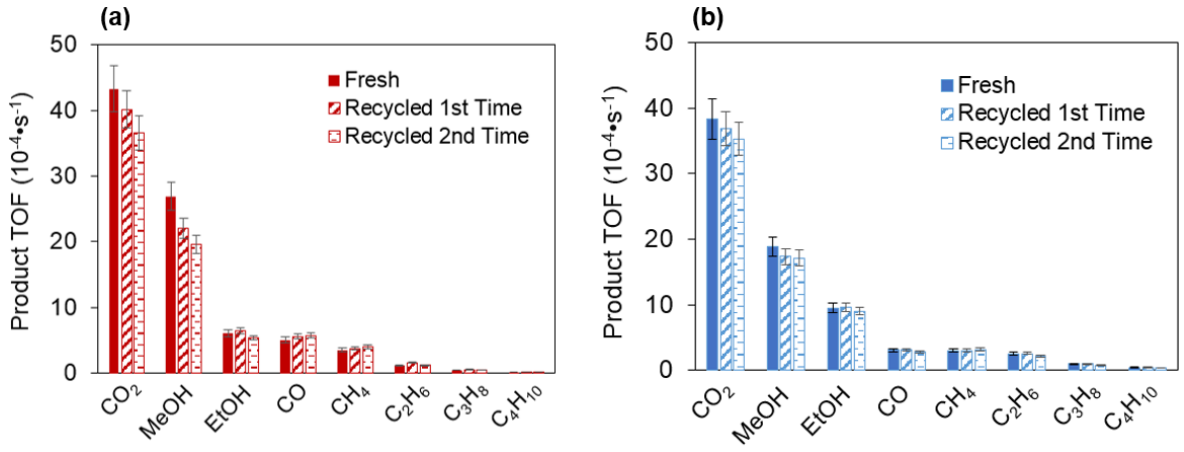

Figure 5.8 Product TOFs for (a) Cu/Mo_2C and (b) Fe/Mo_2C over the fresh and reused catalysts.

5.4 Discussion

Results presented in this chapter allow us to understand the effects of the metal type and temperature on the performance of Mo_2C supported metal catalysts for CO_2 hydrogenation, and the potential reaction pathways for these catalysts.

There are limited reports regarding CO_2 hydrogenation over Mo_2C-based catalysts, and other than our prior work [34], the experiments were carried out with gas phase reactants. Table 5.5 compares results from our work with those in the literature that are at similar temperatures. The CO_2 conversion TOFs are of the same order of magnitude. This is particular interesting given the lower CO_2 and H_2 concentrations in the liquid phase (0.10 and 0.18 mol/L for CO_2 [16] and H_2 [15], respectively, in 1,4-dioxane at 200 ℃, 10 bar CO_2, and 30 bar H_2) compared to those for experiments carried out in the gas phase (0.3, 0.77 mol/L for CO_2 [35] and H_2 at 200 ℃, 10 bar CO_2, and 30 bar H_2). We also note that CO and CH_4 were the predominant products for CO_2 hydrogenation in the gas phase, while alcohols including C_2H_5OH and C_{2+} hydrocarbons were the predominant products for our work in the liquid phase. This difference in selectivity was likely due to the different

reactant densities in the liquid and gas phase media. Different synthesis and pretreatment protocols could also contribute to the differences. Recall that we directly employed freshly-synthesized Mo_2C catalyst without surface passivation. Xu et al. [8] and Dubois [6] et al. described a pretreatment of the passivated Mo_2C via recarburization or H_2 reduction prior to the reaction. This could introduce different types or distributions of the active sites over the Mo_2C surface and ultimately alter the product selectivities.

Table 5.5 Comparing CO_2 hydrogenation activities and selectivities on Mo_2C-based catalysts between the literature and this study.

Catalyst	T (℃)/ P(bar)	CO_2/H_2 ratio	Phase	TOF (s^{-1}•10^4)	Selectivity (%)					Reference
					CO	CH_3OH	C_2H_5OH	CH_4	C_{2+}	
Mo_2C	200/40	0.33	Liquid	20	5	53	16	17	9	This work
Cu/Mo_2C	200/40	0.33	Liquid	41	9	62	14	10	6	This work
Fe/Mo_2C	200/40	0.33	Liquid	38	7	58	16	8	11	This work
α-MoC_{1-x}	200/20	0.2	Gas	14	52	28	1	11	5	[28]
β-Mo_2C	200/20	0.2	Gas	106	39	21	1	29	8	[28]
Cu/Mo_2C	220/60	3	Gas	219	49	32	0.4	14	4	[26]

Results presented in this chapter are consistent with different active sites for the formation of alcohols and hydrocarbons. Recall that activation energies obtained for CH_3OH (60-76 kJ/mol) and hydrocarbons (96-110 kJ/mol) were different (Table 5.3) implying different rate determining steps and perhaps different pathways. Xu et al. [8] indicated that selectivities during CO_2 hydrogenation were highly dependent on the Mo/C ratio and crystalline phases present. They reported that β-Mo_2C catalyst was more active than α-MoC_{1-x} but produced primarily CO and CH_4, while α-MoC_{1-x} catalyst was more selective to CH_3OH. Porosoff et al. [9] also reported that a β-Mo_2C catalyst exhibited high selectivities to CO albeit at atmospheric pressure. Recall that the Mo_2C used in the current

study was a mixture of α-MoC_{1-x} and β-Mo_2C, therefore, it is plausible that α-MoC_{1-x} produced primarily CH_3OH, and β-Mo_2C produced primarily CO (via RWGS) and perhaps C_1-C_4 hydrocarbons via FTS. The supported metals likely influenced the properties of sites already on the Mo_2C surface; it is also possible that the metals introduced new sites. Previously we reported experimental and computational results suggesting that, for Pt/Mo_2C catalysts, highly active sites for WGS were located at the interface between the Pt and Mo_2C [4]. These sites were much more active than those associated solely with Mo_2C or Pt. Results presented in this current chapter do not allow us to determine if there were active sites for CO_2 hydrogenation at the interface between the metal and Mo_2C, however, the presence of the supported metal clearly contributed to the catalytic properties.

The addition of Cu and Pd resulted in a significant increase in the CO_2 conversion rates and selectivities to CH_3OH at 135 and 200 ℃ (Table 5.2). Copper [36-38] and Pd [39-41] are known to be selective for CO_2 hydrogenation to CH_3OH, and their addition to Mo_2C would be expected to improve the CH_3OH selectivity. Copper and Pd have also been reported to function synergistically with metal oxides (e.g. ZrO_2 and ZnO) by facilitating H_2 dissociation, which makes atomic H available to the support (likely via H_2 spillover) for CO_2 hydrogenation [42, 43]. The possibility of synergy between Cu and Mo_2C is currently being explored. While Cu and Pd affected CH_3OH selectivities, the Co/Mo_2C and Fe/Mo_2C catalysts yielded significant amounts of C_{2+} hydrocarbons and ethanol. Weatherby [44] reported that oxide supported Co and Fe facilitate the formation of C_{2+} products during CO_2 hydrogenation and suggested that the hydrocarbons were produced via CO hydrogenation. Our results are consistent with this finding, in particular that CO is likely a primary intermediate for hydrocarbons over the Mo_2C catalyst. We postulate that

Mo_2C produces CO via the RWGS and CO hydrogenation occurs on both the Fe or Co particles [45-47] and the Mo_2C surface. Ethanol may have been produced via a CO-insertion or oxygenate-based mechanism [24].

Figure 5.9 summarizes what we understand about the reaction pathways for CO_2 hydrogenation over Mo_2C supported metal catalysts under the experimental conditions employed for our research. Similarities between the hydrocarbon formation rates and distributions for CO hydrogenation and CO_2 hydrogenation are consistent with CO being a common intermediate.

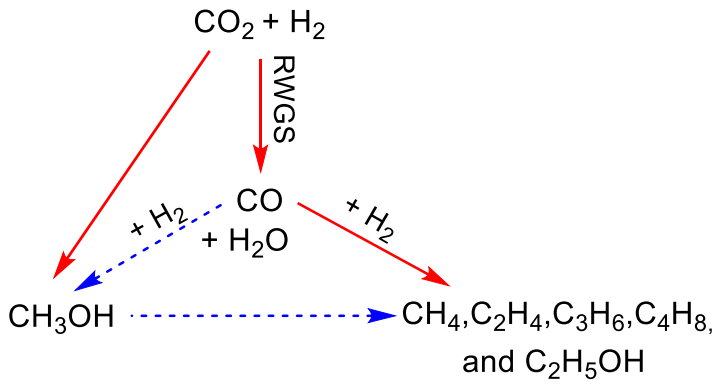

Figure 5.9 Proposed reaction pathways to produce alcohols and hydrocarbons from CO_2 and H_2. The solid arrows denote major pathways and the dashed arrows denote minor pathways. The pathways are applicable to the following experimental conditions: 200 ℃, 10 bar CO_2, and 30 bar H_2 in 1,4-dioxane.

A useful way to compare the hydrocarbon distributions is via Anderson-Schulz-Flory chain propagation probabilities (α). These α values were determined using the Anderson-Schulz-Flory equation (Equation (1)):

$$W_n/n = (1-\alpha)^2 \bullet \alpha^{n-1} \qquad \text{Eq. 5.2}$$

where W_n is the weight fraction of hydrocarbons containing n carbon atoms and α is the chain propagation probability, i.e. the probability that a molecule continues reacting to

form a longer chain. The α value is obtained by taking the linear slope of log (Wn/n) and n (the ASF plots can be found in Figure. A4). The α values for CO and CO_2 hydrogenation are identical (see Table 5.6). Also note that α values for the Fe/Mo_2C and Co/Mo_2C catalysts were higher than those for other catalysts for both CO_2 and CO hydrogenation. These results are consistent with literature indicating that Fe and Co are effective for chain propagation during FTS [45, 48], while Cu or Pd produce surface intermediates that lead to C_1 products, i.e. CH_4 and CH_3OH [40, 49, 50]. While CH_3OH was an additional source of CH_4, the contribution was insignificant such that the α values were not affected.

Table 5.6 Chain propagation probabilities for the M/Mo_2C catalysts.

Catalysts	Chain propagation probability (α)	
	CO_2 Hydrogenation	CO Hydrogenation
Mo_2C	0.21 ± 0.02	--
Cu/Mo_2C	0.22 ± 0.01	0.22 ± 0.02
Pd/Mo_2C	0.21 ± 0.02	--
Co/Mo_2C	0.27 ± 0.01	--
Fe/Mo_2C	0.31 ± 0.02	0.31 ± 0.02

Three mechanisms have been suggested for the formation of C_{2+} products during CO hydrogenation [51, 52]: the carbide, oxygenate, and CO insertion mechanisms. Recently, a mechanistic study performed by Schaidle et al. [53] implicated that the chain growth over Mo_2C-based catalysts was primarily via the oxygenate mechanism. This mechanism involves the molecular adsorption of CO and subsequent hydrogenation to produce surface methoxy species (–CHO); C-C coupling then occurs via condensation of the –CHO species and hydrogenation steps. This pathway produces alcohols as the side products during the chain growth to form hydrocarbons, which is consistent with ethanol

formation at 200 ℃ for our study. Iron-based catalysts have also been reported to perform chain propagation via the oxygenate mechanism [29]. In fact, Mo_2C-based catalysts are known to dissociatively and associatively adsorb CO, with the latter being responsible for chain propagation [53]. Given our results, we believe the addition of Fe introduced additional associative adsorption sites over Mo_2C, which modifies Mo_2C and results in an enhancement in C_{2+} hydrocarbon formation.

Two pathways have been suggested for CH_3OH production; one involving surface formate and formaldehyde species and the other involving CO as the major intermediate [54-56]. In comparing the CH_3OH production rates during CO and CO_2 hydrogenation, we found that CO contributed insignificantly (3-7%) to the total CH_3OH production implicating surface formates and aldehydes as principal intermediates. Interestingly, neither formic acid nor aldehyde were detected during the reaction. We believe that these species were rapidly converted, given the thermodynamic favorability (Appendix A, Table A1).

5.5 Conclusions

In summary, a series of Mo_2C-supported metal catalysts were evaluated for CO_2 hydrogenation at 135-200 ℃ in 1,4-dioxane solvent. At 135 ℃, the catalyst favors CH_3OH with selectivities up to 95%, while at 200 ℃, the selectivity shifts to C_2H_5OH (~15%) and C_2-C_4 (5-10%) hydrocarbons with a reduced selectivity to CH_3OH formation (50-70%). A comparison of the product distributions over the M/Mo_2C catalysts revealed that the addition of Cu and Pd enhanced CH_3OH synthesis, while the deposition of Co and Fe enhanced C-C coupling to produce C_2-C_4 hydrocarbons and ethanol. Our analysis of the reaction pathway suggests that CO was the intermediate for hydrocarbon production via

FTS, while CO_2 was the primary source for CH_3OH likely via surface formate/aldehyde intermediates. The M/Mo_2C catalysts were robust and experienced minimal changes in catalytic activity and physical/surface properties as a consequence of use for CO_2 hydrogenation. The results also suggested that Mo_2C possessed distinct sites for the production of alcohols and hydrocarbons. The activities of these sites can be altered by, for example, depositing metals or changing the synthesis/treatment protocols. The findings from this study advance our understanding of the low temperature CO_2 hydrogenation activities of carbide supported metal catalysts and provide insights for the design of these types of materials for other reactions.

5.6 References

[1] S. Oyama, Catal. Today 15 (1992) 179-200.
[2] P.M. Patterson, T.K. Das, B.H. Davis, Appl. Catal., A 251 (2003) 449-455.
[3] J.J. Patt, Carbide and Nitride Catalysts for the H_2O Gas Shift Reaction, University of Michigan, 2003.
[4] N.M. Schweitzer, J.A. Schaidle, O.K. Ezekoye, X. Pan, S. Linic, L.T. Thompson, J. Am. Chem. Soc. 133 (2011) 2378-2381.
[5] W. Setthapun, S. Bej, L. Thompson, Top. Catal. 49 (2008) 73-80.
[6] J.-L. Dubois, K. Sayama, H. Arakawa, Chem. Lett. 21 (1992) 5-8.
[7] A.B. Vidal, L. Feria, J. Evans, Y. Takahashi, P. Liu, K. Nakamura, F. Illas, J.A. Rodriguez, J. Phys. Chem. Lett. 3 (2012) 2275-2280.
[8] W. Xu, P. Ramirez, D. Stacchiola, J. Rodriguez, Catal. Lett. 144 (2014) 1-7.
[9] M.D. Porosoff, X. Yang, J.A. Boscoboinik, J.G. Chen, Angew. Chem. 126 (2014) 6823-6827.
[10] Y. Liu, W. Zhang, T.J. Pinnavaia, J. Am. Chem. Soc. 122 (2000) 8791-8792.
[11] M.J. Verhoef, P.J. Kooyman, J.A. Peters, H. van Bekkum, Microporous Mesoporous Mater. 27 (1999) 365-371.
[12] J.A. Schaidle, N.M. Schweitzer, O.T. Ajenifujah, L.T. Thompson, J. Catal. 289 (2012) 210-217.
[13] B.M. Wyvratt, J.R. Gaudet, L.T. Thompson, J. Catal. 330 (2015) 280-287.
[14] H.P. Klug, L.E. Alexander, X-Ray Diffraction Procedures: For Polycrystalline and Amorphous Materials, 2nd ed., Wiley-VCH, 1974.
[15] E. Brunner, J. Chem. Eng. Data 30 (1985) 269-273.
[16] D. Kassim, H. Zainel, S. Al-Asaf, E. Talib, Fluid Phase Equilib. 41 (1988) 287-294.
[17] P. Canton, G. Fagherazzi, M. Battagliarin, F. Menegazzo, F. Pinna, N. Pernicone, Langmuir 18 (2002) 6530-6535.

[18] S. Alayoglu, F. Tao, V. Altoe, C. Specht, Z. Zhu, F. Aksoy, D. Butcher, R. Renzas, Z. Liu, G. Somorjai, Catal. Lett. 141 (2011) 633-640.
[19] J. Evans, M. Wainwright, A. BridgeH_2O, D. Young, Appl. Catal. 7 (1983) 75-83.
[20] R.C. Reuel, C.H. Bartholomew, J. Catal. 85 (1984) 63-77.
[21] D. Panayotov, M. Khristova, D. Mehandjiev, J. Catal. 156 (1995) 219-228.
[22] E. Guglielminotti, The Journal of Physical Chemistry 98 (1994) 4884-4891.
[23] P. Dowben, M. Grunze, Langmuir 2 (1986) 368-372.
[24] J.A. Schaidle, Carbide and Nitride Based Catalysts for Synthesis Gas Conversion, University of Michigan, 2011.
[25] M. Saito, R.B. Anderson, J. Catal. 67 (1981) 296-302.
[26] H. Ren, W. Yu, M. Salciccioli, Y. Chen, Y. Huang, K. Xiong, D.G. Vlachos, J.G. Chen, ChemSusChem 6 (2013) 798-801.
[27] Y. Jin, A.K. Datye, J. Catal. 196 (2000) 8-17.
[28] T. Herranz, S. Rojas, F.J. Pérez-Alonso, M. Ojeda, P. Terreros, J.L.G. Fierro, J. Catal. 243 (2006) 199-211.
[29] B.H. Davis, Catal. Today 141 (2009) 25-33.
[30] T.E. King, Carbide and Nitride Supported H_2O-Gas Shift Catalysts, University of Michigan, 2007.
[31] W. Setthapun, Carbide and Nitride Supported CH_3OH Steam Reforming Catalysts, University of Michigan, 2007.
[32] S. Srinivas, P.K. Rao, J. Catal. 148 (1994) 470-477.
[33] V.V.e. Rozanov, O.V. Krylov, Russian chemical reviews 66 (1997) 107-119.
[34] Y. Chen, S. Choi, L.T. Thompson, ACS Catal. 5 (2015) 1717-1725
[35] G.C. Kennedy, Amer. J. Sci 252 (1954).
[36] M. Behrens, F. Studt, I. Kasatkin, S. Kühl, M. Hävecker, F. Abild-Pedersen, S. Zander, F. Girgsdies, P. Kurr, B.-L. Kniep, M. Tovar, R.W. Fischer, J.K. Nørskov, R. Schlögl, Science 336 (2012) 893-897.
[37] I. Kasatkin, P. Kurr, B. Kniep, A. Trunschke, R. Schlögl, Angew. Chem. 119 (2007) 7465-7468.
[38] S. Natesakhawat, J.W. Lekse, J.P. Baltrus, P.R. Ohodnicki, B.H. Howard, X. Deng, C. Matranga, ACS Catal. 2 (2012) 1667-1676.
[39] X. Jiang, N. Koizumi, X. Guo, C. Song, Applied Catalysis B: Environmental 170–171 (2015) 173-185.
[40] T. Fujitani, I. Nakamura, Bulletin of the Chemical Society of Japan 75 (2002) 1393-1398.
[41] S.E. Collins, J.J. Delgado, C. Mira, J.J. Calvino, S. Bernal, D.L. Chiavassa, M.A. Baltanás, A.L. Bonivardi, J. Catal. 292 (2012) 90-98.
[42] C. Schild, A. Wokaun, A. Baiker, Fresenius' J. Anal. Chem. 341 (1991) 395-401.
[43] F. Arena, K. Barbera, G. Italiano, G. Bonura, L. Spadaro, F. Frusteri, J. Catal. 249 (2007) 185-194.
[44] G.D. Weatherbee, C.H. Bartholomew, J. Catal. 87 (1984) 352-362.
[45] S. Li, S. Krishnamoorthy, A. Li, G.D. Meitzner, E. Iglesia, J. Catal. 206 (2002) 202-217.
[46] H. Arakawa, A.T. Bell, Industrial & Engineering Chemistry Process Design and Development 22 (1983) 97-103.

[47] T. Riedel, M. Claeys, H. Schulz, G. Schaub, S.-S. Nam, K.-W. Jun, M.-J. Choi, G. Kishan, K.-W. Lee, Appl. Catal., A 186 (1999) 201-213.
[48] D. Schanke, S. Vada, E. Blekkan, A. Hilmen, A. Hoff, A. Holmen, J. Catal. 156 (1995) 85-95.
[49] Y. Yang, J. Evans, J.A. Rodriguez, M.G. White, P. Liu, Phys. Chem. Chem. Phys. 12 (2010) 9909-9917.
[50] A.A. Peterson, F. Abild-Pedersen, F. Studt, J. Rossmeisl, J.K. Nørskov, Energy Environ. Sci. 3 (2010) 1311-1315.
[51] B.H. Davis, Fuel Process. Technol. 71 (2001) 157-166.
[52] G.P. Van Der Laan, A. Beenackers, Catalysis Reviews 41 (1999) 255-318.
[53] J.A. Schaidle, L.T. Thompson, J. Catal. 329 (2015) 325-334.
[54] J. Ye, C.-j. Liu, D. Mei, Q. Ge, J. Catal. 317 (2014) 44-53.
[55] L.C. Grabow, M. Mavrikakis, ACS Catal. 1 (2011) 365-384.
[56] J. Weigel, R.A. Koeppel, A. Baiker, A. Wokaun, Langmuir 12 (1996) 5319-5329.

CHAPTER 6

CHEMOSELECTIVE HYDROGENATION OF CROTONALDEHYDE IN A SOLID-POLYMER-ELECTROLYTE REACTOR

6.1 Introduction

The work described in Chapters 2-5 of this dissertation illustrated the use of cascade systems for the low temperature selective hydrogenation of CO_2 and other C=O containing species, including formic acid, formate ester, and DMF to produce CH_3OH using thermochemical routes. In this chapter, we investigated the electrochemical route for the low temperature chemoselective hydrogenation of multifunctional organics. In particular, we targeted the selective hydrogenation of α,β-unsaturated aldehydes (containing both C=O and C=C functional groups), with the corresponding unsaturated alcohols being the desired products.

The chemoselective hydrogenation of multifunctional organic compounds serves as a key process to produce higher value chemicals from low-value starting materials and is of great importance to the chemical industry. These reactions account for almost 20% of the reaction steps in a typical chemical process [1], with applications in pharmaceutical, cosmetics, and manufacturing industries [2].

Commercial selective hydrogenation reactions are typically performed in thermo-catalytic reactors; however, there are two major limitations associated with these conventional systems. First, the reactions are usually carried out at high temperatures (> 250 °C) and pressures (> 50 bar) and therefore require significant capital and operating costs. Second, the mass transport of gaseous H_2

through the liquid phase to the solid catalyst surface and the poor H_2 solubility in the solvents restricts the reaction rates.

Recently, solid-polymer-electrolyte (SPE) reactors have been reported as an alternative to thermochemical reactors for chemical syntheses [3-7]. The reactor has a similar structure to a fuel cell, in that it is composed of an anode, a cathode and an ion- exchange-membrane. However, unlike fuel cells which produce electricity, this reactor uses electricity as the driving force to carry out the reactions. This process is potentially sustainable if electricity is derived from a common renewable source, such as solar, wind, and hydroelectric [8]. Several multifunctional organic hydrogenation reactions have been successfully performed in an SPE reactor, including triglyceride hydrogenation [3, 9, 10] and nitrobenzene reduction [6, 7].

Compared to a traditional thermo-catalytic reactor, an SPE reactor can perform the reactions at low temperatures and ambient pressures, decreasing the equipment and operation costs. Mild reaction temperatures are also beneficial if the desirable products are generated from exothermic processes. Furthermore, using an SPE reactor reduces the mass transport limitations by providing the hydrogen in the form of protons at the catalyst surface under the applied potential. This latter attribute eliminates the problem of low hydrogen solubility in the solvent [10].

Research described in this chapter investigated the use of an SPE reactor for the selective hydrogenation of multifunctional organic compounds containing C=C and C=O groups. Crotonaldehyde (CH_3-CH=CH-CHO) was selected as the model molecule for its simple chemical structure while still containing both C=C and C=O groups [10]. The key findings of this research provide a scientific basis to perform the hydrogenation of other organic compounds with similar functional groups in the SPE reactor and create a more energy-efficient means of chemical synthesis.

6.2 Background

The following subsections will introduce the structure of a typical SPE reactor and review several hydrogenation reactions that have been successfully performed in this type of reactor. Additionally, the previous work regarding hydrogenating crotonaldehyde using both electrochemical and thermocatalytic reactors will be discussed.

6.2.1 SPE Reactor

A typical SPE reactor consists of bipolar plates, fluid channels and a membrane electrode assembly (MEA), as shown in Figure 6.1 [8]. The two stainless steel bipolar plates are directly connected to the electrical power supply for conducting electricity. The graphite plates with patterned fluid channels are used to distribute the substrate to the membrane surface.

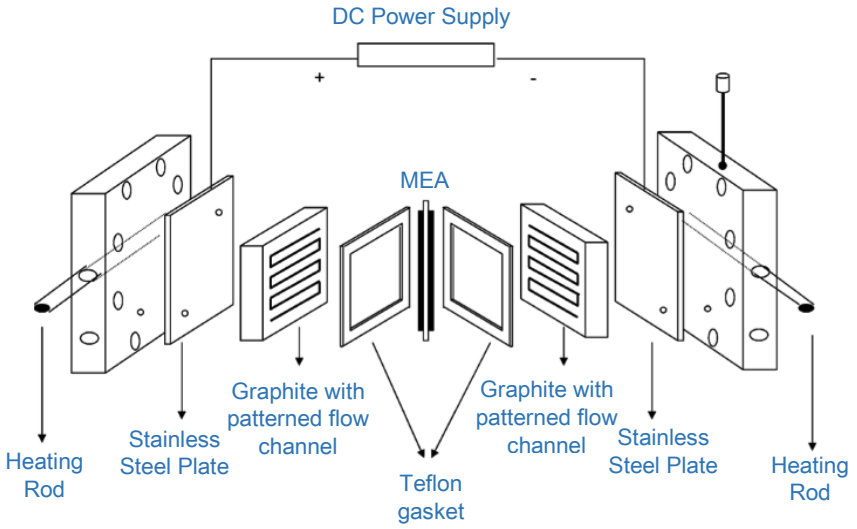

Figure 6.1 Scheme diagram of an SPE reactor. Taken from [10].

The core component of the reactor is the MEA. A typical MEA has an ion-exchange membrane, e.g. Nafion®, in the middle with gas-diffusion layers (GDLs), usually carbon paper or carbon cloth, loaded with catalysts hot-pressed onto each side of the membrane. A GDL with

catalysts on its surface serves as an electrode. The MEA is tightly inserted between two flow channels by the Teflon® gasket for efficient proton transport. In a hydrogenation reaction, H_2 is fed to the anode and oxidized to protons. The protons migrate through the membrane to reach the cathode surface, where they are reduced to atomic hydrogen on the surface for further hydrogenation or to molecular H_2, i.e. the hydrogen evolution reaction (HER). This is an undesirable reaction, as it reduces the efficiency of the selective hydrogenation reactions.

6.2.2 Hydrogenation Reaction in a SPE Reactor

Several studies on hydrogenation reactions of multifunctional organic compounds have been carried out in SPE reactors. In 1998, An et al. examined the hydrogenation of triglycerides in an SPE reactor at 50-80 ℃ and 1 atm H_2 [9]. The reactions were operated with a constant current density of 0.1A/cm^2 and used RuO_2 as the anode catalyst and Pd black or Pt black as the cathode catalyst. During the reaction, hydrogen reacted with the triglycerides to generate various products. The products included the *cis* and the undesirable *trans* isomers; however, the *trans* isomer yield (4%) was significantly lower when compared to the conventional thermocatalytic process (36.5%) [4]. Their findings suggested that at optimal electrochemical conditions, the SPE reactor could result in superior selectivities to the desired product than the conventional thermo-catalytic reactor.

In 2000, Yuan et al. reported work on nitrobenzene hydrogenation in an SPE reactor. In the study, they achieved cogeneration of cyclohexylamine and electrical power [7]. The reaction was conducted at 70 ℃ and 2 atm H_2 using 20% Pt/C as the catalysts for both the cathode and the anode. Potential hydrogenation products for this reaction include aniline (AN) and cyclohexylamine (CHA), where the latter was the desired product for its value in the metal-coating and pharmaceutical industry. They studied the effects of H_2 flow rate on the selectivity of the products and achieved a CHA selectivity of 57.3% using a flow rate of 20 mL/min H_2. A maximum power density of 1.5

mW/cm^2 was also achieved as the cogenerated electrical power. This study demonstrated the feasibility of using an SPE reactor for selective chemical synthesis with concurrent power generation.

6.2.3 Crotonaldehyde Hydrogenation Reaction

A reaction scheme for crotonaldehyde (CAL) hydrogenation and the thermodynamic properties associated with each step [11, 12] is shown in Figure 6.2. Selective hydrogenation can occur on the C=O bond to generate crotyl alcohol (COL), or on the C=C bond to form butyraldehyde (BAL). Further hydrogenation of COL or BAL produces n-butanol (BOH). The desired (high-value) product is COL, which is used in the flavor, fragrance, and pharmaceutical industries [10]. Obtaining each hydrogenation product is thermodynamically down-hill but producing COL is more challenging than the other two products, indicated by a higher ΔG° (Figure 6.2). Therefore, the major research focus is to understand which factors influence the reaction activity and selectivity.

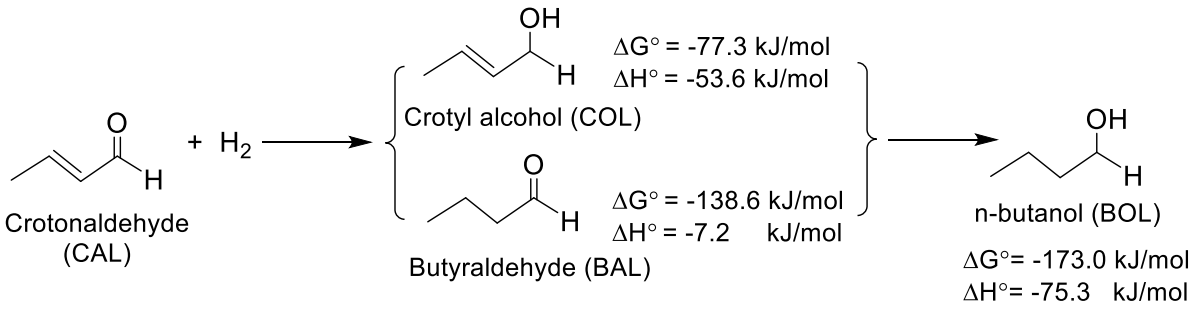

Figure 6.2 Crotonaldehyde hydrogenation reaction scheme and thermodynamic properties.

6.2.4 Crotonaldehyde Hydrogenation in Electrochemical Reactors

In 1982, G. Horanyi et al. [13] performed CAL reduction on a platinum electrode in a liquid electrolyte-based three-electrode cell. The reaction was conducted under a constant voltage of 60 mV using 1M H_2SO_4 as the electrolyte. No H_2 was fed into the system; instead, protons from H_2SO_4 provided the hydrogen for reduction. Some gaseous hydrocarbons were formed as products, including propane, butane, and butene. The authors proposed a scheme for the reaction shown in

Figure 6.3; the final products were mainly hydrocarbons. This observation indicated that at these electrochemical conditions, the reactions did not stop at the primary or secondary hydrogenation products, e.g. COL, BAL, or BOL, but proceeded with the hydrogenation or deoxygenation to produce hydrocarbons.

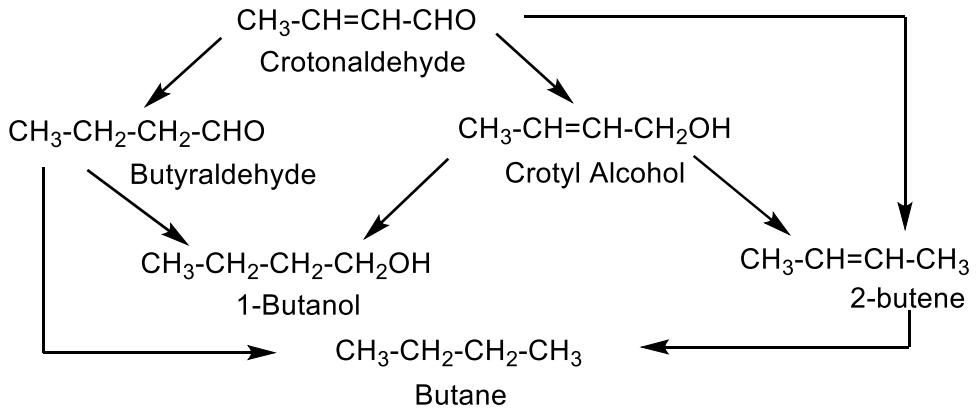

Figure 6.3 Proposed crotonaldehyde hydrogenation scheme.

Barnes et al. also examined the electrochemical reduction of CAL at a dropping mercury electrode [13]. They reported that the product distribution was greatly dependent on the pH value of the electrochemical environment. The results showed that in acidic media, an unsaturated diol (a dimer of CAL) was the major product; however, in a basic environment the *trans*-COL was primarily produced. This study demonstrated the feasibility of producing COL via electrochemical CAL reduction.

6.2.5 Crotonaldehyde Hydrogenation in Thermocatalytic Reactors

The majority of published research regarding CAL hydrogenation were performed in thermocatalytic reactors. Several representative studies are summarized in Table 6.1. In these studies, CAL hydrogenation was carried out at relatively high pressures (>10 bar) and moderate temperatures, i.e. higher than room temperature but less than 150 ℃. The catalysts utilized in this

study were mostly noble metals, such as Pt, Ru, or Ag, supported on metal oxides. The selectivity to COL was reported to be highly dependent on both the catalysts and the operating conditions.

Table 6.1 Thermocatalytic crotonaldehyde hydrogenation: conditions and results.

Authors	Year	T(˚C)	P (atm)	Catalysts	Selectivity % to COL
X. Yang et al. [15]	2009	140	30	Ag/SiO_2,Au/SiO_2, Pt/SiO_2	50%
B. Campo et al. [16]	2009	80	10	Au/CeO_2	29%
Šebkoá et al. [17]	2003	80	80	Pt/SnO_2, Ru/SnO_2	60%

6.3 Experimental

6.3.1 Description of SPE Reactor System

Figure 6.4 illustrates the experimental apparatus designed for CAL hydrogenation in an SPE reactor. A stream of H_2, monitored by a mass flow meter, was hydrated in a humidifier and then was flowed into the anode side. The hydrated H_2 kept the membrane moisturized during the reaction to ensure that the cation-exchange-membrane functioned properly. On the other side of the membrane, a stream of 5 vol% CAL in isopropanol was pumped into the cathode block. The stream was placed in a circulation loop to allow sufficient contact time between CAL and the catalyst surface. The cathode effluent was sampled after 3, 6, 9, and 24 h and sent to a GC for further analyses.

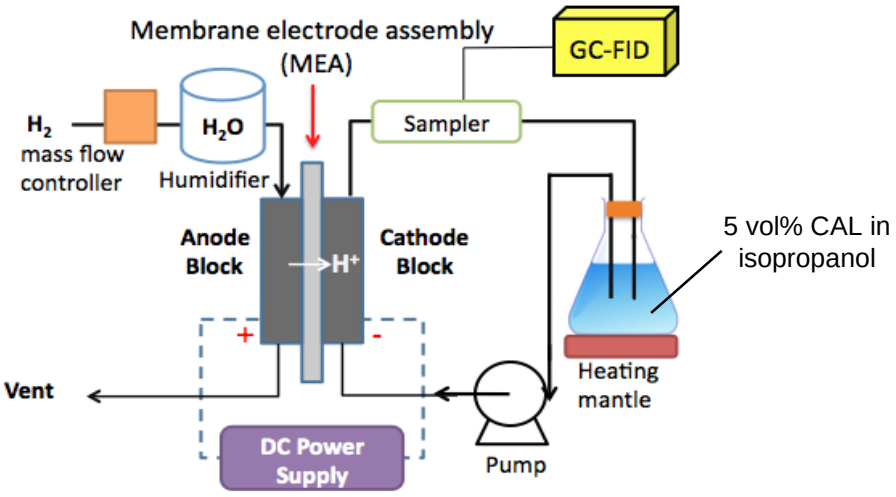

Figure 6.4 Schematic diagram of experimental apparatus for crotonaldehyde hydrogenation.

6.3.2 MEA Fabrication

Membrane electrode assemblies (MEAs) were fabricated based on a FuMA-Tech FKB® membrane. The details for selecting this membrane will be described in Section 6.4.1 of this chapter. The fabrication was accomplished via three steps. First, the catalyst suspension was prepared as a mixture of 20% Pt/C (Alfa Aesar, 190 m^2/g) and a binder, i.e. the FKB solution with a mass ratio of 3:20. The FKB solution was 5 wt% of FKB ionomer (Fumasep®) in dimethylacetamide (Sigma-Aldrich, 99%). The suspension was stirred for 24 h on a magnetic stir plate to ensure thorough mixing. The carbon GDLs (Toray TGP-H-090) were cut to the size of 6.45 cm^2 before loading the catalysts. Second, the catalyst slurry was painted onto the surface of the GDLs and these painted GDLs were then dried in a vacuum oven at 150 ℃. The painting step was repeated until the desired metal loading of 0.1 mg Pt/cm^2 was achieved by monitoring the weight increase on the GDLs. Fumasep® FKB membrane was pretreated using 0.5 mol/L sulfuric acid (Fischer Scientific) and ultra pure H_2O (18MΩ*cm, Millipore Hilli-Q Advantage A10) to

remove the organic impurities. Finally, the MEA was placed between two copper plates and hot pressed at 210 ℃ and 20 MPa for 5 minutes.

6.3.3 Gas Chromatography Analysis

The products were analyzed using a Varian 450 GC with FID and Varian MS-220 (Mass Spectroscopy) for product identification. The column used for separation was CP-WAX 57CB (25 m $\times$ 0.25 mm $\times$ 0.1 μm). The products were identified by their retention time and confirmed by comparison to standard MS spectra. Mass spectroscopy was also used to determine any unknown species from the GC spectrum. Standard solutions of CAL, BAL, COL, and BOL were calibrated in the GC to determine the retention time and response factor of each species.

6.3.4 Conversion and Selectivity Calculations

In this study, CAL conversion and selectivity were defined by Eq. 6.1 and Eq. 6.2 respectively in the following:

$$X = \frac{c_0 - c}{c_0} \times 100\% \qquad \text{Eq. 6.1}$$

$$S_i = \frac{c_{p,i}}{\sum_{i=1}^{m} c_{p,i}} \times 100\% \qquad \text{Eq. 6.2}$$

Where

X	=	conversion of CAL [%]
c_0	=	initial concentration of CAL [mol/L]
c	=	concentration of CAL in the products stream [mol/L]
S_i	=	selectivity of species i [%]
$c_{p,i}$	=	concentration of species i in the products [mol/L]
$\sum_{i=1}^{m} c_{p,i}$	=	the sum of concentrations of all the species in the products

6.4 Results and Discussion

6.4.1 Proton-Exchange-Membrane Selection

Several initial trials were performed at 60 ºC using Nafion 117 ® as the proton-exchange membrane in the MEA; however, a significant amount of CAL crossed over the membrane which caused a decrease in reactant concentration. Also, there was evidence of CAL absorbed on the membrane. This significant loss of the reactant via crossover or absorption with Nafion 117 made it difficult to analyze the carbon balance of the reaction system.

To replace the Nafion membrane and improve the carbon balance analysis, we performed a diffusion test on Nafion 117 ® and three other FuMA-Tech® membranes, FKB, FKE and FZP. The chemical composition and physical properties of each membrane are summarized in Table 6.2.

Table 6.2 Composition and physical properties of Nafion, FKB, FKE, and FZP.

Membrane type	Composition	Conductivity[a] ($mS \bullet cm^{-1}$)	H_2O uptake[b] (wt%)
Nafion117 (Dupont.)	Polymer of sulfonated tetrafluoroethylene	100	37
FKB (Fumatech.)	Polymer of sulfonated polyetherketone; Thickness (120 μm)	15	25
FKE (Fumatech.)	Polymer of sulfonated polyetherketone Thickness (50 μm)	16	27
FZP (Fumatech.)	Polymer of sulfonated tetrafluoroethylene with inorganic additive, e.g. zirconium phosphate	80	27

[a] The conductivity is measured in H^+ form at T=25 °C in H_2O [18, 19].
[b] The H_2O uptake is the saturated amount of H_2O that membrane absorbed at 25 °C [18, 19].

The purpose of the membrane diffusion test is to determine the CAL loss caused by crossover through the membrane and other factors, such as adsorption on the membrane and side reactions with the membrane. The test was performed in an H-cell, which was composed of two cylindrical glass chambers separated by the tested membrane, as shown in Figure 6.5. Initially, the L-side of the cell contained 15 ml of decane used as the solvent; the R-side of the cell held 15 ml of 5 vol% CAL in decane. The H-cell was left undisturbed for 24 h and a 1ml sample was taken from each chamber at 0, 3, 9 and 24 h. The samples were then analyzed by a GC to determine the concentration of CAL. The amount of crossover was determined by measuring the increase of CAL on the L-side. The degree of membrane absorption was obtained by taking the difference between the CAL on the R-side and the L-side. The results for each membrane are shown in Figure 6.6.

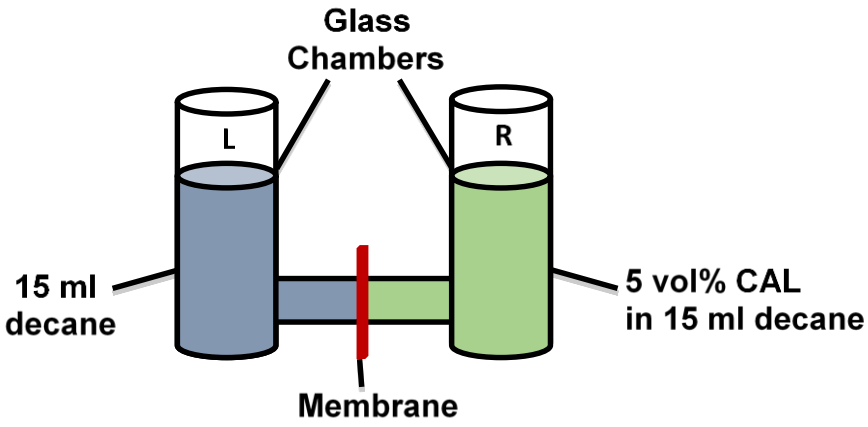

Figure 6.5 Scheme diagram of H-cell for diffusion test.

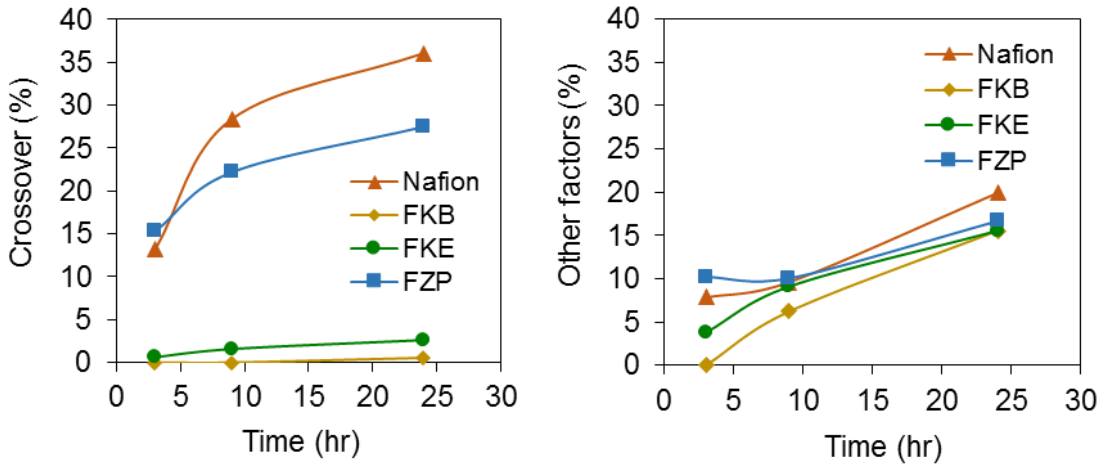

Figure 6.6 Crotonaldehyde loss through (a) crossover and (b) other factor as a function of time on the four tested membranes.

Figure 6.6a shows that both the Nafion and FZP membranes allowed relatively high crossover of CAL, while FKE and FKB had much lower crossover. Since FKB had the least crossover and the least loss of CAL through adsorption or side reactions, it was selected as the proton-exchange membrane for the experiments discussed later.

6.4.2 Crotonaldehyde Hydrogenation: Influence of Applied Potential

Crotonaldehyde hydrogenation was performed at room temperature (25 ℃) at potentials ranging from 0.0-1.0V (with 0.25 V increments), where 0.0 V represents a control experiment with no applied potential. The half-cell reactions that can occur at the anode and cathode are indicated by the following equations:

Anode:

$H_2 \rightarrow 2H^+ + 2e^-$ Eq. 6.3

Cathode:

$2H^+ \rightarrow 2H_{electro}$ Eq. 6.4a

$2H_{electro} + CH_3CH{=}CHCHO \rightarrow CH_3CH{=}CHCH_2OH;$ $\Delta E° = 0.40$ V Eq. 6.4b

$2H_{electro} + CH_3CH{=}CHCHO \rightarrow CH_3CH_2CH_2CHO;$ $\Delta E° = 0.72$ V Eq. 6.4c

$2H_{electro} + CH_3CH{=}CHCH_2OH \rightarrow C_4H_{10}OH;$ $\Delta E° = 0.50$ V Eq. 6.4d

$2H_{electro} + CH_3CH_2CH_2CHO \rightarrow C_4H_{10}OH;$ $\Delta E° = 0.18$ V Eq. 6.4e

$4H_{electro} + CH_3CH{=}CHCHO \rightarrow C_4H_{10}OH;$ $\Delta E° = 0.45$ V Eq. 6.4f

where, $H_{electro}$ represents the hydrogenation generated electrochemically via the applied potential.

Table 6.3 shows the steady state currenct density, CAL conversion rate and reaction selectivity at potentials from 0.0V to 1.0V. The current density varied linearly with the applied potential ($R^2 = 0.998$ using a linear fitting), indicating the overall cell potential remained constant during the reaction. The CAL conversion rate also increased with increasing potential. This finding suggested that CAL was hydrogenated through an electrochemical process, where the rate limiting steps were likely governed by the amount of $H_{electro}$ or directly related to the applied potential.

Table 6.3 Reaction rate, selectivity, and steady state current density at different applied potentials for crotonaldehyde hydrogenation.

Applied Potential (V)	Steady State Current Density (mA/cm^2)	CAL Conversion Rate ($\mu mol/s/m^2_{Pt}$)	Selectivity (%)	
			COL	BOL
0	0	0	N/A	N/A
0.25	2.9 ± 0.1	11 ± 0.7	25 ± 0.4	75 ± 0.4
0.50	6.4 ± 0.3	92 ± 7	34 ± 0.9	66 ± 0.9
0.75	9.2 ± 0.7	125 ± 9	40 ± 0.8	60 ± 0.8
1.00	11.9 ± 0.9	150 ± 13	47 ± 0.8	53 ± 0.8

[a] Experiments were carried out at 25 °C and 1 atm H_2, 0.066 mmol of CAL, in 100 mL isopropanol. 20% Pt/C was used as the catalyst for both anode and cathode with a loading of 0.1 $mgPt/m^2$.

Figure 6.7a shows the influence of applied potential on reaction rate, as measured by the rates of formation of the hydrogenation products. Each data point represents the average from at least 3 reproducible trials. The control experiment at 0.0 V did not form any hydrogenation products, indicating that the hydrogen participating in this reaction was generated electrochemically, as indicated in Eq 6.4a. We observed that both COL and BOL started to form at 0.2 V. This finding suggested that the production of COL and BOL over the Pt/C required the overpotentials of 0.6 V and 0.65 V, respectively. The formation rates of COL and BOL also increased with the increase of applied potential from 0.2 V to 1.0V, although different kinetics were observed. The formation rate of COL seemed to increase linearly with the applied potential, while the rate for BOL increased substantially from 0.2 V to 0.5 V and gradually from 0.5 V to 1.0V. These observations indicated that the rate-determining steps to produce these products were electrochemical reactions, governed by the applied potential. The nonlinearity of BOL formation rate versus the applied potential likely suggested a change in the rate-determining step.

Figure 6.7b illustrates the selectivity to hydrogenation products at different applied potentials. The selectivity to COL moderately increased with the applied potential, suggesting the product distribution can be tuned by modifying the applied potential in the current reaction system.

Two possible reasons may explain the increase trend in COL selectivity. First, it's possible that at higher applied potential, more COL was formed without being further hydrogenated to BOL. This explanation was plausible as increasing potential generated more $H_{electro}$, likely resulting in an increased surface coverage of $H_{electro}$ at the cathode surface. This increased H surface coverage may diminish the number of sites available to accommodate the organic reactants or intermediates involved in this reaction. Possibly, COL has desorbed from the cathode surface at a faster rate at higher potential instead of remaining on the surface to be further converted. Second, it is possible the rate to produce BOL from other sources, e.g. directly from CAL or from BAL, may not increase as significantly with the increased potential as that for COL, leading to relatively higher COL composition, i.e. selectivity, in the product species.

Figure 6.7c shows the Faradaic efficiency (FE) as a function of the applied potential, which indicates the electrochemical selectivity of the reaction system. The FE of all the hydrogenation products must add up to 100%. In this case the discrepancy was balanced by H_2 generated at the cathode through the HER. The HER was an undesired reaction as it consumed the $H_{electro}$ to produce hydrogen instead of being used for CAL hydrogenation. The FE reached a maximum of ~ 50% at 0.5 to 0.6 V, after which it dropped to around 30% as the potential increased to 1.0V. This observation indicated that after 0.6V, the HER on the cathode surface became more prevalent compared to the hydrogenation reactions, thus deteriorating the overall FE. The results support the rationale that at the higher potential, as more $H_{electro}$ was available and the overpotential for HER was estimated to be less than the overpotentials to produce COL and BOL. A similar trends in FE in an electrochemical hydrogenation reaction in a SPE reactor were also observed by Lausche et al. [19] in a previous study on selective hydrogenation of triglyceride.

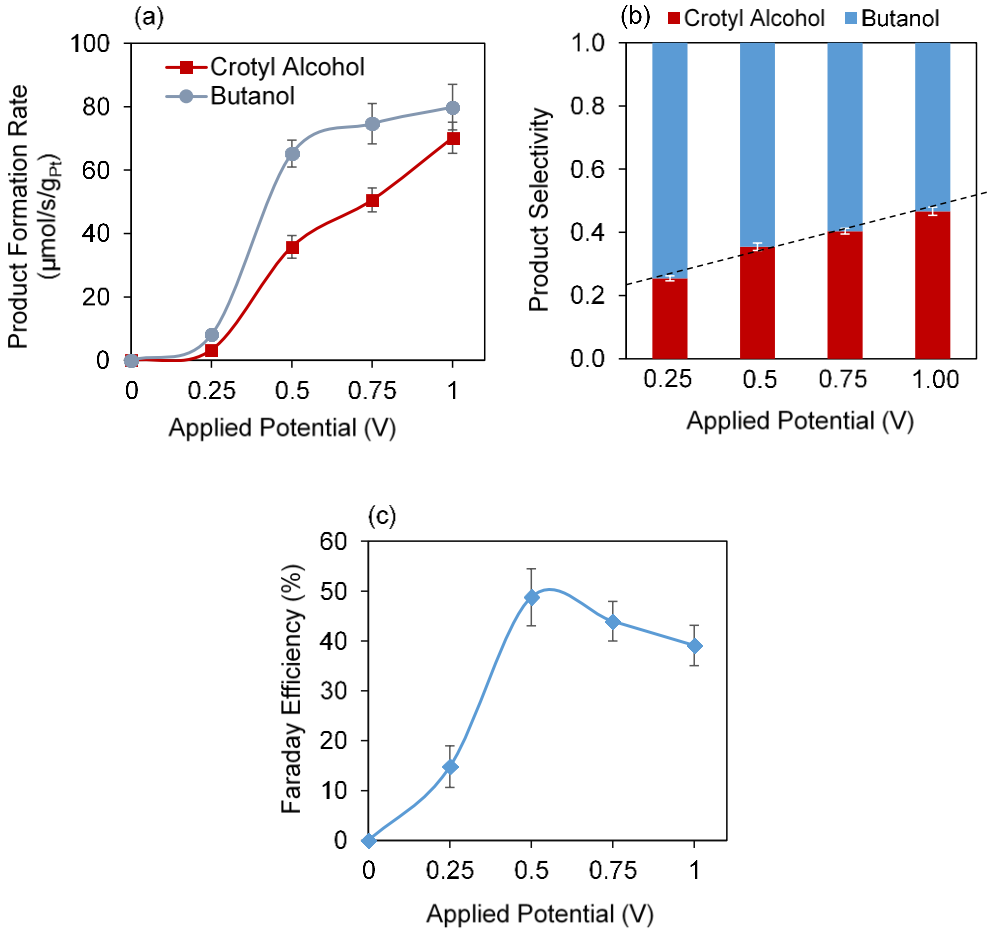

Figure 6.7 Crotonaldehyde hydrogenation performance: (a) Production formation rate, (b) selectivity, and (c) faraday efficiency as a function of applied potential. Experiments were carried out at 25 ℃ and 1 atm using 20% Pt/C as the anode and cathode catalysts.

Isopropyl crotonate, the ester of crotonic acid and isopropanol was also detected in addition to the hydrogenation products. The ester was formed in the control experiments (at 0.0V) and was also produced in similar amounts in all other experiments conducted at varied applied potentials. This finding indicated that crotonate ester came from a thermochemical rather than an electrochemical process. As this work focused on the electrochemical performance for CAL hydrogenation and ester was not produced electrochemically from hydrogenation reaction, it was not included as a product in the previous discussion. The proposed pathway for producing the

crotonate ester and the ester formation profile at different applied potentials can be found in Appendix B.

6.4.3 Reaction Pathway Investigation

The classical pathway for CAL hydrogenation should generate COH and BAL as the primary hydrogenation products and BOH as the secondary hydrogenation product [11]. The formation of BAL is more thermodynamically favorable than COH, however, BAL was not detected in any of the experiments. Two pathways could potentially explain this observation: (i) BAL was not formed in CAL hydrogenation because it was not kinetically favored compared to other products; (ii) BAL was a reaction intermediate, where it was first generated but consumed instantaneously and therefore was not observed in the product. To investigate these suggested pathways, a series of experiments were performed using COH and BAL as the reactants. Table 6.4 summarizes the results of these experiments performed at both 0.0V (the control experiments with no applied potential) and 0.5V. We selected 0.5 V as the applied potential because experiments performed at this potential achieved relatively high conversions and current efficiencies for CAL hydrogenation (Table 6.3).

Table 6.4 Reaction activity, selectivity, current density, and faraday efficiency the for the BAL and COL hydrogenations.[a]

Trial	Applied Potential (V)	Substrate	Steady State Current Density (mA/cm^2)	Conversion Rate ($\mu mol/s/m^2_{Pt}$)	Faraday Efficiency (%)	Selectivity to BOH (%)
1	0.0	BAL[b]	0	0	N/A	0
2	0.5	BAL[b]	149 ± 2.4	92 ± 7	10.4 ± 0.9	100
3	0.0	COL	0	0	N/A	0
4	0.5	COL	155 ± 3.7	125 ± 9	15.6 ± 1.2	100

[a] Experiments were carried out at 25 °C and 1 atm H_2, 0.02 mmol of BAL or COL, in 100 mL isopropanol. 20% Pt/C was used as the catalyst for both anode and cathode reaction with a loading of 0.5 mg/m^2.

[b] Butyric acid was also produced in Trial 1 and 2 in comparable amounts, therefore, it was considered as the side product from the control experiment (baseline reaction) and was not included in the hydrogenation products.

When there was no applied potential (Trial 1 and 3), no hydrogenation reactions occurred, indicating H_2 did not diffuse through the membrane to react with either BAL or COL. When 0.5 V was applied (Trial 2 and 4), both BAL and COL were hydrogenated to BOL with 100% selectivity. The rate of COL hydrogenation was slightly more active by ~ 36% than that of BAL hydrogenation. This trend was expected as the conversion of COL to BOL is more thermodynamically favorable than the conversion of BAL to BOL.

To quantitatively describe the reaction rates for all the possible steps for the CAL hydrogenation system, we fitted the reaction rate data into a rate model containing 5 elementary steps as shown in Figure 6.8.

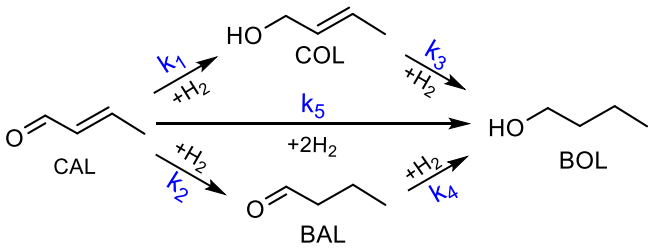

Figure 6.8 Crotonaldehyde hydrogenation reaction scheme, with rate constant associated with each individual hydrogenation step.

Based on the previous activity measurement, the reaction rates seemed to follow first order kinetics with respect to the disappearance of CAL, COL, and BAL. Assuming each step within the reaction system is a first order elementary reaction, the reaction rate laws can then be expressed with the following equations (Eqs. 6.5 – 6.9):

$$\frac{d[CAL]}{dt} = -k_1[CAL] - k_2[CAL] - k_5[CAL] \qquad \text{Eq. 6.5}$$

$$\frac{d[COL]}{dt} = k_1[CAL] - k_3[COL] \qquad \text{Eq. 6.6}$$

$$\frac{d[BAL]}{dt} = k_2[CAL] - k_4[BAL] \qquad \text{Eq. 6.7}$$

$$\frac{d[BAL]}{dt} = 0 \qquad \text{Eq. 6.8}$$

$$\frac{d[BOL]}{dt} = k_5[CAL] + k_3[COL] + k_4[BAL] \qquad \text{Eq. 6.9}$$

The rate constants k_1-k_5 were solved using Polymath 4.1 and the calculated values are shown in Table 6.5. The results indicated that CAL was consumed to produce COL and BOL in parallel. However, the conversion of CAL to BAL was negligible, with a k_2 value at least three orders of magnitude smaller than the other rate constants, which explained the absence of BAL during the reaction. The calculated rate constants also suggested that BOL was produced through two sources: directly from CAL and via the crotyl alchol intermediate.

Table 6.5 Reaction rate constant for each individual step for crotonaldehyde hydrogenation to crotyl alcohol, butyraldehyde, and butanol.

Reaction step	Rate constants ($h^{-1} \bullet 10^3$)
k_1	0.66
k_2	≈0 (< 10^{-3})
k_3	1.98
k_4	1.28
k_5	1.06

To validate the accuracy of this reaction model, we compared the simulated (by Polymath 4.1) and the measured concentrations of reaction species as shown in Figure 6.9. The experimentally measured and simulated values matched well within statistical errors for both the products (COL and BOL) and the substrate, suggesting the model was effective in predicting the reaction performance.

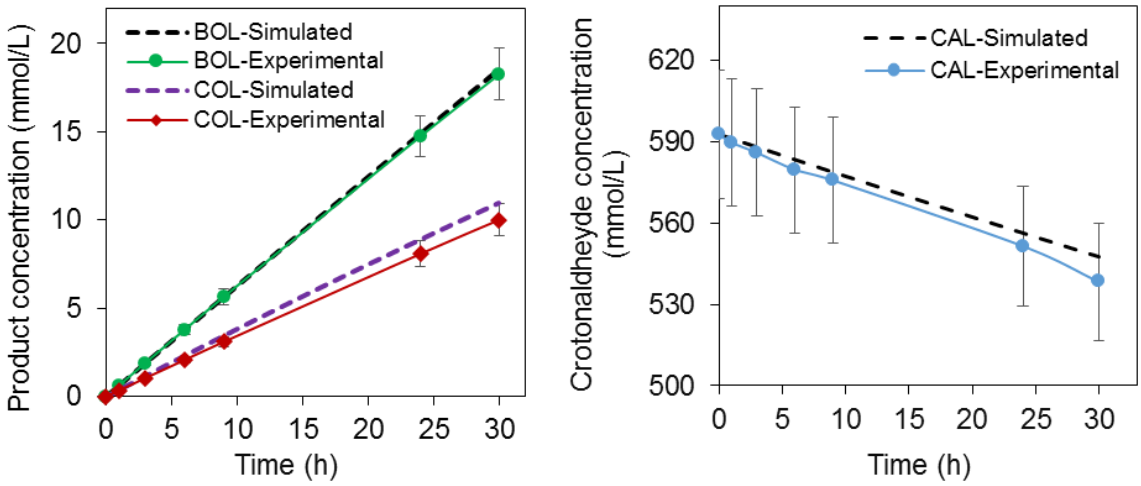

Figure 6.9 Comparison of simulated and experimental concentrations of (a) products (BOL and COL) and (b) substrate (CAL). Experiments were carried out at 25 ℃ and 1 atm H_2, 0.066 mmol of CAL, in 100 mL isopropanol. 20% Pt/C was used as the catalyst for both anode and cathode.

The Pt/C catalyst used for this study consists of mostly Pt (111) crystallites (~ 60 wt%) as suggested by XRD analysis (Appendix B). The DFT calculations performed for the CAL hydrogenation over Pt (111) surface by Cao et al. [21] seemed to provide theoretical support to our experimental data. They performed the free energy calculations over all the possible intermediates (Figure 6.10) for the hydrogenation of CAL and estimated the TOF for each pathway to produce the hydrogenation products, including COL, BAL, and BOL as shown in Table 6.6.

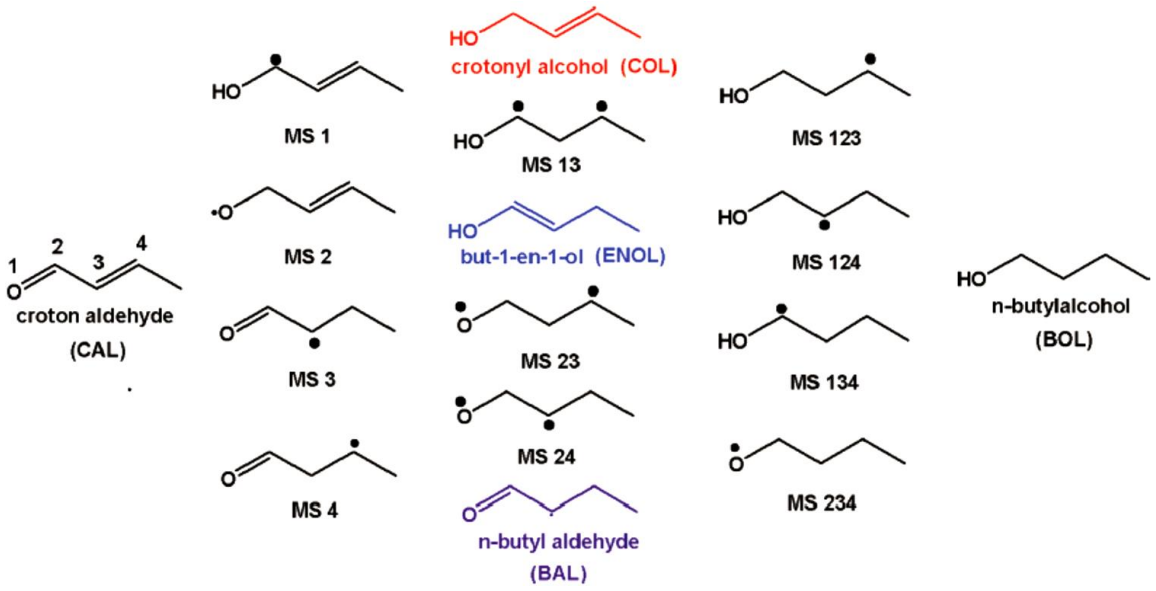

Figure 6.10 All the possible intermediates in the process of CAL hydrogenation on Pt(111). The four available attack sites are numbered from 1 to 4, corresponding to O_1, C_2, C_3, and C_4, respectively. From the left to right, transcrotonaldehyde, mono-hydrogenation intermediates, di-hydrogenation intermediates, tri-hydrogenation intermediates, and full hydrogenation product n-butylalcohol (BOL), respectively. Taken from [21].

These calculations indicated that COL was mainly produced by first hydrogenating the O1 atom in CAL through MS1 intermediate, while BOL was primarily produced by hydrogenating a series of open-shell intermediates, via MS 1, MS 13, and MS 134 (Figure 6.10). Crotyl alcohol appeared to be the second most significant intermediate to produce BOL, as suggested by a total

7.8×10^{-5} s^{-1} TOF for BOL formation combining +1234 and + 1243 pathways. This calculation was consistent with the observation from our experiments, where CAL and COL both served as the sources for BOL. In our study, the contribution from CAL to produce BOL was slightly more significant than that from COL but was still in the same order of magnitude suggested by similar rate constants reported in Table 6.5. The TOFs and selectivity values calculated from our system were comparable to the theoretical values for both COL and BOL production (Table 6.6), suggesting that COL and BOL were likely produced via the same pathways as proposed by this theoretical study.

Table 6.6 Turnover frequency (TOF) of each hydrogenation pathway and the selectivity of products over Pt(111) predicted from DFT calculation [21] and the experimental values from this work.

Product	TOF (s^{-1})			selectivity	Results from this work[b]	
	pathway[a]		final		TOF (s^{-1})	selectivity
COL	+12	6.78×10^{-3}	6.78×10^{-3}	46.3%	4.6×10^{-3}	47%
	+21	2.36×10^{-7}				
BAL	+14	1.12×10^{-3}	1.12×10^{-3}	7.7%	0	0
	+41	1.13×10^{-7}				
	+34	2.87×10^{-12}				
	+43	3.95×10^{-10}				
BOL	+1234	5.15×10^{-5}	6.73×10^{-3}	46.0%	5.3×10^{-3}	53%
	+1243	2.68×10^{-5}				
	+1423	4.59×10^{-11}				
	+1432	2.47×10^{-10}				
	+1324	1.77×10^{-5}				
	+1342	6.63×10^{-3}				

[a] Numbers in bold denote the most predominant pathway to produce each species. Taken from [21].

[b] TOF = (mmol of product)/(mmol of Pt(111))/(mol% of CAL)/(% of Pt dispersion). 10% of Pt dispersion was assumed. TOF and selectivity were calculated based on experiments carried out at 25 °C and 1 atm H_2, 0.066 mmol of CAL, in 100 mL isopropanol at 1.0 V applied potential. 20% Pt/C was used as the catalysts for both anode and cathode with 0.5 mg/m^2 loading.

6.5 Conclusions

The study described in this chapter investigated the feasibility of using an SPE reactor for the chemoselective hydrogenation of crotonaldehyde at ambient conditions. Both crotyl alchol, the high-value product, and butanol were formed as hydrogenation products at potentials higher than 0.25 V. The reaction rates, selectivities, and current efficiencies proven to be functions of applied potential. The highest crotonaldehyde conversion rate of ~ 150 μmol/s/m^2_{Pt} and highest selectivity to COL of 47% were achieved at the applied potential of 1.0V. The highest Faraday efficiency of 49% is achieved at the applied potential of ~ 0.5 V. The reaction pathway study suggested that butanol was produced directly from complete hydrogenation of crotonaldehyde and also from a sequential hydrogenation through a crotyl alcohol intermediate, while butyraldehyde was not produced in the reactor system. The rates and selectivities from this study were in good agreement with the theoretical values reported in the literature. Future work should focus on identifying electrocatalysts that can selectively inhibit the pathway to produce butanol to enhance the selectivity to the desired product, crotyl alcohol. The experimental techniques and results from this study will help advance the use of SPE reactors to carry out the selective hydrogenation of other multifunctional organic compounds.

6.6 References

[1] S. McGovern, G. Harish, C. Pai, W. Mansfield, J. Taylor, S. Pau, R. Besser, Catalyst-Trap Microreactor for Hydrogenation of a Pharmaceutical Intermediate, The 2006 Spring National Meeting, 2006.

[2] H.U. Blaser, C. Malan, B. Pugin, F. Spindler, H. Steiner, M. Studer, Advanced Synthesis & Catalysis 345 (2003) 103-151.

[3] G. Yusem, P. Pintauro, Journal of the American Oil Chemists' Society 69 (1992) 399-404.

[4] R. Hastert, Journal of the American Oil Chemists' Society 58 (1981) 169-174.

[5] Z. Ogumi, K. Nishio, S. Yoshizawa, Electrochimica Acta 26 (1981) 1779-1782.

[6] Z. Ogumi, M. Inaba, S.-i. Ohashi, M. Uchida, Z.-i. Takehara, Electrochimica acta 33 (1988) 365-369.

[7] X.-Z. Yuan, Z.-F. Ma, Q.-Z. Jiang, W.-S. Wu, Electrochem. Commun. 3 (2001) 599-602.

[8] V. Roldugin, B. Tinsley, Journal of Atmospheric and Solar-Terrestrial Physics 66 (2004) 1143-1149.
[9] W. An, J.K. Hong, P.N. Pintauro, K. Warner, W. Neff, Journal of the American Oil Chemists' Society 75 (1998) 917-925.
[10] P. Pintauro, M.P. Gil, K. Warner, G. List, W. Neff, Ind. Eng. Chem. Res. 44 (2005) 6188-6195.
[11] P. Claus, Top. Catal. 5 (1998) 51-62.
[12] J.C. Wu, C.-Y. Chen, S.D. Lin, Catal. Lett. 102 (2005) 223-227.
[13] G. Horanyi, K. Torkos, Journal of Electroanalytical Chemistry and Interfacial Electrochemistry 136 (1982) 301-309.
[14] D. Barnes, P. Zuman, Journal of the Chemical Society B: Physical Organic (1971) 1118-1121.
[15] X. Yang, A. Wang, X. Wang, T. Zhang, K. Han, J. Li, The Journal of Physical Chemistry C 113 (2009) 20918-20926.
[16] B. Campo, G. Santori, C. Petit, M. Volpe, Appl. Catal., A 359 (2009) 79-83.
[17] K. Liberková-Šebková, L. Červený, R. Touroude, Research on chemical intermediates 29 (2003) 609-617.
[18] Dupont Fuel Cells: Dupont Nafion PFSA Membranes. Information available at http://www2.dupont.com/FuelCells/en_US/assets/downloads/dfc101.pdf.
[19] FumaTech Cation-Exchange-Membranes. Information available at http://www.fumatech.com/EN/Onlineshop/fumasep-for-Electro-membrane-processes/Kationenaustauschermembranen/.
[20] A.C. Lausche, K. Okada, L.T. Thompson, Electrochem. Commun. 15 (2012) 46-49.
[21] X.-M. Cao, R. Burch, C. Hardacre, P. Hu, The Journal of Physical Chemistry C 115 (2011) 19819-19827.

CHAPTER 7

CONCLUSIONS AND FUTURE WORK

7.1 Summary

The overall goal of this dissertation was to investigate the use of heterogeneous-based catalysts for designing the cascade catalytic systems for the hydrogenation of CO_2 or C=O containing species, including formic acid and formate esters to produce CH_3OH (Chapters 2-5). We also extended this work to evaluate the selective hydrogenation of crotonaldehyde, also containing the C=O group, to produce the crotyl alcohol (desired product) using an electrochemical SPE cell (Chapter 6).

Our work on cascading CO_2 hydrogenation is inspired by a few literature examples where the reaction was performed using homogeneous cascade catalysis, but also identified major challenges with catalyst compatibility and recyclability [1-3]. Copper-based heterogeneous catalysts were also demonstrated to drive the cascade pathway to convert CO_2 to CH_3OH through formic acid and ester intermediates [4]. However, a rate-limiting step always existed because a single catalyst did not provide equal active sites for each sub-step within the overall reaction system. Therefore, we aim to combine multiple heterogeneous catalysts to sequentially facilitate sub-reactions in these cascade processes, with better cocatalyst compatibility, greater thermal stability, and easier separation of catalyst from the reaction mixture.

Using CO_2 hydrogenation to CH_3OH as the primary test reaction, we first identified the pathways and desired intermediates to achieve this transformation. Then the most effective heterogeneous catalyst was selected for each sub-reaction within the overall transformation. Finally, the most promising catalyst from each sub-reaction were combined to create the cascade system.

We first evaluated a series of mixed-phase homo-/heterogeneous cascade systems, for example, the system containing a $Ru(PMe_3)_4OAcCl$ and a Cu/Mo_2C catalyst for CO_2 hydrogenation to CH_3OH through formic acid/ester intermediates (Figure 7.1a). However, the surface interaction between these two catalytic components resulted in both the deactivation of Cu/Mo_2C and the decomposition/ligand shedding of the Ru-phosphine complex. In other words, the homogeneous complex acted as a reactant to the heterogeneous catalyst. Nevertheless, the coupling of homo- and hetero-geneous catalysts for cascade CO_2 hydrogenation greatly expands the design matrix for cascade systems by providing a broader selection of catalysts and reaction pathways. Minimizing the surface interactions between the homo- and hetero-geneous species would potentially lead to a feasible application of these mix-phased cascade systems. Section 7.2 will mention several strategies to reduce surface interactions to improve the material compatibility.

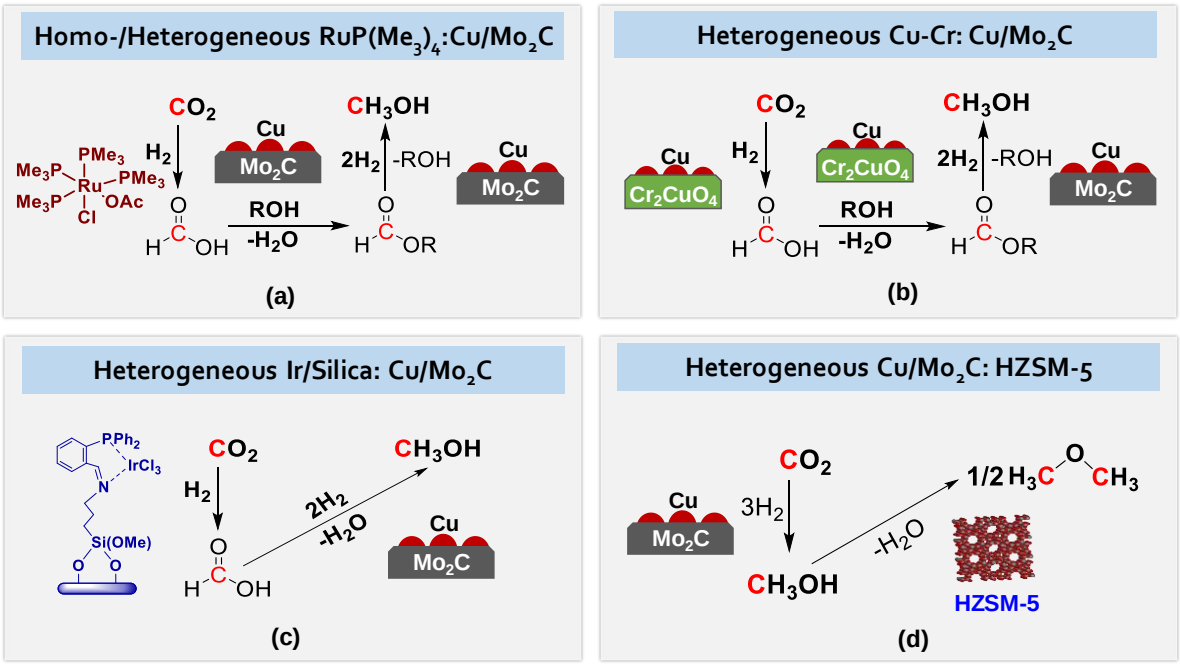

Figure 7.1 Representative cascade systems for CO_2 hydrogenation developed via research described in this dissertation.

We also evaluated all-heterogeneous based cascade systems for the hydrogenation to CO_2 to CH_3OH, DME, and hydrocarbons (Figure 7.1b-d). The results demonstrated that these heterogeneous catalysts worked cooperatively to achieve enhanced performance compared to each individual catalyst at mild reaction temperatures, 135-200 ℃. In fact, there was no reported activities to CH_3OH or DME from CO_2 at 135 ℃ prior to our work. These systems effectively eliminated the incompatibility issue that occurred in the homogeneous-based cascade systems. All-heterogeneous cascade systems have great potential to be further applied to other challenging processes; one example is the biomass conversion, a complex reaction system that typically contains various types of transformations [5, 6]. These heterogeneous-based cascade systems are also promising to facilitate electrochemical reactions to achieve

higher selectivities and Faradaic efficiencies, especially for the multi-electron transfer processes [7, 8].

During the screening of heterogeneous catalysts for CO_2 hydrogenation, Mo_2C-based catalysts were identified to be catalytically active and relatively selective (~70%) for CH_3OH production from CO_2 at low temperature (135 ℃). The deposition of active metals, e.g. Cu and/or Pd, onto the Mo_2C surface significantly enhanced the CH_3OH production. We further investigated the influence of metal type and reaction temperature on the catalytic performance for CO_2 hydrogenation over the Mo_2C-based catalysts. Increasing the reaction temperature from 135 ℃ to 200 ℃ enabled C-C coupling that resulted in the formation of C_2-C_4 hydrocarbons. Experiments with CO as reactant indicated that these hydrocarbons were produced as a consequence of CO hydrogenation. Furthermore, we demonstrated that the catalytic properties of Mo_2C were tunable by introducing different metals onto the surface: the addition of Cu or Pd mainly enhanced CH_3OH production and the addition of Co or Fe enhanced the C_2-C_4 hydrocarbon and ethanol formation through Fischer Tropsch Synthesis (FTS). A summary of the reaction pathway and the role of different metals onto Mo_2C on activities and selectivities for CO_2 hydrogenation are illustrated in Figure 7.2.

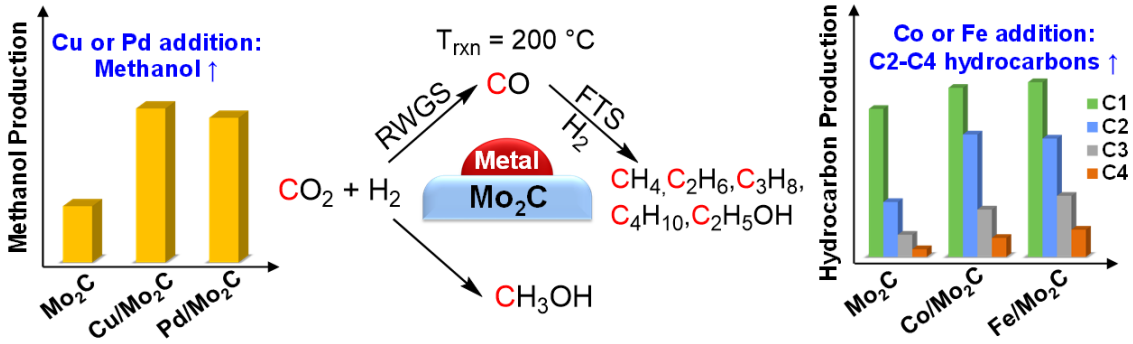

Figure 7.2 Proposed reaction pathways and the role of different metals on Mo_2C for CO_2 hydrogenation at 200 ℃.

7.2 Recommendations and Future Works

The research described in this dissertation can be further expanded in several directions to advance the design of heterogeneous-based cascade systems for CO_2 hydrogenation.

(i) Transitioning from a batch system to a flow-through system

During the catalyst screening phase this work, we only utilized a batch reactor system due to its ease of operation and to allow direct comparisons with homogeneous systems. A flow-through reactor system is desirable for measuring the intrinsic reaction rates and evaluating catalyst stability. Figure 7.3 shows an example of a flow-through system for liquid phase cascading CO_2 hydrogenation. Both liquid and gas phase samples can be analyzed online to fully quantify the products. The catalyst stability can be easily assessed by collecting the activity data versus reaction time on stream. When needed, the system can also be modified to recycle the reactant species to increase overall conversion. In these flow systems, we can also compare a one-pot reactor and multiple reactors operating in series to investigate the influence of intermediate lifetime and other operating factors on the catalytic performance of a cascade system.

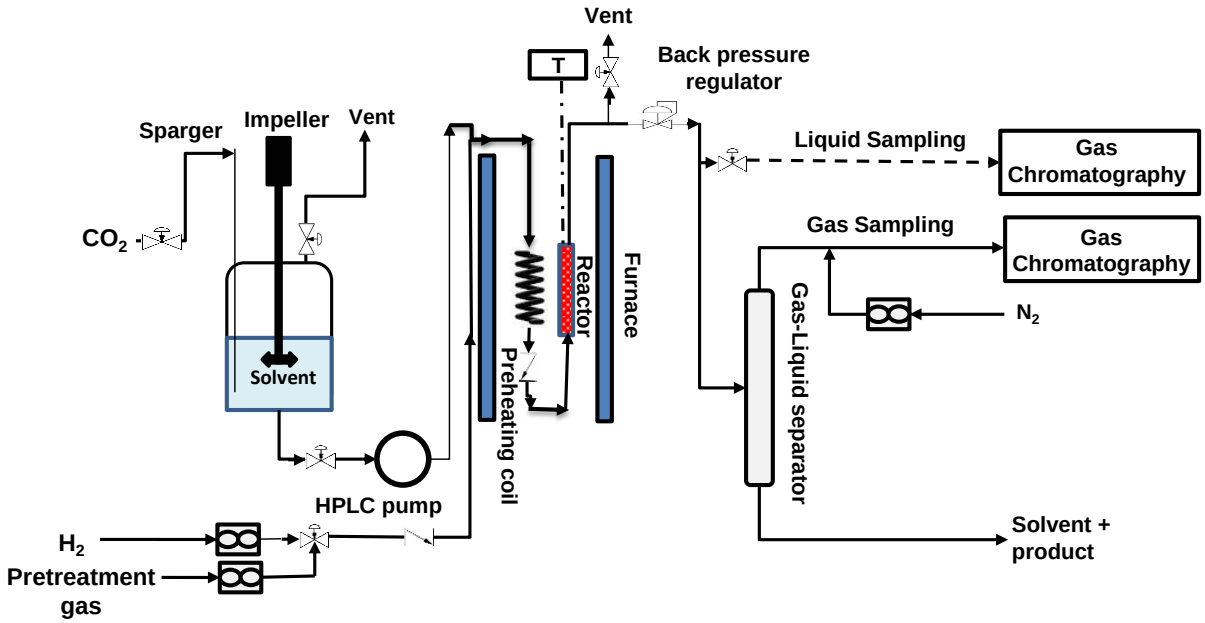

Figure 7.3 A schematic diagram of a flow-through system for liquid phase CO_2 hydrogenation. The design is based on a flow system reported in [9].

(ii) Creating cascade systems for C_{2+} products

The ultimate goal of this project is to use the cascade catalysis strategy to selectively produce industrially relevant chemicals, preferably high carbon-containing products, starting from CO_2. From the research in this dissertation, two major pathways were mapped out to produce C_{2+} products from CO_2 as shown in Figure 7.4.

One pathway directly utilizes CH_3OH as an intermediate and couples with the methanol-to-olefin/gasoline (MTO/MTG) processes to produce C_{2+} products. We already achieved the production of dimethyl either (DME) from CO_2 using a Cu/Mo_2C:HZSM5 cascade system. Our system afforded a total CO_2 conversion of 24%, with selectivities to CH_3OH:DME:CO:CH_4 = 17%:78%:1%:4%, at 135 ℃ and 40 bar at 54 h time on stream. We compared our results to a representative study in the literature using a mixture of Cu-Zn-Al and HZSM-5 catalysts for the gas phase CO_2 hydrogenation to DME [10]; this study achieved

an overall CO_2 conversion of 30% and selectivities of CH_3OH:DME:CO = 7%:53%:40% at 260 ℃ and 50 bar. Our results exhibited higher selectivities to the desired CH_3OH and DME (by~ 40%). This result was not surprising given the processes of producing both CH_3OH and DME are exothermic and favored at lower operating temperatures. To accomplish the conversion of CO_2 to C_2+ products, a promising strategy would be to introduce an additional catalyst that converts DME to other higher carbon-containing products. The BEA zeolite supported Cu catalyst reported by Schaidle et al. is a great candidate for the direct conversion of DME to 2,2,3-trimethylbutane through homologation [11].

Another pathway uses CO as the intermediate to produce higher hydrocarbons through FTS, which requires the combination of an effective RWGS catalyst and a FTS catalyst that work cooperatively in one-pot. Once the most promising cascade systems have been identified, process simulation tools (such as ASPEN) can also be utilized to identify appropriate reaction parameters, including temperatures, pressures, and catalyst loading and ratios to optimize the performance.

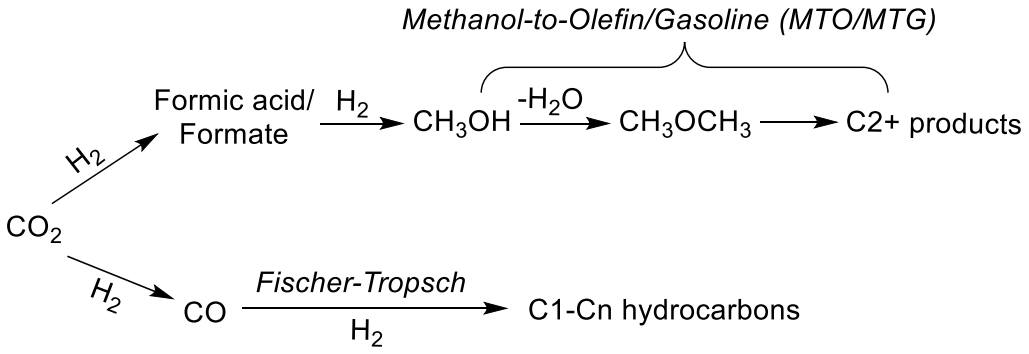

Figure 7.4 Two possible pathways in parallel for cascade CO_2 hydrogenation to C_2+ products.

(iii) Refining homo-/heterogeneous cascade systems

Cooperative homo- and hetero-geneous cascade systems can be envisioned by improving the compatibility between these two classes of materials. We have demonstrated a cooperative cascade system by combining an Ir-complex tethered on SBA-15 (high surface area silica) and a Cu/Mo_2C catalyst to produce CH_3OH from CO_2 via a formic acid intermediate. A similar tethering strategy can be applied to other active homogeneous complexes to maintain physical separation from the heterogeneous active sites. Heterogeneous supports including high surface area silica, alumina, zeolite, and metal-organics frameworks (MOFs) are attractive candidates to tether the homogeneous materials. Ultimately, for the most promising systems, we might be able to place both the homogeneous and heterogeneous active sites on the same support (Figure 7.5). This arrangement can provide better accessibility to the active sites for the intermediates and more effective cooperation between the active sites. Quickly accessing the adjacent active sites is also beneficial for converting the short-lived intermediates to the product instead of undergoing the reverse reaction to form the reactant. The feasibility of synthesizing such catalytic systems needs to be assessed.

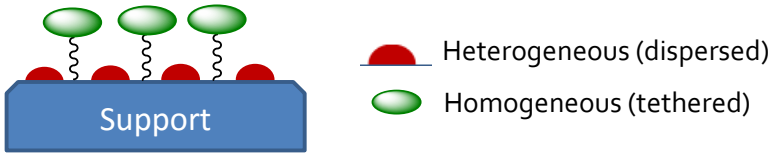

Figure 7.5 A schematic diagram of both homogeneous and heterogeneous active sites present on the same support.

7.3 Sustainability and Economics Considerations for Cascading CO_2 Hydrogenation

A series of factors have to be considered when developing sustainable and economically viable processes for CO_2 hydrogenation. This section will briefly discuss several key factors,

including the source of CO_2, the source of H_2, solvent use, and their potential influences on the process sustainability and economics.

(i) Source of CO_2

Major sources for CO_2 include flue gases from chemical plants, such as those used for ammonia synthesis and refineries, and the atmosphere. [12] The former are typically CO_2 enriched (30-65% concentrations), while the latter contains dilute CO_2 (0.4-0.5 vol% in the atmosphere), requiring more energy and effort in separation. Currently, flue gases are projected to provide CO_2 at a low price ($60-$450/ton) and a capacity of 1.5 Gton/year. [13] This capacity provides sufficient amount of carbon for the initial phase of developing CO_2 recycling technology [12]. Furthermore, CO_2 conversion can be performed onsite close to the flue gas to reduce the costs for CO_2 storage and transportation. In the long term, advances in CO_2 capture technologies are expected to provide lower-cost CO_2 from the atmosphere at a capacity of 3.6 Gton/year. [14]

(ii) Source of H_2

While methane steam reforming (MSR) is the commercial route for the production of most H_2, the overall process generates ~ 0.55 mole of CO_2 for every mole of H_2 produced according to a life cycle assessment analysis (LCA) by Utgikar and Thiesen. [15] This high CO_2:H_2 ratio could result in greater CO_2 emissions than consumption (typically fewer than 0.5 mole of CO_2 is consumed per mole of H_2 used [16]) considering the overall CO_2 hydrogenation reaction; the resulting process would therefore become unsustainable. To ensure the sustainability of this process, alternative H_2 production methods need to be considered. A promising technique is to couple electricity production via renewable sources (e.g. wind, solar, and nuclear) and water electrolysis to produce H_2 (e.g. renewable H_2). [12] Biomass conversion through ethanol steam reforming or gasification can also provide hydrogen with lower CO_2 emissions compared to the

conventional methane SR. [15] However, the relatively high cost for renewable H_2 remains a significant challenge to achieving economic viability for CO_2 hydrogenation. According to the DOE (Department of Energy) target, the unit price of H_2 should stay below $2/kg to be considered competitive [17]. Currently, renewable H_2 from solar or wind costs $8-10/kg and its cost is projected to decrease to $5-6/kg by 2020, still 2-3 times higher than the target cost [18]. The price for the renewable H_2 can be further reduced if an excess amount of cheap electricity is available, by enhancing the efficiency of renewable electricity generation or using electricity derived from nuclear energy.

(iii) Solvent use

Solvents can greatly influence the catalytic performance of the liquid phase cascading CO_2 hydrogenation. The solvent not only determines the reactant gas solubilities but can also alter or participate the reaction pathways; for example, the use of an alcohol solvent would result in the formation of ester [4]. 1,4-Dioxane was selected as the solvent for most of the studies in this dissertation due to its relative inertness, high boiling point compared to the reactant and product species and relatively high CO_2 and H_2 solubilities compared to other organic solvents tested, including tetrahydrofuran, toluene, and ethanol. However, the solubilities for CO_2 and H_2 in these organic solvents are still relatively low compared to the gas phase densities, resulting in lower reaction rates, as reported in Chapters 4 and 5 in this dissertation. Alternatively, ionic liquids (e.g., imidzolium-based) can be considered as the solvent for CO_2 and H_2. [19] These ionic liquids provide solubilities (up to ~ 20 M), at least one order of magnitude higher than that in organic solvents. [19, 20] The enhancement in gas solubilities should lead to improved catalytic activities for CO_2 hydrogenation. Meanwhile, the non-volatility of ionic liquids also eliminates vapor loss and allows easy down-stream separation, reducing the cost for the overall process.

7.4 Future Prospects for Cascade Catalysis

The concept of cascade catalysis represents a promising platform for the rational design of catalytic systems that accomplish complex chemical transformations involving multiple elementary steps. This strategy offers a number of advantages for developing a sustainable process for chemical synthesis, including the efficient use of feedstock, reduced separation efforts between reaction steps, and the ease of rational reactivity tuning.

We anticipate cascade catalysis will play a significant role in designing both homogeneous and heterogeneous catalytic processes to produce valuable chemicals of industrial importance, preferably from abundant and sustainable feedstocks, such as methane, CO_2, and biomass. Heterogeneous-based cascade systems are especially attractive as they offer the benefits of greater compatibility and recyclability of catalytic components compared to their homogeneous counterparts. Although significant progress has been made recently in this field with a number of promising demonstrations, heterogeneous cascade catalysis is still underexploited. Tremendous research effort is still needed to advance our understanding of these heterogeneous-based cascade systems. Future investigations should not only focus on developing thorough knowledge of the catalytic materials through systematic characterization, but also a deep understanding of the physical and chemical features of the reaction mechanisms to design more efficient cascade sequences. [21]

7.4 References

[1] C.A. Huff, M.S. Sanford, J. Am. Chem. Soc. 133 (2011) 18122-18125.
[2] C.A. Huff, J.W. Kampf, M.S. Sanford, Organometallics 31 (2012) 4643-4645.
[3] S. Wesselbaum, T. vom Stein, J. Klankermayer, W. Leitner, Angew. Chem., Int. Ed. 124 (2012) 7617-7620.
[4] L. Fan, Y. Sakaiya, K. Fujimoto, Appl. Catal., A 180 (1999) L11-L13.
[5] M. Shiramizu, F.D. Toste, Angew. Chem., Int. Ed. 52 (2013) 12905-12909.
[6] Y. Román-Leshkov, C.J. Barrett, Z.Y. Liu, J.A. Dumesic, Nature 447 (2007) 982-985.

[7] L. Tong, A. Iwase, A. Nattestad, U. Bach, M. Weidelener, G. Götz, A. Mishra, P. Bäuerle, R. Amal, G.G. Wallace, Energy Environ. Sci. 5 (2012) 9472-9475.
[8] J. Gobrecht, R. Potter, R. Nottenburg, S. Wagner, J. Electrochem. Soc. 130 (1983) 2280-2283.
[9] J.G. Dickinson, P.E. Savage, J. Mol. Catal. A: Chem. 388 (2014) 56-65.
[10] S.P. Naik, T. Ryu, V. Bui, J.D. Miller, N.B. Drinnan, W. Zmierczak, Chemical Engineering Journal 167 (2011) 362-368.
[11] J.A. Schaidle, D.A. Ruddy, S.E. Habas, M. Pan, G. Zhang, J.T. Miller, J.E. Hensley, ACS Catal. 5 (2015) 1794-1803.
[12] E.A. Quadrelli, G. Centi, J. Duplan, S. Perathoner, ChemSusChem 4 (2011) 1194-1215.
[13] Information obtained from International Panel on Climate Change webpage http://www.ipcc.ch/. .
[14] T. Nauclér, W. Campbell, J. Ruijs, McKinsey & Company, sl (2008).
[15] V. Utgikar, T. Thiesen, International Journal of Hydrogen Energy 31 (2006) 939-944.
[16] W. Wang, S. Wang, X. Ma, J. Gong, Chem. Soc. Rev. 40 (2011) 3703-3727.
[17] G. Centi, E.A. Quadrelli, S. Perathoner, Energy Environ. Sci. 6 (2013) 1711-1731.
[18] (!!! INVALID CITATION !!!).
[19] C. Cadena, J.L. Anthony, J.K. Shah, T.I. Morrow, J.F. Brennecke, E.J. Maginn, J. Am. Chem. Soc. 126 (2004) 5300-5308.
[20] R. Singh, E. Marin-Rimoldi, E.J. Maginn, Ind. Eng. Chem. Res. (2014).
[21] M.J. Climent, A. Corma, S. Iborra, M.J. Sabater, ACS Catal. 4 (2014) 870-891.

Appendix A

Supporting Information for Chapter 5

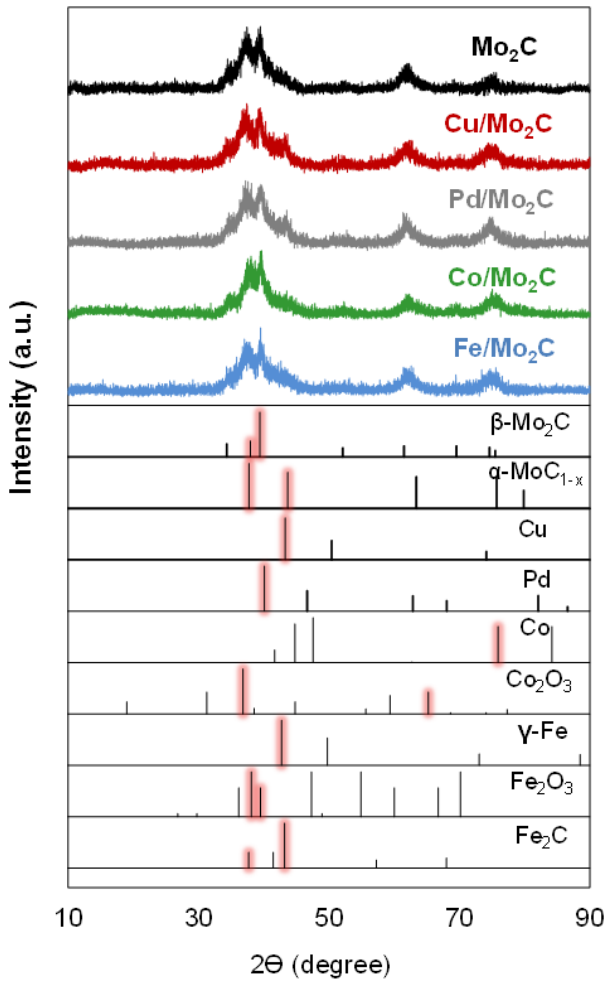

Figure A.1 X-ray diffraction patterns for M/Mo_2C catalysts and standard peaks.

All the XRD patterns were collected after passivating the metal/Mo_2C catalysts in 1% H_2/O_2 for 5 h. The relevant standard spectra are included below the metal/Mo_2C patterns. The peaks that are overlapped with the Mo_2C peaks from the metal-containing species are highlighted in red in the standard spectra.

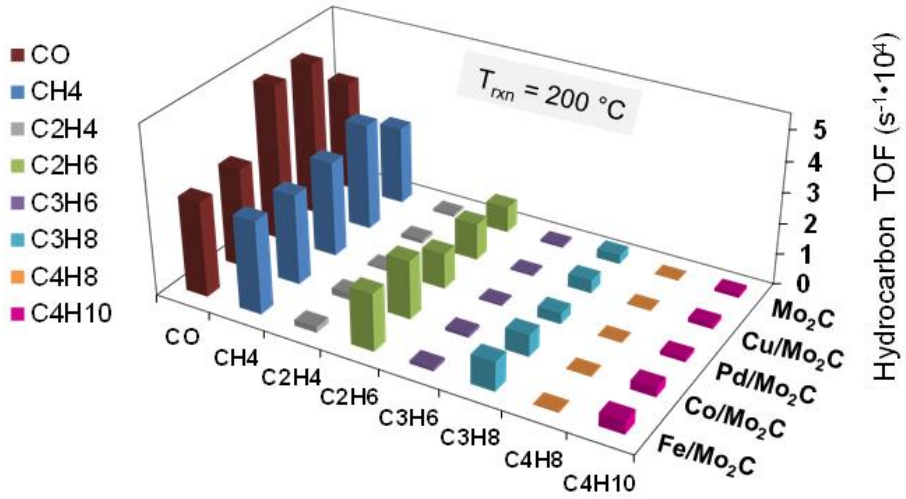

Figure A.2 CO and hydrocarbons (paraffins and olefins) distribution from CO_2 hydrogenation at 200 ℃.

CH_3OH Hydrodeoxygenation (HDO):

$$CH_3OH + H_2 \rightarrow CH_4 + H_2O, \quad \Delta G_{200°C} = -106\ kJ/mol \qquad \text{Eq. S1}$$

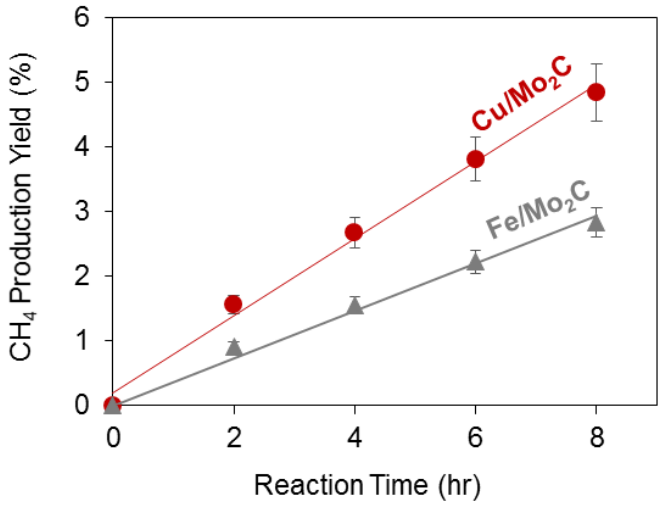

Figure A.3 Product yield (%) as a function of reaction time for CH_3OH HDO over Cu/Mo_2C and Fe/Mo_2C catalysts. Experiments are performed at 200 ℃, 10 bar N_2, 30 bar H_2, 7 mmol CH_3OH, 37.5 ml 1,4-dioxane, and 200 mg M/Mo_2C catalyst.

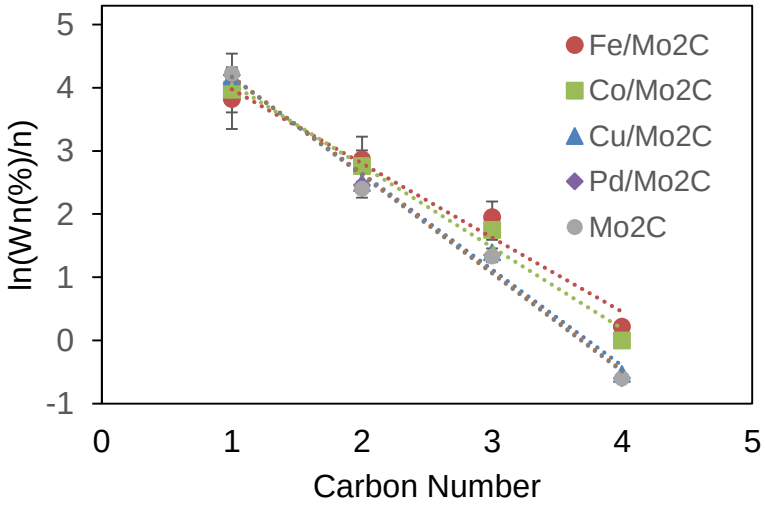

Figure A.4 Anderson-Schultz-Flory plot for C_1-C_4 hydrocarbon distributions at 200 ℃ over M/Mo_2C catalysts.

The ASF plot was generated based on the following equation:

$$W_n/n = (1-\alpha)^2 \bullet \alpha^{n-1} \qquad \text{Eq. S2}$$

Where Wn is the weight fraction of hydrocarbons containing n carbon atoms and α is the chain propagation probability, i.e. the probability that a molecule continues reacting to form a longer chain. The α value is the linear slope of log (Wn/n) and n.

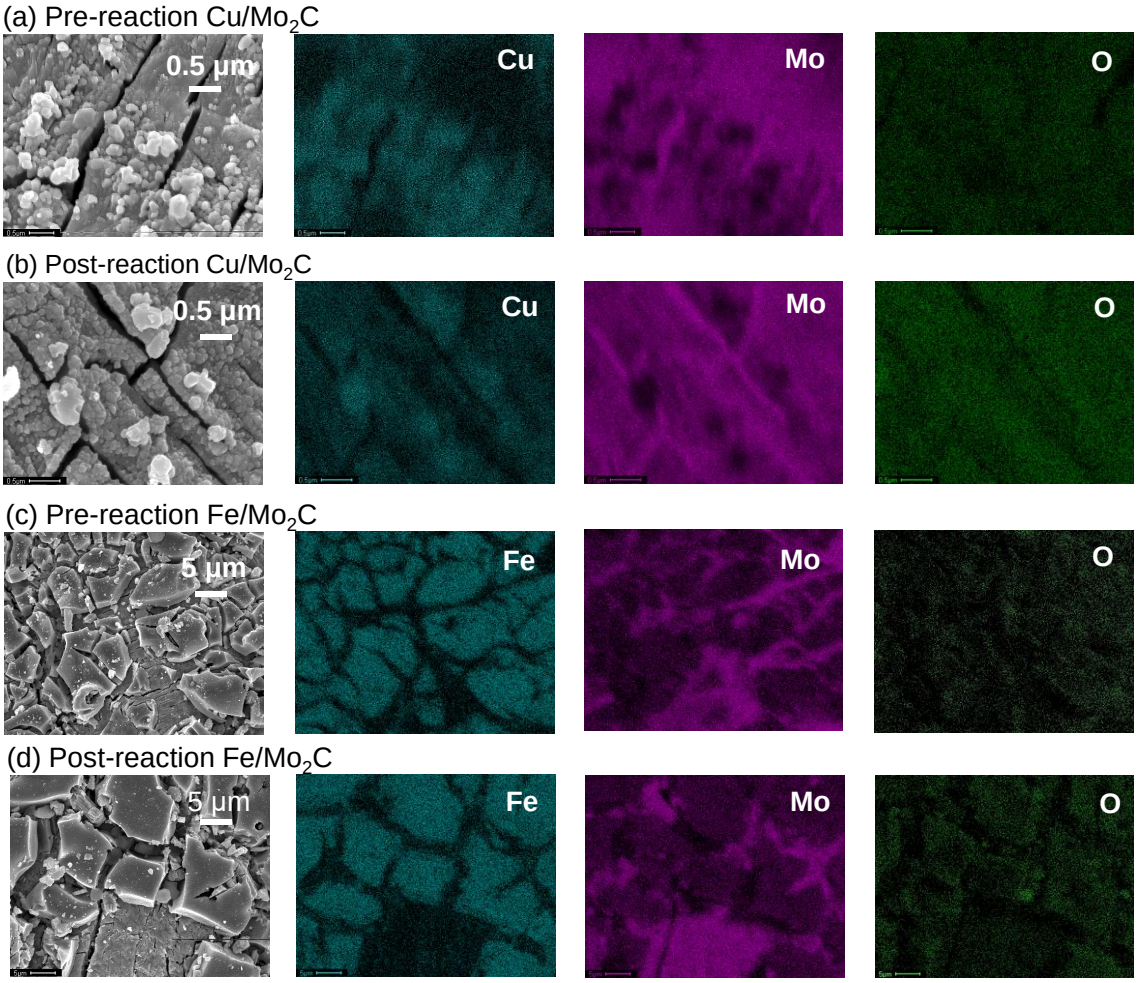

Figure A.5 Scanning electron micrographs and the corresponding EDX spectra for (a) pre-reaction Cu/Mo_2C, (b) post-reaction Cu/Mo_2C, (c) pre-reaction Fe/Mo_2C, and (d) post-reaction Fe/Mo_2C catalysts.

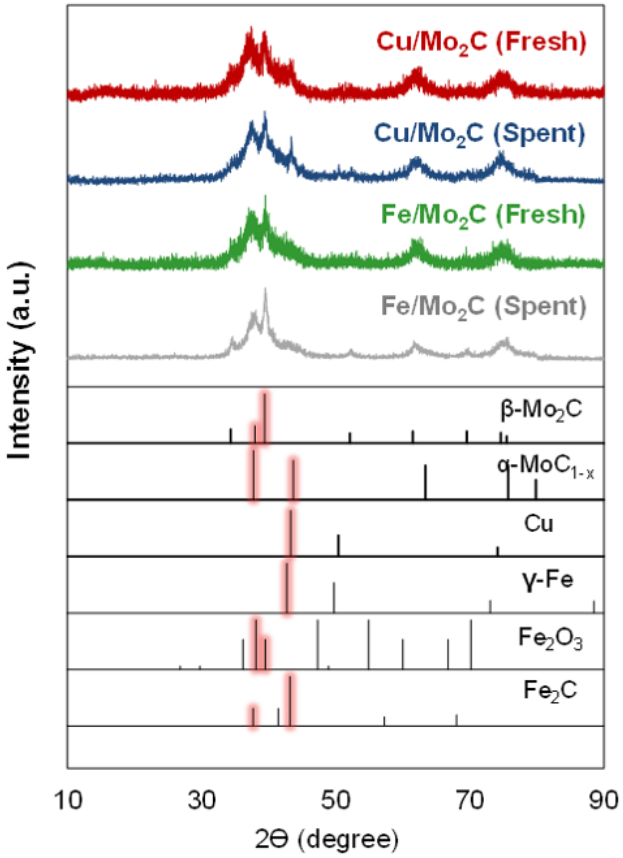

Figure A.6 XRD diffraction patterns for pre- and post-reaction Cu/Mo_2C and Fe/Mo_2C catalysts.

Table A.1 Thermodynamic properties of CH_3OH and hydrocarbon formation from CO_2 or CO hydrogenation.

Chemical Equations	$\Delta H_{25℃}$ (kJ/mol)[a]	$\Delta G_{25℃}$ (kJ/mol)[a]	$\Delta G_{135℃}$ (kJ/mol)[b]	$\Delta G_{200℃}$ (kJ/mol)[b]
$CO_2 + 3H_2 \rightarrow CH_3OH + H_2O$	-49.5	4.2	24.0	35.8
$CO_2 + H_2 \rightarrow CO + H_2O$	41.2	28.6	24.0	21.3
$CO_2 + 4H_2 \rightarrow CH_4 + 2H_2O$	-164.7	-113.3	-94.3	-83.1
$CO_2 + \frac{7}{2}H_2 \rightarrow \frac{1}{2}C_2H_6 + 2H_2O$	-132.0	-78.8	-59.1	-47.4
$CO_2 + \frac{10}{3}H_2 \rightarrow \frac{1}{3}C_3H_8 + 2H_2O$	-125.0	-70.9	-50.9	-39.1
$CO_2 + \frac{13}{4}H_2 \rightarrow \frac{1}{4}C_4H_{10} + 2H_2O$	-121.6	-67.0	-46.8	-34.9
$CO + 2H_2 \rightarrow CH_3OH$	-24.4	-0.22	0.03	14.5
$CO + 3H_2 \rightarrow CH_4 + H_2O$	-205.8	-141.9	-118.3	-104.4
$CO + \frac{5}{2}H_2 \rightarrow \frac{1}{2}C_2H_6 + H_2O$	-173.2	-107.4	-83.1	-68.7
$CO + \frac{7}{3}H_2 \rightarrow \frac{1}{3}C_3H_8 + H_2O$	-166.2	-99.6	-74.9	-60.4
$CO + \frac{9}{4}H_2 \rightarrow \frac{1}{4}C_4H_{10} + H_2O$	-162.7	-95.6	-70.8	-56.2
$HCOOH + 2H_2 \rightarrow CH_3OH + H_2O$	-80.4	-54.5	-44.9	-39.2
$HCOH + H_2 \rightarrow CH_3OH$	-92.6	-59.0	-46.6	-39.2

[a] The calculations are performed based on thermodynamic properties of reactants and products in their standard states at 25 ℃ and 1 atm. The thermodynamic values are obtained from the NIST Chemistry WebBook.

[b] Calculated based on $\Delta G(T) = \Delta H° - T*\Delta S°$, assuming $\Delta H°$ and $\Delta S°$ remain constant at different reaction temperatures.

Appendix B

Supporting Information for Chapter 6

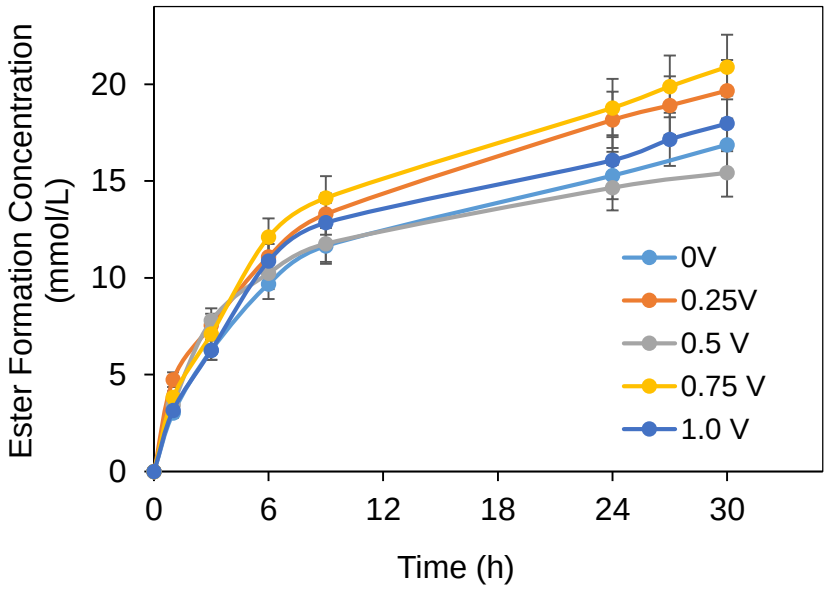

Figure B.1 Isopropyl crotonate concentration profile as a function of reaction time at different applied potentials from 0.0V to 1.0V.

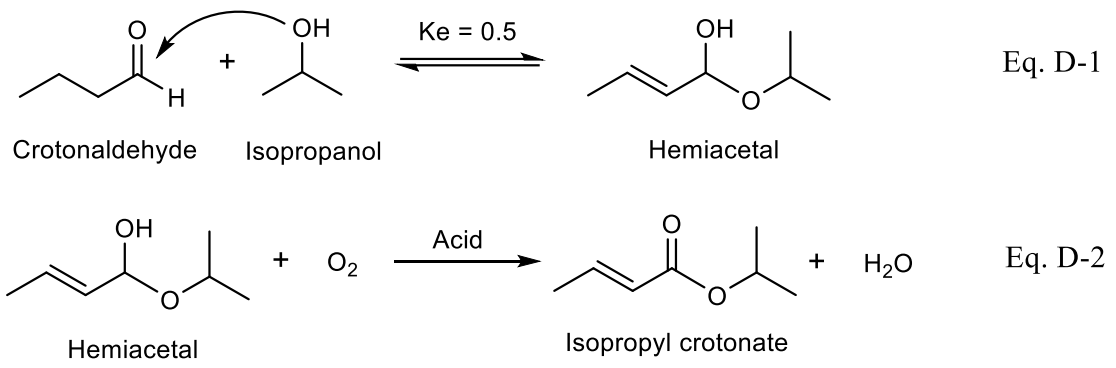

Figure B.2 Proposed pathways for isopropyl crotonate formation.

The formation of ester was likely to occur through two steps as shown in Figure B.2. The first step was the formation of hemiacetal, as a consequence of mixing crotonaldehyde and isopropanol (the solvent). The presence of hemiacetal was also confirmed by GC-FID as shown in Figure B.3. This reaction was reported to occur at room temperature in the presence of acid or base with an equilibrium constant of Ke = 0.5. The second step was the oxidation of the hemiacetal, which generated the ester, i.e. the isopropyl crotonate, while releasing an equivalent mole of H_2O. The formation of an oxidation product was a little surprising given the experiment was conducted in a reducing environment. However, as hemiacetal is typically an unstable intermediate, the formation of ester should be thermodynamically downhill. Meanwhile, the Nafion membrane used in the SPE cell is a strong acid that can catalyze this oxidation reaction (Eq. B.2).

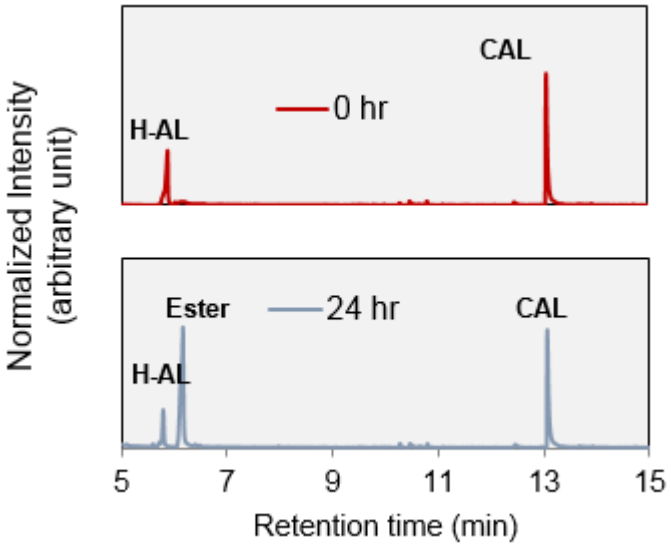

Figure B.3 GC-FID spectra from blank experiments, samples from 0 h and 24 h. 0.0 V, room temperature, 1 atm, 20% Pt/C as the catalysts. H-AL=Hemiacetal, ester = isopropyl crotonate, and CAL = crotonaldehyde.

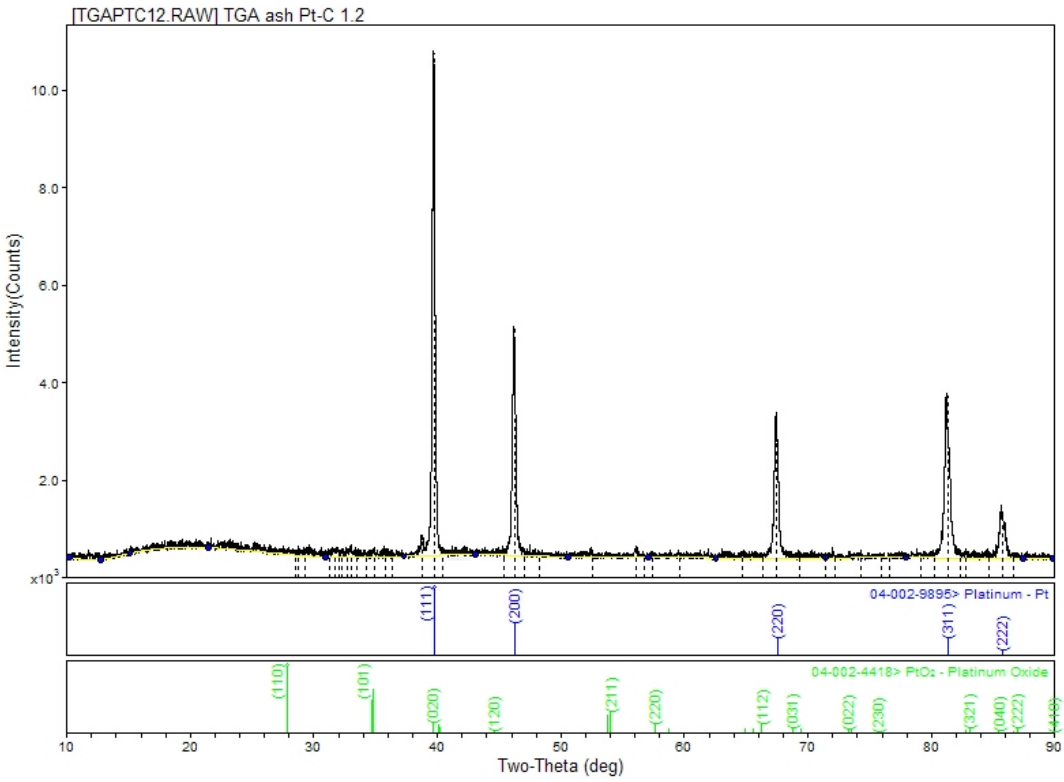

Figure B.4 XRD pattern for 20% Pt/C used for crotonaldehyde hydrogenation in the SPE reactor.